EFFICIENCY STUDIES OF Cu_2ZnSnS_4 THIN FILM SOLAR CELL

A Thesis submitted to
The Graduate School of Engineering and Science of
İzmir Institute of Technology
in Partial Fulfillment of the Requirements for the Degree of

MASTER OF SCIENCE

in Energy Engineering

by
Ece MERİÇ

July 2018
İZMİR

We approve the thesis of **Ece MERİÇ**

Examining Committee Members:

Prof. Dr. Lütfi ÖZYÜZER
Department of Physics, İzmir Institute of Technology

Asst. Prof. Dr. Enver TARHAN
Department of Physics, İzmir Institute of Technology

Asst. Prof. Dr. Özge SAĞLAM
Department of Mechanical Engineering, İzmir University of Economics

03 July 2018

Prof. Dr. Lütfi ÖZYÜZER
Supervisor, Department of Physics
İzmir Institute of Technology

Asst. Prof. Dr. Gürcan ARAL
Co-Supervisor, Department of Physics
İzmir Institute of Technology

Prof. Dr. Gülden GÖKÇEN AKKURT
Head of the Department of
Energy Engineering

Prof. Dr. Aysun SOFUOĞLU
Dean of the Graduate School of
Engineering and Sciences

ACKNOWLEDGEMENTS

Firstly, I would like to thank my supervisor, Prof. Dr. Lütfi ÖZYÜZER for giving a chance for carrying out my thesis with his invaluable experience and knowledge. I feel very lucky because of his guidance, suggestions and encouragement. I also would like to thank Prof. Dr. Gülnur AYGÜN ÖZYÜZER for her valuable contributions throughout my thesis.

I would like to thank TÜBİTAK for funding the project number of "114F341'' during my study.

I want to thank my the committee members of my thesis Asst. Prof. Dr. Enver TARHAN and Asst. Prof. Dr. Özge SAĞLAM for their participation and valuable comments.

I would like to thank CZTS team members Ayten CANTAŞ, Fulya TURKOĞLU, Fatime Gülşah AKÇA and Dilara Gökçen BULDU as a last member of this team for their support and assistance. I would also like to thank Hasan KÖSEOĞLU for sharing his experience with me. I am grateful to all OZYUZER research members who created friendly work environment. Also, I would like to thank Dr. Mehtap ÖZDEMİR KÖKLÜ, Dr. Mehmet Ali OLGAR and Mutlu Devran YAMAN for all their contributions to my thesis. I would like to thank Prof. Dr. Hasan EFEOĞLU from Atatürk University for LBIC measurements.

I am also very thankful to Dilce ÖZKENDİR, Hasan AYDIN, Barış AKBALI and Alper YANILMAZ for their friendship and help during my study.

I am especially thankful to Burak MIZRAK who has unlimited love and support throughout the thesis. I know that he will always be with me in all future successes and failures.

Last but not least, I want to thank my family. Firstly, I want to thank my father Engin MERİÇ who encourages me with all his hearth. I could never achieve all these things without his support. I also want to thank my mother Nüket MERİÇ who makes my life easier. I can overcome all difficulties with her unlimited patience and love. Especially, I would like to convey my deepest thanks to my sister Banu MERİÇ ARSLAN who is also my best friend and partner in crime. I also would like to thank my brother Mustafa ARSLAN who has been one of my best friends since 2009. I could not do anything without the support my family who are my biggest luck in life.

ABSTRACT

EFFICIENCY STUDIES OF Cu_2ZnSnS_4 THIN FILM SOLAR CELLS

Cu_2ZnSnS_4 (CZTS) is a promising candidate as an absorber layer for thin film solar cells due to not only its low cost but also nontoxic properties contrary to alternative materials such as CdTe and $Cu(In,Ge)Se_2$ (CIGS). Recently, CZTS and similar chalcogenides have attracted remarkable attention because of their suitable properties.

In my thesis; I studied the efficiency of Cu_2ZnSnS_4 thin film solar cells for various stoichiometric cases. Besides, the effect of back contact, buffer layer thickness and sulfurization time were investigated. CZTS thin films were fabricated by DC magnetron sputtering method on Molybdenum (Mo) coated Soda Lime Glass (SLG) and Ti foil substrates. Cu, Sn, Zn, Cu layers were, respectively, deposited on the substrates, and then sulfurization process was followed as the second step in the growth process to obtain a desirable CZTS formation. The as grown CZTS structure was investigated using Raman and X-Ray Diffraction (XRD) spectroscopies. Scanning electron microscopy (SEM) was used to investigate the surface morphology of the films. Energy dispersive spectroscopy (EDS) was used to define the chemical structure of the surface of the films. Next, a CdS buffer layer was deposited on CZTS absorber layer using CBD method at 85^oC for varying times (60, 75 and 90 min). Then, ZnO and Al doped ZnO (AZO) layers were deposited on CdS. J-V curves were obtained for SLG/Mo/CZTS/CdS/ZnO/AZO solar cell structure. The photovoltaic characteristic of solar cells was studied and their dependence on CdS deposition time were found. Among all the device we produced, the highest efficiency was obtained for the device with the lowest CdS deposition time. In addition; effect of sulfurization time on the solar cell conversion efficiency was studied.

ÖZET

Cu_2ZnSnS_4 İNCE FİLM GÜNEŞ HÜCRELERİNİN VERİM ÇALIŞMALARI

Cu_2ZnSnS_4 (CZTS) sadece ucuz maliyetli olması nedeniyle değil aynı zamanda CdTe ve $Cu(In,Ge)Se_2$ (CIGS) ile karşılaştırıldığında zehirli olmaması dolayısıyla ince film güneş hücrelerinde kullanılan soğurucu katman tabakası için ümit vadeden bir adaydır. Son zamanlarda, CZTS ve benzer dörtlü bileşikler uygun özellikleri bakımından dikkat çekmektedir.

Bu tezde; çeşitli stokiometrik durumlar için Cu_2ZnSnS_4 ince film güneş pillerinin verimlilik çalışmalarını inceledik. Ayrıca, arka kontak, tampon tabaka kalınlığı ve sülfürizasyon süresinin etkisi araştırıldı. CZTS ince filmleri, Molibden (Mo) kaplı cam alttaş üzerine ve Titanyum (Ti) folyo üzerine DC magnetron saçtırma yöntemi ile üretilmiştir. Cu, Sn, Zn, Cu tabakaları sırasıyla alttaş üzerine biriktirilmiştir ve bunu CZTS yapısına ulaşmak için ikinci adım olarak sülfürleme süreci takip etmiştir. Büyütülen CZTS yapısı Raman ve X-Ray Saçtırma (XRD) analizi kullanılarak incelenmiştir. Yüzey yapısının incelenmesi için taramalı elektron mikroskopu (SEM) kullanılmıştır. Dahası, enerji dağıtıcı spektroskopisi (EDS) kullanılarak filmlerin yüzeylerinin kimyasal yapısı tanımlanmıştır. Mo kaplı camın alttaş olarak kullanılmasıyla devam edilen çalışmada, CdS tampon katmanı farklı zamanlarda (60,75 ve 90 dak) kimyasal banyo biriktirme metoduyla 85 ^oC'de CZTS soğurucu tabaka üzerine biriktirilmiştir. Sonrasında, güneş hücresi aygıtını tamamlamak amacıyla, ZnO ve Al katkılı ZnO (AZO) tabakaları CdS katmanı üzerine biriktirilmiştir. SLG/Mo/CZTS/CdS/ZnO/AZO güneş hücresi yapısı için J-V eğrileri saptanmıştır. Güneş hücrelerinin fotovoltaik özelliği incelenmiş ve CdS birikim süresine bağlılığı bulunmuştur. En yüksek verimlilik CdS'nin en düşük biriktirme süresi için elde edilmiştir. Buna ek olarak; güneş hücresi verimi üzerinde sülfürleme süresinin etkisi araştırılmıştır.

To my Family…

TABLE OF CONTENTS

LIST OF FIGURES

Figure **Page**

LIST OF TABLES

Table **Page**

CHAPTER 1

INTRODUCTION

1.1. Overview of Renewable Energy Sources

The motivation of my thesis comes from the increase in the amount of CO_2 emission to Earth's atmosphere which cause climate change. Most of the CO_2 emission is due to human activities such as the combustion of carbon-containing fuels (fossil fuels: petroleum, natural gas, coal, etc.). The increasingly negative air quality due to CO_2, is the main cause of rise in the greenhouse effect in the atmosphere. (The sun's rays reflected from the earth cause it to warm up when it returns to the earth without going out.) The consequences of this problem will be terrifying for planet if no precaution is taken immediately. The annual world energy consumption data reported in BP Statistical Review of World Energy (BP 2017). It is shown in Figure 1.1 which also show some feature predictions.

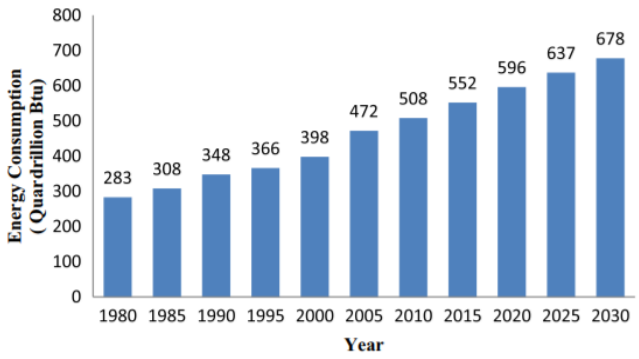

Figure 1. 1. Past and Predicted World Annual Energy Consumption Graph.
(Source: Manish Kumar and Kumar 2017)

Many countries focus on renewable energy sources as alternatives for the conventional ones. Renewable energy sources such as solar, wind, geothermal, hydropower and biomass are sustainable, ecofriendly and unlimited. By the end of 2015, approximately 23.7% of the world's electricity was produced from renewable energy

sources (Seyboth et al., 2016). Among the renewable energy sources, solar energy is one of the most invested ones (Figure 1.2). Solar energy attracted great attention due to its supply being available always. In addition to this, it is suitable for large and small scale manufacturing. Solar energy reaches the Earth's surface within an hour ($4.3x10^{20}$ J) is almost equal to annual energy consumption ($4.1x10^{20}$ J) of the whole world (Zhu, Long, and Ort 2008).

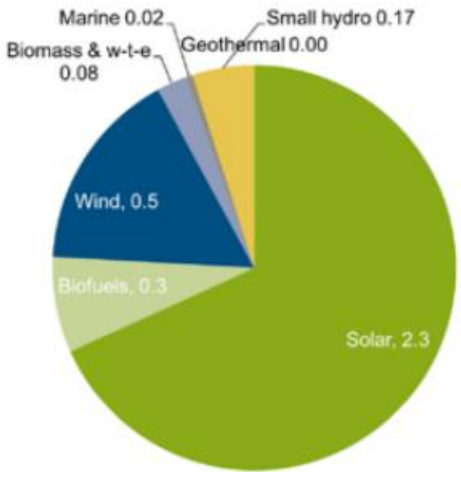

Figure 1. 2. New Investment in Renewable Energy by Sector
(Source: McCrone et al., 2017).

1.2. Analysis of Solar Energy

Sun is one of the crucial energy source for humanity. Since many centuries, solar radiation was used for many purposes. The first evidence was recorded in 7th century B.C. in order to make fire using sun ray (Jha et al., 2017). The most important invention was attained in 1839 with photovoltaic effect (H. Zhu et al. 2011). Photovoltaics (PV) is a term which covers alteration of light into electricity using semiconductor materials which show photovoltaic effect. To better understanding, photovoltaic effect can be explained as creation of voltage or electric current in material under sun light exposure. Therefore, all we need is sun. Huge amount of energy is generated from the sun and collected by the earth is 174.000 terawatt (TW). On the other hand; 30% of the total energy is reflected while the rest of it is absorbed. Emitted photons which have the wavelength from 100 nm to 10^6 nm energy and frequency change at different wavelength

can be seen Figure 1.2. Electromagnetic spectrum is used to characterize these waves. The amplitude is the height of wave from the center and a measure of light intensity. Wavelength is the distance between wave peaks. Frequency, other important term, is number of waves that pass a point in a period of time.

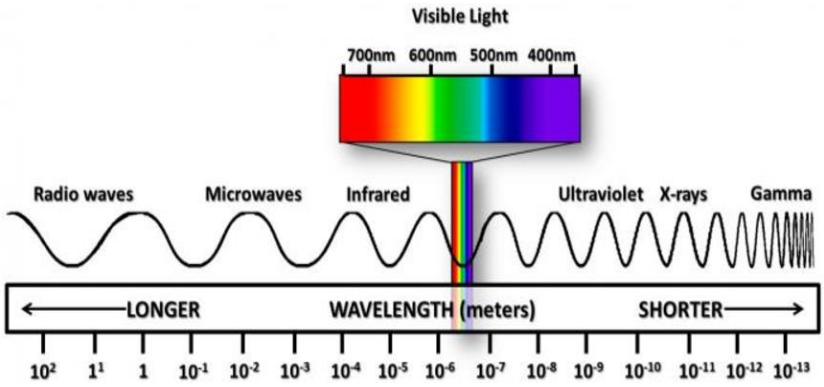

Figure 1. 3. The Electromagnetic Spectrum.

In order to understand the air mass calculations, we have to define some terms. ‘’AM 0’’ and ‘’AM 1.5’’ give us the spectrum of irradiance. Absorption and scattering depend on the line length of sunlight through the atmosphere. In other words, the sun’s elevation angle above the horizon becomes important. Air mass spectrum changes depending on zenith angle. Figure 1.3. shows us the illustration of light path. Z is an angle from the zenith and h is an angle from the horizon. If we assumed that the path length of light is s and atmosphere thickness is d, s=d/cosh. Air mass (AM) is given by s/d=1/cosh. In Figure 1.4, red line represents AM0, while blue line represents AM1.5. Green line shows us blackbody irradiance of the sun. Also, visible region can also be seen. If the light has an angle of 48.2° between the sun positions and the zenith, it is called AM1.5. Since AM1.5 radiation value is close to maximum irradiance value collected at the earth’s surface, it was confirming to standards for photovoltaic systems.

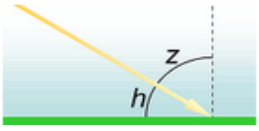

Figure 1. 4. Illustration of sunlight path.

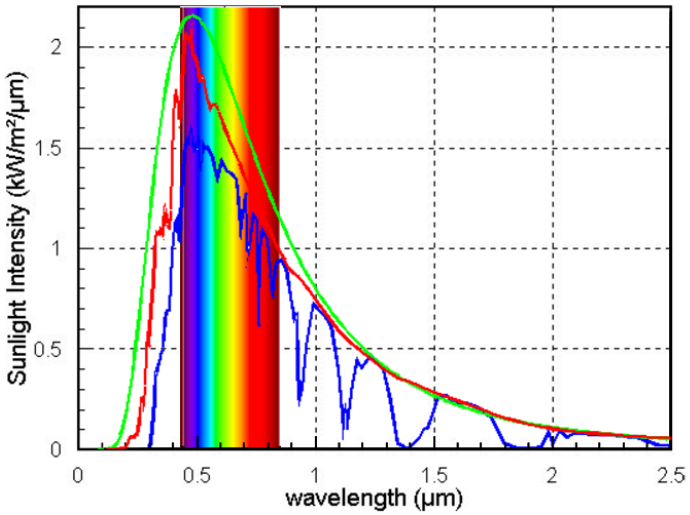

Figure 1. 5. Solar Radiation
(Source: Sekular and Blake 1985).

1.3. The Goal of This Thesis

New compound semiconductor material which is ecofriendly, non-toxic and earth abundant is studied for photovoltaic applications in this thesis. Cu_2ZnSnS_4 thin film solar cells is investigated. Optimize Zn(O,S), ZnO, Al:ZnO layers are our the other target to formed solar cell device. CdS buffer layer thickness effect on CZTS solar cell conversion efficiency is studied. Besides, sulfurization time effect on solar cell efficiency is explained. To achieve high performance for our solar cell devices, various of characterization techniques should be used. Scanning Electron Microscope (SEM), X-Ray Diffraction Analysis (XRD), Energy Dispersive Spectroscopy (EDS) are fundamental techniques to determine high quality CZTS absorber layer. The order of our work is;

- Growth of absorber layer on different substrates
- Characterization of CZTS absorber layer
- Substrate selection
- CdS, Zn(O,S), ZnO, Al:ZnO layers optimization
- Investigate CdS thickness effect on solar cell performance
- Sulfurization time effect on solar cell device which is used Zn(O,S) as a buffer layer.

CHAPTER 2

THIN FILM SOLAR CELLS

2.1. Thin Film Photovoltaics

Photovoltaics is one of the most available option for energy conversion. Motivation of thin film photovoltaics comes from opinion of low cost for production. Thin film solar cells are formed by depositing of semiconductor materials on a substrate. Device thickness varies from nanometers to micrometers. It is much thinner than conventional one which is crystalline silicon (c-Si) solar cell. This allows us solar cell flexibility and lower in weight. Besides, thin film materials have direct band gap. They have also high absorption coefficient. Therefore, thin film photovoltaics is more preferable option for energy conversion. Figure 2.1 shows the basic illustration of thin film solar cell.

Figure 2. 1. Illustration of Cu_2SnZnS_4 Thin Film Solar Cells

2.1.1. Amorphous Silicon (a-Si) Solar Cell

First studies were recorded about a-Si due to the reasons which are mentioned below (Chittick, Alexander, and Sterling 1969). a-Si solar cells are categorized in second generation solar cells. It is a non-crystalline form of silicon. In general, p-i-n or n-i-p

photo-diode sequence is used as shown in Figure 2.2. Under a large electric field, transport mechanism occurs result of either the diffusion or the drift collection (Petrich 2007). Generally, silicon is deposited by using chemical vapor deposition (CVD), or plasma-enhanced (PE-CVD) on glass, metal or plastic (Bharam 2012). In the literature, the highest efficiency is 14.0% for a-Si (Green et al., 2017). For high performance thin film solar cell;

- ✓ Absorption of a large division of the incident solar radiation
- ✓ Efficient collection of both photo-generated electrons and holes
- ✓ Low internal series resistance is required (Carlson and Wronski 1976).

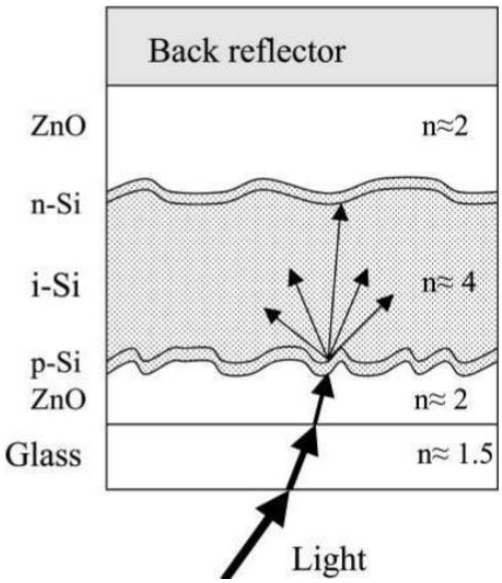

Figure 2. 2. Schematically Sketch of a p-i-n Thin Film Solar Cell.
(Source:Shah et al., 2004)

2.1.2. Cadmium Telluride (CdTe) Solar Cell

CdTe is preferable material due to its direct band structure. In addition, it has high absorption coefficient (>10^5 cm^{-1} at λ=700 nm) in the visible region (Loferski 1956). Its high absorption coefficient, allows us 99% of photons absorbing within 0.5μm (Birkmire and McCandless 2010). The highest conversion efficiency (22.1%) is announced for CdTe solar cell (Green et al., 2017). Figure 2.3 shows us a basic structure for CdTe. Through the glass substrate light get in. Transparent conductive oxide (TCO) is used as

front contact. In order to diminish shunting, high resistance oxide is used. Because of the toxicity problems, the use of CdTe is restricted.

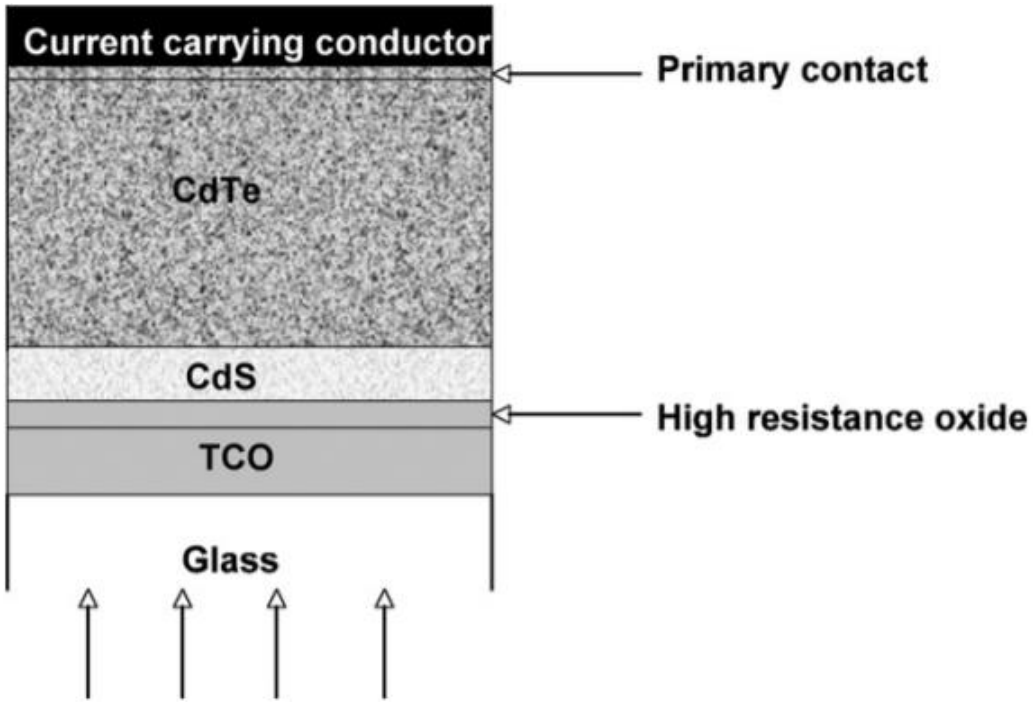

Figure 2. 3. Schematic cross section view of CdTe/CdS thin film solar cell.
(Source: Birkmire and McCandless 2010)

2.1.3. Copper Indium Gallium Diselenide (CIGS) Solar Cell

In 1976, first CIGS thin films were produced with conversion efficiency of 4.5% (Kazmerski et al., 2008). As seen Figure 2.4, soda lime glass (SLG) is used as substrate. Molybdenum is coated on SLG as a back contact. CIGS which is a p type and CdS which is a n type semiconductor is coated on back contact, respectively. ZnO and Al:ZnO are deposited after these layers. When it is compared with crystalline silicon which is 170-200 μm, CIGS which is about 4μm is much thinner. The highest conversion efficiency was reported as 22.0% (Green et al., 2017). Although high conversion efficiencies were reached, there are some problems. Indium and Gallium are expensive materials which effect solar cell cost. Besides, using toxicity selenium is unwanted situation. When

considered its disadvantages, other materials are needed for research. The solar cell structure with CIGS absorber layer can be seen in Figure 2.4.

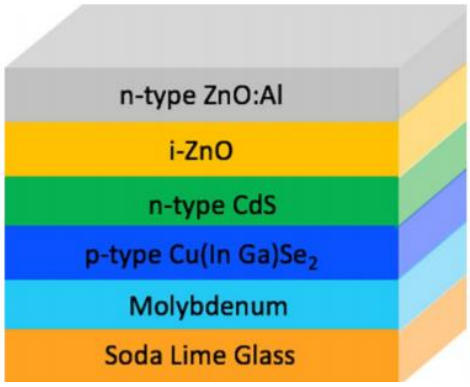

Figure 2. 4. Basis Illustration of CIGS Solar Cell

2.1.4. Copper Zinc Tin Sulfide (CZTS) Solar Cell

Up to now, types of solar cells were introduced. Among all, Cu_2ZnSnS_4 (CZTS) is a bright candidate for solar cell industry due to CZTS has direct band gap which is 1.5 eV and high absorption coefficient. Besides, it consists earth abundant elements which is important large volume production. After initial study by Ito (Ito and Nakazawa 1988) following work Katagiri (Katagiri et al., 2001) was done. The efficiency of this type of solar cell enhanced during last decades, however developments are still needed. In the following sections, detailed observation about CZTS solar cells are presented.

CHAPTER 3

PHYSICAL DESCRIPTION OF SOLAR CELL

3.1. What is Semiconductor?

In order to understand what transistors and diodes do, working principle of semiconductors should be examined. Solids can be categorized as conductors, semiconductors and insulators according to conduction electrons in their construction. Difference between these materials can be explained using band theory. Figure 3.1 shows schematic presentation of insulator, semiconductor and conductor. Darker rectangular represent valance band while others represent conduction band.

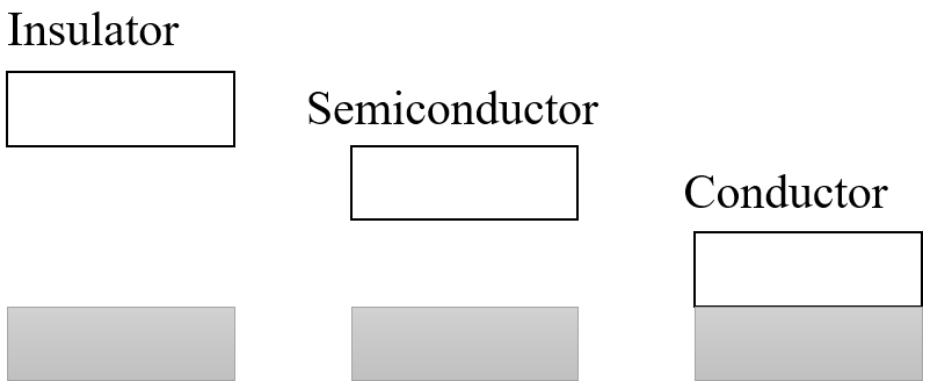

Figure 3. 1. Schematic representation for Insulator, Semiconductors and Conductor.

Thanks to number of atoms, a solid can be formed. In that moment, wave functions of electrons of these atoms contact each other and occur quantum states. Energy band is formed due to this formation. Pauli principle says that each state can be utilized only by one electron. Besides, Fermi energy level should be understood. Fermi level describes electron energy levels at absolute zero temperature. Fermi-Dirac statistic explains this concept. Electrons call fermions and cannot occupy same energy levels. At zero temperature, electrons gather in lowest available energy states. Electrons have not enough energy to rise above this states. For understanding of the electrical and thermal properties

of solids, fermi energy is important. At higher temperatures, a division that characterized by Fermi function will exist above the Fermi level. Position of the energy bands and the Fermi energy level shows us three different case as Figure 3.1.

If there are electrons in conduction band, conduction process can be discussed. As seen below; if electrons in the valance band is separated a large gap (> 5 eV) from conduction band, this material is an insulator. In conductors, valance band overlaps in conduction band. When it comes to semiconductor, there is a small gap (< 5 eV) between valance and conduction band. With a small percentage of doping material conductivity can develop. Addition of foreign atoms in regular lattice creates strong alteration in their electrical properties, producing n-type or p-type semiconductors.

We can categorize as two group that are elemental and compound semiconductors. Elemental semiconductors are from IV A group and whereas compound semiconductors combination of III-V A and II-VI A element as seen Table 3.1.

Table 3. 1 List of semiconductor materials.

Elemental Semiconductors	✓ Germanium (Ge) ✓ Silicon (Si) ✓ Tin (Sn)
Compound Semiconductors	✓ Cadmium telluride (CdTe) ✓ Cadmium selenide (CdS) ✓ Gallium arsenide (GaAs) ✓ Zinc sulfide (ZnS) ✓ Zinc oxide (ZnO)

Table 3.2. shows a portion of periodic table. More common semiconductor materials are displayed in blue. For example; silicon is the most used semiconductor material for integrated circuits chips and solar cells.

Table 3.3 shows the properties of crucial semiconductors. Terms should be explained in the table. For example; the values are for mobilities obtained in pure and simple suitable to date. In addition, band structure such as Ge, Si and GaAs label Ge-like, Si-like and GaAs-like structure respectively. Suitable materials for applications can be utilized by using these properties. Lattice constants or band gap crucial to determine material quality. The combination of different semiconductor types together generates

devices with special electrical properties, which allow control of electrical signals. Semiconductors are employed in the manufacture of electronic devices and integrated circuits.

Table 3. 2. A portion of Periodic Table.

1B	2B	3A	4A	5A	6A
		B	C	N	O
		Al	Si	P	S
Cu	Zn	Ga	Ge	As	Se
Ag	Cd	In	Sn	Sb	Te
Au	Hg				
	...				

Table 3. 3. Properties of Important Semiconductors.
(Source: Sze and Ng 2006)

		Lattice constant	Bandgap		Mobility[b] (cm²/V-s)		
Semiconductor		(Å)	(eV)	Band[a]	μ_n	μ_p	Dielectric constant
Element	Ge	5.65	0.66	I	3900	1800	16.2
	Si	5.43	1.12	I	1450	505	11..9
IV-IV	SiC	3.08	2.86	I	300	40	9.66
III-V	AlSb	6.13	1.61	I	200	400	12.0
	GaAs	5.65	1.42	D	9200	320	12.4
	GaP	5.45	2.27	I	160	135	11.1
	GaSb	6.09	0.75	D	3750	680	15.7
	InAs	6.05	0.35	D	33000	450	15.1
	InP	5.86	1.34	D	5900	150	12.6
	InSb	6.47	0.17	D	77000	850	16.8
II-IV	CdS	5.83	2.42	D	340	50	5.4
	CdTe	6.48	1.56	D	1050	100	10.2
	ZnO	4.58	3.35	D	200	180	9.0
	ZnS	5.42	3.68	D	180	10	8.9
IV-VI	PbS	5.93	0.41	I	800	1000	17.0
	PbTe	6.46	0.31	I	600	4000	30.0

Also, the term of extrinsic and intrinsic semiconductor should be mentioned. Actually we defined below their differences. An intrinsic semiconductors called a perfect crystal and its electron have enough energy to go to conduction band and leave behind a

hole. Extrinsic semiconductors are made using different atoms which is called dopant atoms in crystal. We can categorize two type as p-type and n-type.

3.1.1. P Type Semiconductors

In p-type semiconductor, holes are called majority carriers and free electrons are called minority carriers. Carrying out process of doping which should be added specific type of atoms to the semiconductor to enhance the amount of free charge of carriers p-type (p for positive) semiconductor is formed. In order to get away weakly-bound outer electrons from the semiconductor atoms, doping material is added. Vacancy left behind is known as a hole. The aim of p-type doping is to form an abundance of holes. For example, a trivalent atom is substituted into crystal lattice in Si. One electron is missing from one of the four covalent bond normal in order to complete the fourth bond. The dopants are called acceptors since they complete this bond. The dopant atom accepts an electron resulting formation of a hole. One of hole affiliated with nearby negatively-charged dopant ion, so when we consider semiconductor as a hole, it is electrically neutral. Hole behaves as a quantity of positive charge. When we added enough number of acceptor atoms, there are more holes than excited electrons. Thus; in p type materials, holes are accepted as majority carriers, while electrons are the minority carriers. B, Al, Ga and In are examples of p type semiconductors' doping materials. Consequently, p type semiconductors can be thought of as only conducting holes.

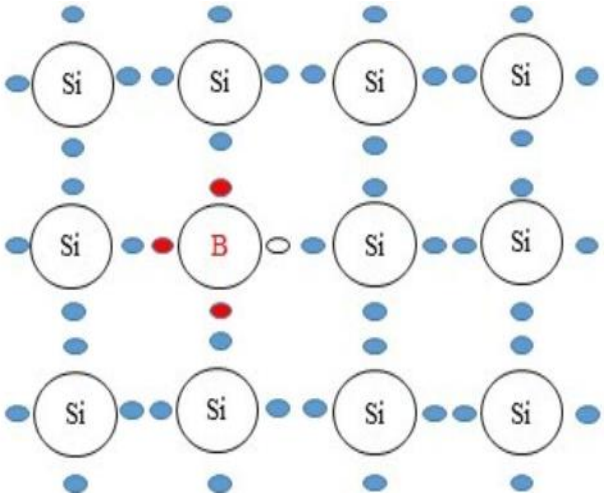

Figure 3. 2. P-type semiconductor.

3.1.2. N Type Semiconductors

Insulators are not good conductors because of large band gap between valance and conduction band. Insulators enhances conductivity with temperature because heat supplies energy to promote electrons to conduction energy levels.

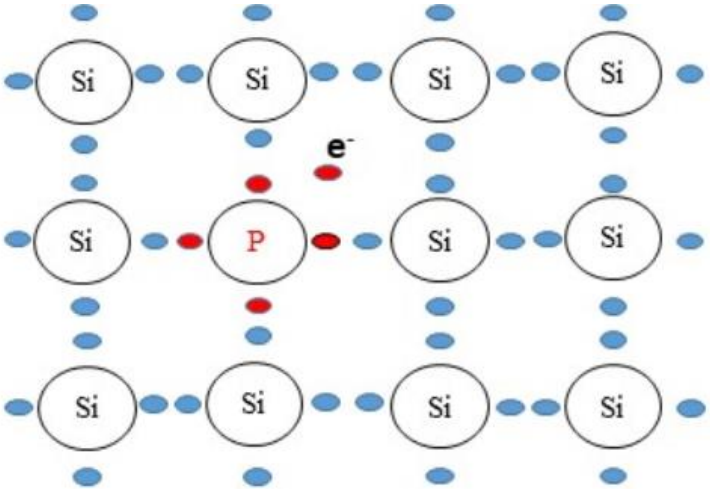

Figure 3. 3. N-Type Semiconductor.

As mentioned before, semiconductors are the middle of this two type of materials behalf of electrical conductivity. Their band gap is small and number of electrons pass from lowest energy levels to conduction band with small promote in temperature. Conductivity promotes with doping. Other elements are added to intrinsic crystal in order to create extrinsic semiconductor. When the dopant atoms provide an extra conduction electron to host material, negative electron charge carriers which creates holes in valance band and loosely held electrons in conduction band are created and the material called n-type semiconductor. Even small thermal agitation can release electrons to conduction band because levels are full of electrons near conduction band. Generally doping atoms have one more electrons than host material. Most common doping materials are from group V elements (Phosphorus, Arsenic, Antimony) which contain five valance electron. From group IV; silicon, germanium, tin which contain four valance electron are used for host material.

3.2. P-N Junction

The p-n junctions are of huge importance both electronic applications and in the understanding of other semiconductor devices. Fundamental theory of current-voltage characteristic of p-n junction was studied by Shockley (W. Shockley 1949). Then, Sah (Sah, Noyce, and Shockley 1957) and Moll (Moll 1958) developed this theory. Fundamental information of solar device is based on crystal materials and its unit p-n junction. Voltage is built inside by positively charged holes and negatively charged electrons are moved to opposite directions which are anode and cathode and collected by electrodes. It is actually explained using concept of diode. Figure 3.4 shows a basic p-n junction.

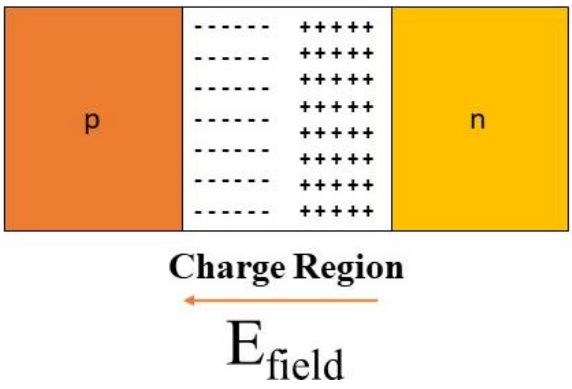

Figure 3. 4. Illustration of a basic p-n junction.

P-type and n-type semiconductor is added to each other, an electric field is established. Firstly, huge density gradient is formed in both electron and hole concentration. Due to the thermal diffusion, they begin to move from n-type zone to p-type zone and majority carrier holes diffuse to n-type zone. Because of leaving n-type region, there are lots of holes called as donor atoms. Also, holes diffusion from p-region to n-region causes construction of negatively charged atoms. These positively and negatively charged ions causes an electric field. Free charge carriers influence from this electric field. Electrons carry positive ions while holes haul negative ions. Electron or hole near the charge region is attracted by electric field and to dragged its original volume. Two contrary flow reach an equilibrium eventually. After that, net electron flow across

the junction is zero. Although net current is zero across the junction, electric field is established which is the basis of p-n junction devices.

3.2.1. P-N Junction Under Bias

When the p part of p-n junction is contacted negative terminal of the battery and n part of p-n junction is contacted positive terminal of battery, negative carrier flows to the positive side of battery while positive carrier flows to the negative side of battery. Therefore; the reverse bias removes the majority carriers increasing the potential barrier. No current can be read. Figure 3.5 shows p-n junction under reverse bias.

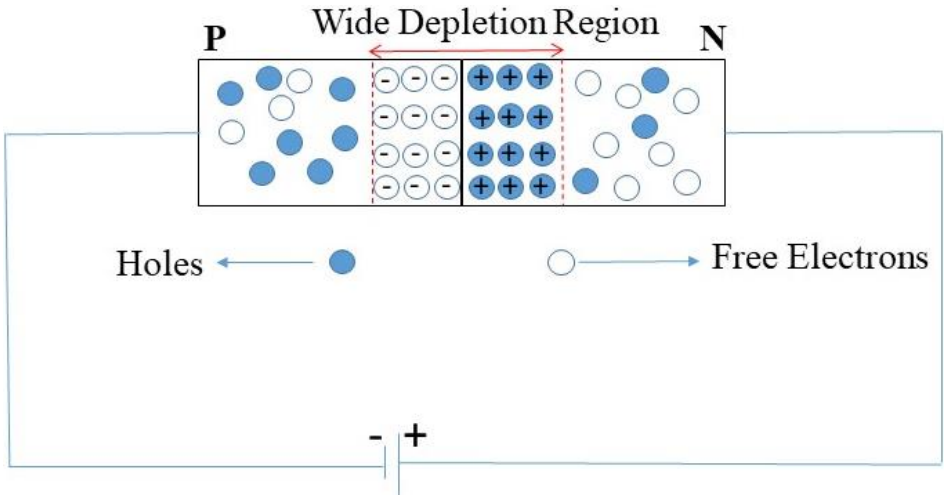

Figure 3. 5. p-n junction under reverse bias.

When the opposite of these case is thought, situation will change. If p side of junction connect positive terminal of battery and n-side of junction connect negative terminal of battery, current flows. Holes and free electrons enter the depletion region because of repulsion at the respective terminals. Decrease in potential difference and width of depletion region cause lots of majority charge carriers in order to diffuse junction. Holes travel to the right and electrons travel to the left as shown Figure 3.5. P-n junction allows current carriers to flow through it if the junction is forward bias. As known, if a device that allows the current only one direction is called diode, so p-n junction can be described as a diode.

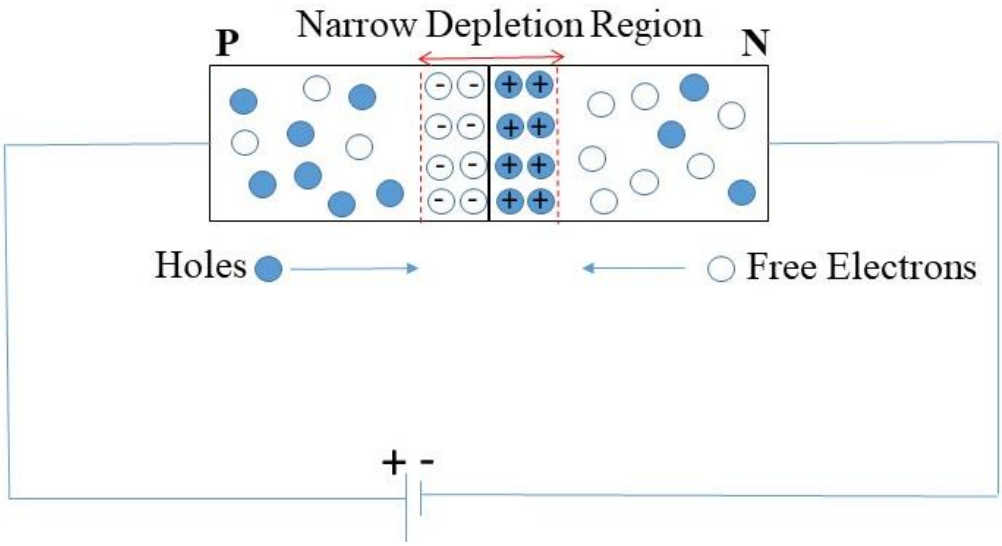

Figure 3. 6. p-n junction under forward bias.

3.2.2. P-N Junction Under Illumination

The most important thing for devices, material's band gap energy should be lower than incident light's band gap energy. If not; there is no absorption and electron-hole pair cannot be observed. Therefore; when a cell is illuminated, there are two different results. If the incident photon energy is greater than band gap of device material, photons are absorbed and electron-hole pairs are occurred which is necessary for current. This current is called photo-current (I_L). This current flows opposite direction to the dark current. Besides, since the illumination causes the photocurrent in the opposite direction of the dark current, I-V curve shifts along the negative current-axis. While the intensity of incident light is increased, the generated current by solar cell increases. Current of the junction is shown equation 3.1 for the case of illumination.

$$I = I_0 \left(e^{\frac{qV}{kT}} - 1 \right) - I_L \tag{3.1}$$

Here, I_0 is saturation current, q is the electron charge, V is voltage, k is Boltzmann's constant and T is absolute temperature in Kelvin unit. To determine a solar cell, device parameters is crucial. Current is the main target for fabrication Therefore, given equation can be used to calculation.

3.2.3. I-V Observation of P-N Junction

The illuminated and dark conditions for a p-n junction can be seen in Figure 3.7. Due to the illuminated p-n junction creates photocurrent in opposite direction of the dark current, so I-V curve alters along the negative current axis. Current for solar cell increases with the increment in the intensity of incident light.

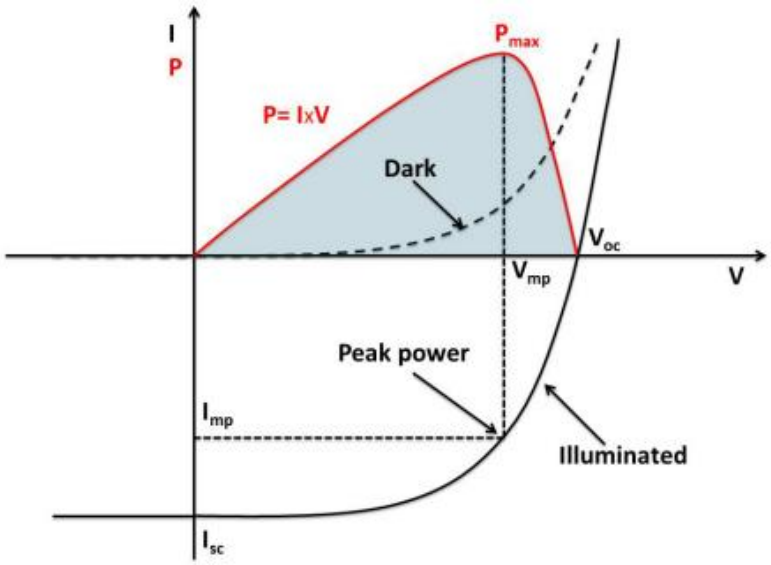

Figure 3. 7. I-V characteristics of solar cell in dark and illuminated condition (Source: Turkoglu 2017).

3.4. Parameters of Solar Cell

In order to analyze and determine the performance of solar cell, there are some electrical parameters such as open circuit voltage (V_{OC}), short circuit current (I_{SC}), fill factor (FF), series resistance (R_S), shunt resistance (R_{SH}) and efficiency of the cell (η). For better understanding, equivalent circuit of a solar cell should be drawn. Figure 3.8. shows circuit for non-ideal solar cell. If the whole parameters can be understood clearly, it is beneficial for solar cell device fabrication. Because, optimized properties supply better fabrication. If the fabrication is important for industry. The main target should be understanding parameters that affect the device performance. The details of these parameters will be discussed in next heading.

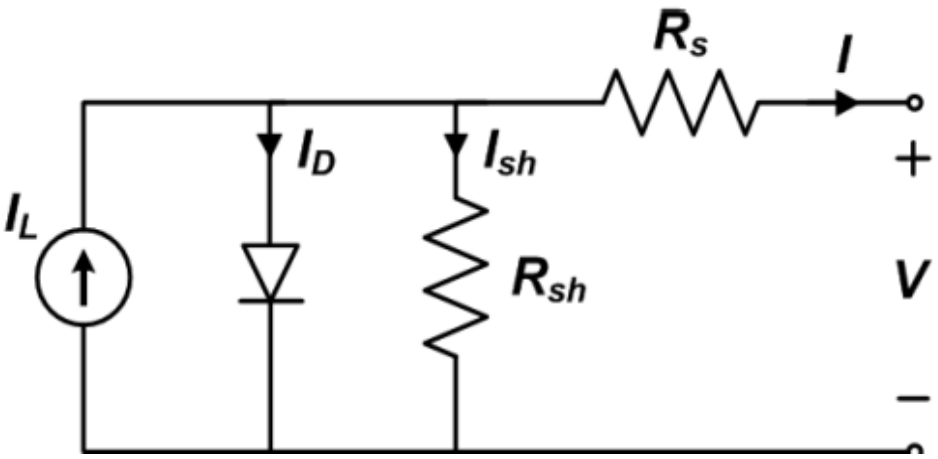

Figure 3. 8. The equivalent circuit of a non-ideal solar cell.

Here, I_L is photocurrent, I_D is diode current, I_{SH} is shunt current and I is output current while R_{SH} shunt resistance and R_S is series resistance. The output current is shown with equation 3.2.

$$I = I_L - I_D - I_{SH} \tag{3.2}$$

The potential both shunt resistance and diode is V_D whereas the output voltage is V is shown with equation 3.3.

$$V_D = I_{SH} R_{SH} \ , \qquad V_D = V + IR_S \tag{3.3}$$

Output current for non-ideal solar cell is given with equation 3.4.

$$I = I_L - I_0 (e^{\frac{q(V+IR_S)}{kT}} - 1) - \frac{V+IR_S}{R_{SH}} \tag{3.4}$$

3.4.1. Open Circuit Voltage (V_{OC})

V_{OC} which is called open-circuit voltage, is highest voltage for solar device and occurs at zero current. It can be explained as amount of forward bias on the solar device

because of the solar cell junction with the light-generated current. Figure 3.9 shows IV curve and open circuit voltage of a solar cell.

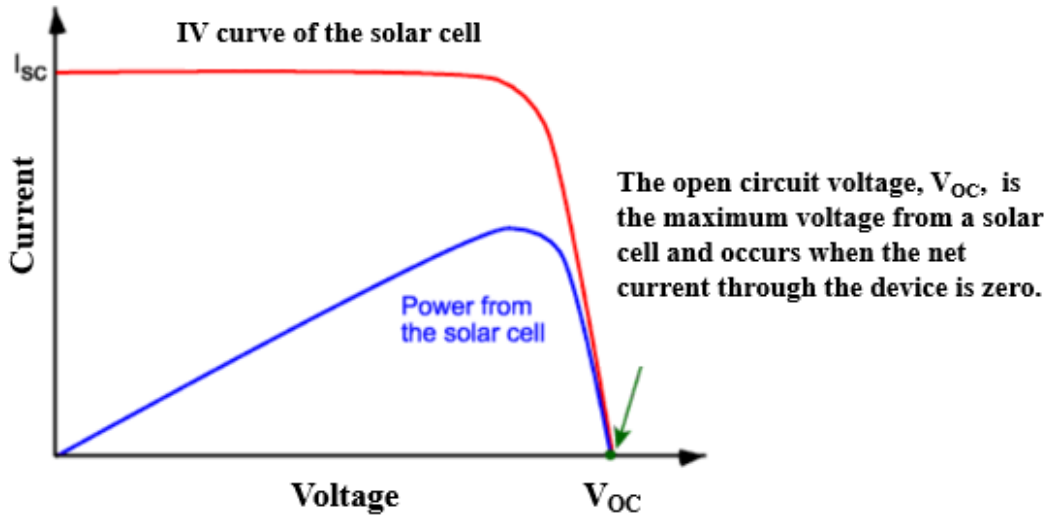

Figure 3. 9. IV curve of a solar cell that shows the open circuit voltage.

3.4.2. Short Circuit Current (I_{SC})

The short circuit current occurs through solar cell when the voltage is zero. Generally, written as I_{SC} and is shown in Figure 3.10 on the IV curve.

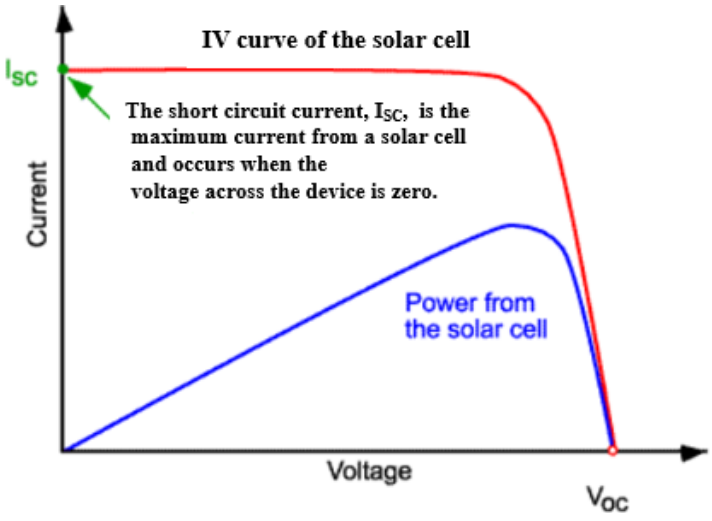

Figure 3. 10. IV curve of a solar cell that demonstrate the short circuit current.

3.4.3. Fill Factor (FF)

Maximum current and voltage from a solar device are short circuit current and open circuit voltage respectively. But, both of this operating points, the power from the solar cell is zero. Fill factor is a parameter which in conjunction with V_{OC} and I_{SC} and is shown FF. Maximum power of a solar cell can be determined using fill factor. The FF is obtained as equation 3.5.

$$FF = \frac{I_{mp} x\, V_{mp}}{I_{sc} x\, V_{oc}} \tag{3.5}$$

Figure 3.11 explains fill factor mechanism. The FF is a measure of squareness of the IV curve. If we have higher voltage, we can get higher possible FF.

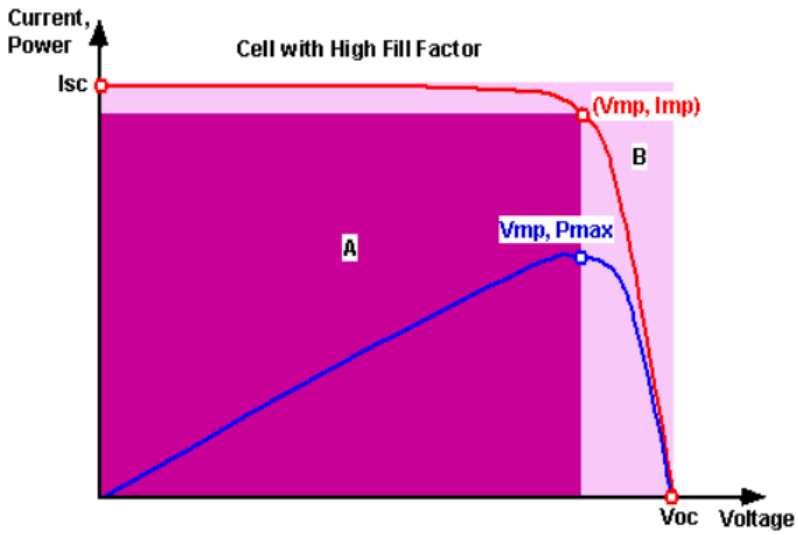

Figure 3. 11. Fill factor from IV curve.

3.4.4. Series Resistance

Two electrical contacts are used for solar cell device as back and front contact. Transparent conductive oxide layer (TCO) is used for front contact aiming for light penetration. Back contact is a metal layer at bottom of the solar cell. Series resistance occurs because of back contact resistance between metal and absorber, front contact

resistance occurs between of the bulk resistance of material and front contact resistance (Kavitha et al., 2016).

Reducing fill factor and also short circuit current at huge values are the main effects. Series resistance should be zero for an ideal solar cell. Schematic illustration of series resistance is shown Fig. 3.12.

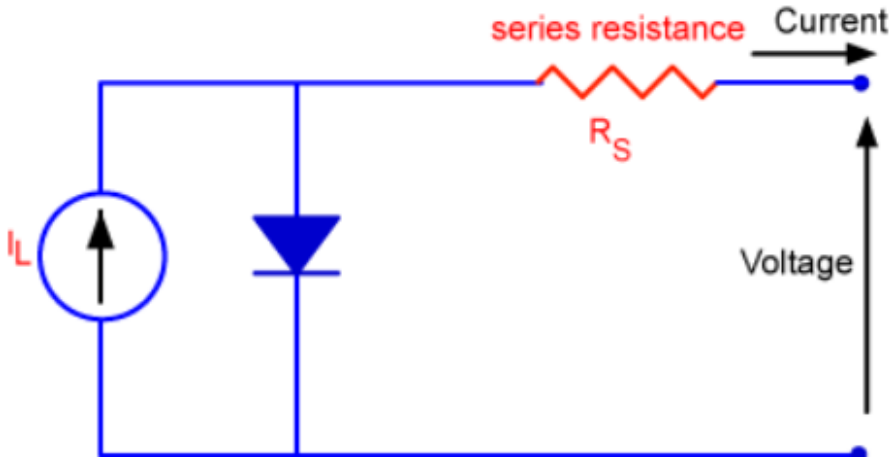

Figure 3. 12. Schematic Illustration of Series Resistance.

Back contact and front contact thickness is important. For instance, when front contact is thin to reduce the optical loss, it causes high sheet resistance which causes series resistance (Markvart 2013). When TCO is thick more light can be absorb, photo carrier decreases.

The missing photon absorption in the buffer layer decreases fill factor (FF) because of augment of series resistance (Buffière et al., 2014).

3.4.5. Shunt Resistance

Because of the local defects in the junction or shunts in the edges, shunt resistance occurs from leakage of the current along the cell (Nelson 2003).Shunt resistance are not good for device performance. In the case of low value of shunt resistance, there is an alternative path for current and causes power losses. When shunt resistance decreases, current diminishes along the solar cell. Due to the losses current, voltage is decreases. Shunt resistance can be calculated using slope of I-V curve. In order to avoid V_{OC} losses,

R_{SH} must be tremendous value when R_S is considered. Schematic illustration of shunt resistance is shown Fig. 3.13.

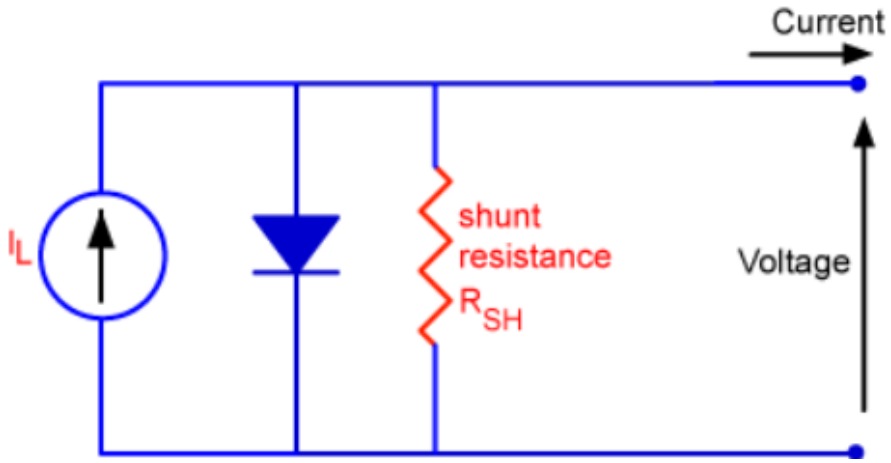

Figure 3. 13. Schematic Illustration of Shunt Resistance.

3.4.6. Efficiency (η)

The ratio between electrical power output (P_{out}) and solar power input (P_{inc}) is called efficiency in photovoltaic cell. P_{out} can be taken maximum when the highest efficiency is achieved. Standard illumination conditions are taken for P_{inc}.

$$\eta = \frac{P_{max}}{P_{inc}} = \frac{V_{OC} x I_{SC} x FF}{P_{inc}} \tag{3.6}$$

3.5. Losses in Solar Cells

If each photon enrols to duty of energy transfer for electron-hole pair, we can say that there are no losses for solar cell, called as ideal solar cell. If this is real, 100% efficiency would be managed. But, there are lots of losses that diminish the solar cell performance. According to studies, solar cell performance limit was reported around 33.7% supposing a single p-n junction with a band gap of 1.4-1.5 eV (William Shockley and Queisser 1961). However, if we don't avoid losses, it must be reduced. If losses are diminished, performance of the cell increases.

3.5.1. Optical Losses

In order to avoid limitation generation of electron-hole pair, optical losses must be minimized. Decreasing short circuit current, optical losses diminish solar cell performance. Optical losses can be summed up as follows;

- If incoming light reflects from top of the solar cell layer or interfaces layers, there will be no photon participation for photo-current.
- Photons with long wavelength can transmit passing absorber layer.
- Shading is also big problem for active area and this inhibit the light entering the solar cell.

3.5.2. Recombination

If the charge carriers which are generated in device are not collected at electrodes, it can be say that there is recombination such as electron–hole recombine which is reduce short circuit current. This result also effects open circuit voltage which is higher for lower recombination. Generally, we can obtain recombination in bulk, at interfaces and surfaces. As a recombination center, lattice defects and impurity atoms of the semiconductor can be assumed.

3.5.3. Thermalization

When the photon energy greater than the materials band gap energy, the excess energy is dissipated as heat. In other words, the waste energy that electron-hole pairs collect from photons is transmitted as a heat into semiconductor. This energy is called thermalization. To avoid thermalization, we should arrange the band gap as big as possible. But, low band gap is suitable to absorb lots of photons without losing them. Hence, theoretical efficiency is around 30% for band gap with 1.4-1.5 eV. Control thermalization is very crucial since it affect the solar cell performance. Identifying the loss mechanisms using the physics and engineering laws, advanced solar cell devices can be fabricated.

3.5.4. Electrical Losses

As it was mentioned before, maximum power of a solar cell can be determined using fill factor. Because of the series resistance and shunt resistance, FF is diminished. As it was shown before in Figure 3.8., I_L is called photo current, I_D is called diode current, I is called output current, I_S is shunt current, R_S is called series resistance and R_{SH} is called shunt resistance.

$$I = I_L - I_D - I_{SH} \tag{3.7}$$

V_D is called potential across the diode and V is called output voltage;

$$V_D = I_{SH} R_{SH} \tag{3.8}$$

$$V = V_D - IR_S \tag{3.9}$$

Output power for non-ideal solar cell is attained as;

$$I = I_L - I_0 \left[\exp\left(\frac{V+IR_S}{kT}\right) - 1\right] - \frac{V+IR_S}{R_{SH}} \tag{3.10}$$

The next chapter of this thesis, we will discuss CZTS structure. The whole layers that we used for solar cell devices will be explained. Secondary phases that can be occur will be introduced. Besides, fabrication methods that we can use will be tabled.

CHAPTER 4

A REVIEW OF DEVICE STRUCTURE

Although there are lots of different semiconductor materials, similar structures are used for thin film solar cell devices. Generally, five different thin film layers are coated on glass substrate for CZTS solar cells. Figure 4.1. shows an example of CZTS device structure. Sun light enters the cell from Transparent Conductive Oxide (TCO) layer which is Aluminium doped zinc oxide. Then, it passes inside the ZnO which is shunt prevent layer and CdS or Zn(O,S) buffer layer. Finally, it enters the CZTS absorber layer. Fundamental mechanism of solar cell which is p-n junction occurs between p-type CZTS layer and n-type CdS or Zn(O,S) buffer layer.

In this chapter, we will introduce materials that we used for the fabrication of solar cell.

Figure 4. 1. Schematic Diagram of CZTS Structure.

4.1. Substrate

A substrate has to be used for thin film solar cells deposition, because they are so thin. The most commonly used substrate is soda-lime glass in terms of its favorable properties. It has highest efficiency (Tajima et al., 2017). Also, we can use flexible substrates such as metal foils which can be used at high temperatures without any defects

of the substrate (Buldu et al., 2018). Moreover, we can eliminate additional back contact layer using metal foils as a substrate. Cost of cell can be minimized using that substrates.

4.2. Molybdenum (Mo) Back Contact Layer

Glass is used for substrate, but we need additional metallic conductive back contact layer. Low resistance, stability, good adhesion behavior and good work function value which must be close to semiconductor value are some of the requirements for a useful back contact. Moreover, high optical reflectance is important to minimize optical losses.

There are many metal and semi metals for back contact, but good electrical contact for CZTS is still hard for fabrication due to the Schottky barrier formation at between CZTS and back contact. Back contact satisfies following condition, if we have an ohmic contact. If not, Schottky barrier is occurred.

$$\Phi_m > E_g + x \tag{4.1}$$

For p-type semiconductor, E_g is band gap and x is electron affinity. Φ_m is work function of a metal.

Molybdenum is commonly used as a back contact for CZTS solar cells. When it is compared with other materials, Mo is good choice on account of suitable features. For instance, it has low electrical resistivity. Also, Mo is stable at high temperatures. Moreover, it has significant adhesion characteristic between CZTS layer and soda lime glass (SLG). In addition to these features, previous reports allege that Na diffusion is beneficial for solar cell performance (Li et al., 2013). At that point, allowance of Na diffusion from SLG to absorber layer is important. Mo back contact allows this process.

Low resistivity and good adhesion are necessary for back contact coating. It must be coated at low deposition pressure for low resistivity whereas the films must be coated under high pressure for good adhesion (Scofield et al., 1995). In order to achieve good quality Mo layer, two pressure deposition steps were developed. First, thin Mo layer is deposited under high pressure as adhesion layer. After that, the other Mo layer is coated under low pressure for low resistivity. To optimize Mo back contact for electrical and

adhesion properties, it is deposited as a bilayer. Mo deposited soda lime glass were obtained from TEKNOMA Technological Materials Industrial and Trading Inc. (www.teknoma.net).

4.3. CZTS Thin Films as an Absorber Layer

Cu_2ZnSnS_4 (CZTS) is a bright candidate as an absorber layer for thin film solar cells (Ito and Nakazawa 1988) due to not only its low cost but also nontoxic properties contrary to CdTe and $Cu(In,Ge)Se_2$ (CIGS). Besides, components of CZTS are earth abundant when compared to the CIGS (Katagiri et al., 2009). Recently, Cu_2ZnSnS_4 (CZTS) and similar chalcogenides have taken remarkable attention because of their low cost and being environmentally friendly. Even though the highest efficiency for thin film solar cells have reached over 20% for CIGS ($Cu(In,Ga)Se_2$) (Jackson et al., 2015), compounds of this chalcopyrite absorber layer contains rare elements such as indium (In) and gallium (Ga) as well as toxic element of selenium (Se). Due to these drawbacks, the long term production is restricted. In order to avoid these kind of problems, researchers have focused on less toxic, more abundant and cheaper elements for thin film solar cells. Among them, Cu_2ZnSnS_4 (CZTS) is a good candidate for absorber layer, since it has 1.4–1.6 eV bandgap energy and absorption coefficient higher than 10^{-4} cm^{-1} (Katagiri et al., 1997). Recent studies have shown that efficiency for kesterite-type Cu_2ZnSnS_4 is improved to 10.00% (Green et al., 2018) and for kesterite-type $Cu_2ZnSn(S,Se)_4$ is 12.6% (W. Wang et al., 2014), respectively. However, theoretical calculations based on Shockley-Queisser limit allege that approximately 33.7% maximum conversion efficiency can be accomplished for single p-n junction with a bandgap of 1.4 eV (William Shockley and Queisser 1961).

CZTS structure starts formation below 300ºC with ZnS, SnS and CuS phases. Between 350 ºC - 450 ºC temperature, Cu_2SnS_3 and ZnS phases are occur in addition to CZTS. Formation occurs from binary metal sulfides and ternary Cu-Sn sulfides (Hergert and Hock 2007). They report two step reaction as following;

$$Cu_{2-x}S + SnS_2 \longrightarrow Cu_2SnS_3$$

$$Cu_2SnS_3 + ZnS \longrightarrow Cu_2ZnSnS_4$$

In literature, there are CZTS formation results derive from various mixture of ternary and binary sulfide compounds as following below (Schorr et al., 2009);

$$2CuS + SnS + ZnS \longrightarrow Cu_2ZnSnS_4$$
$$Cu_2S + SnS_2 + ZnS \longrightarrow Cu_2ZnSnS_4$$
$$Cu_2SnS_3 + ZnS \longrightarrow Cu_2ZnSnS_4$$

4.3.1. Structure of CZTS

CZTS phase occurs as two fundamental structures which are kesterite and stannite type (Hall, Szymanski, and Stewart 1978). These formations are similar. For instance, they have tetragonal structures. Also, they consist of cubic closed packed array of sulfur anions, with cations by occupy one half of the tetrahedral voids. Similar zinc blend stack occurs. The difference between two type of CZTS structure is different locations of Cu and Zn atoms along the c-axis as seen Figure 4.2.

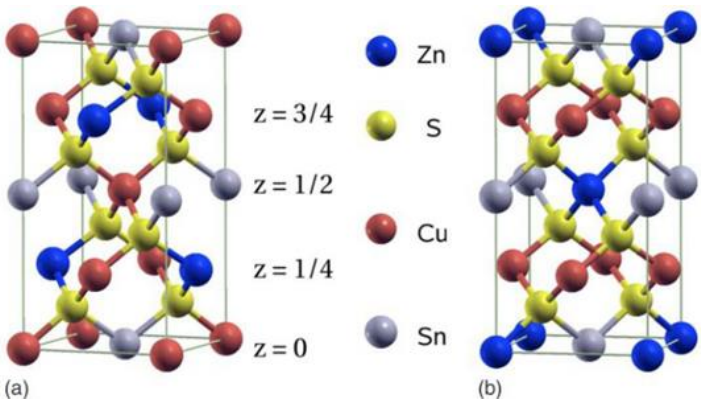

Figure 4. 2. Crystal Structure of (a) Kesterite (b) Stannite CZTS
(Source: Paier et al., 2009).

Studies said that CZTS phase appears in kesterite phase because of thermodynamically more stable when it is compared with stannite structure (Maeda, Nakamura, and Wada 2011). Generally, CZTS samples have been obtained as a kesterite structure.

In kesterite structure; along the c-axis, the cationic layers are aligned in Cu-Sn, Cu-Zn, Cu-Sn and Cu-Zn trend. One of the Cu atoms locate in position 2a with potential

of -15.04 V whereas Zn atom and the other Cu atom locate in position 2d and 2c with potentials of -21.88 and -15.21 V, respectively.

In stannite structure, Zn-Sn cationic layer between Cu-Cu layers is repeated. Cu atoms locate at 4d position and Zn atom locates at 2a position with potentials of -15.30 and 21.62 V, respectively. Sn atom locates at position 2b in kesterite and stannite structure (Persson 2010).

Lattice constants for kesterite CZTS structure are a=0.546 nm and c=1.093 nm (Paier et al., 2009). However, different measurement can be obtained in other studies (Schorr 2011).

4.3.2. Secondary Phases on CZTS

It is quite difficult to form pure CZTS structure. Management of phase stability is important for high quality CZTS absorber layer. Ternary and quaternary compounds can be occurred during process because of having low thermal stability and narrow single phase region of the compounds.

Cu_2S: Generally, Cu-rich, Zn-poor and Sn-poor situations causes copper sulfide phases. That elements are semiconductor with low band gap (1.2 eV). They have high absorption coefficient due to the metallic feature. Thus they cause shunt the solar cell. In addition; this phase increase recombination for holes and electrons. In order to avoid this phase, KCN (potassium cyanide) is used for chemical etching of samples.

Cu_2SnS_3: In Zn-poor conditions, Cu2SnS3 phases form. They have similar metallic features like copper secondary phases. Thus, they can improve the recombination and shunt the cell (Wu et al., 2007).

ZnS: In Sn and Cu poor, Zn-rich situations, zinc sulfide phases form. Since they have high band gap (~3.60 eV), they are insulator and due to this feature, they can obstruct the current flow in absorber layer. Using Raman spectroscopy, we can detect them if they locate on surface. In order to remove these phases, HCl mixture with a concentration of 5-10% at 75^{o}C temperature can be used (Marchionna et al., 2013).

SnS_2: In Sn-rich and Cu-poor conditions, tin sulfide phases occur. This secondary phase is an n-type semiconductor and it has 2.2 eV band gap energy. In addition; this phase causes high photo-carrier recombination acting insulator (Kumar et al., 2015).

SnS-Sn_2S_3: SnS has 1.2-1.5 eV direct band gap and 1.0-1.2 eV indirect band gap. Because of low band gap, low open circuit voltage can occur. $(NH_4)_2S$ can use in order to remove SnS formations. Sn_2S_3 phase a mixed formation with direct band gap of 0.97 eV and indirect band gap of 0.82 Ev, because of Sn and S deformity (Singh 2016).

All in all; many different secondary phases can occur. Each of them can cause any effect in solar cell. Determining and removing is important for these phases in order to reach high performance in solar cell applications.

4.3.3. Fabrication Methods of CZTS

Numerous methods have been used to the coat CZTS absorber layer. According to desirable properties, any fabrication method can be used. These methods can be categorized as vacuum and non-vacuum. Vacuum methods consist of atomic beam sputtering (Ito and Nakazawa 1988), e-beam evaporation (Araki et al., 2008), thermal evaporation (Shi et al., 2012), magnetron sputtering (Jimbo et al., 2007), pulsed laser deposition (Moholkar et al., 2011), chemical vapor deposition (Washio et al., 2012). Non-vacuum methods are electrodeposition (Ennaoui et al., 2009), spray pyrolysis (Yoo and Kim 2011), spin coating (W. Wang et al., 2014).

Table 4. 1. Fabrication techniques of CZTS thin films.

Vacuum Technique	**Non-vacuum Technique**
Sputtering	Electrodeposition
Evaporation	Spray pyrolysis
Pulsed laser deposition	Spin coating
Chemical Vapor Deposition	

It is reported that the vacuum based techniques have better efficiencies for the CZTS solar cells (Katagiri et al., 2008). In all of these experiments, having Cu-poor and

Zn-rich compositions of CZTS samples show better device performances compared with stoichiometric ones (Katagiri et al., 2009). Cu-poor composition improves Cu vacancies, which causes surface acceptors in CZTS, while Zn-rich situation suppresses the substitution of Cu in Zn sites, which appears deep acceptors (S. Chen et al., 2010). Energy dispersive spectroscopy (EDS) is used to reach chemical composition for a selected area. The working principle of the EDS can be explained as the bombardment of the sample with focused beam of electrons and excitation of an electron in an inner shell, ejecting it from the shell while creating an electron hole.

4.4. Buffer Layer

In order to complete p-n junction formation, buffer layer is coated on p-type CZTS absorber layer. Besides, buffer layer protects absorber layer from any processes such as damage during other layer sputtering stage. Also, it helps to minimize interface recombination. Buffer layer must absorb almost whole incident light to create photo-generated carriers with minimum recombination losses. Thickness of the buffer layer should be thin in order to avoid series resistance and band gap of the layer should be large. Carrier density of buffer layer should be larger than absorber layer for extend space charge region into absorber. In that region electric field helps to distinguish charge carriers (Klenk 2001).

4.4.1. Zinc Oxysulfide (Zn(O,S)) as a Buffer Layer

Using II-VI compound semiconductors, zinc oxysulfide (Zn(O,S)) thin films are fabricated as a buffer layer. Thanks to compositional and crystal structure tunability, Zn(O,S) buffer layer has getting attention in solar cell industry. When it is compared to other materials, it is earth abundant and non-toxic. Instead of common CdS as buffer layer, Zn(O,S) is a magnificent candidate since it is adaptable with absorber layers (Platzer-Björkman et al., 2006).

Zn(O,S) is called as $ZnO_{1-x}S_x$. S/(S+O) ratio can be altered using O_2/Ar. When this ratio is changed, fundamental parameters can be altered such as bandgap, conductivity (Sinsermsuksakul et al., 2013). Besides, recombination at the buffer layer

can be minimized managing sulphur composition (Platzer-Björkman et al., 2006). In addition; we can tune of the conduction band offset (CBO) value changing S and O contents. This alteration plays a significant role for solar cell performance diminishing interface recombination without loss in current.

Many deposition technic are used for Zn(O,S) layer such as chemical vapour deposition (CBD) (Kushiya 2004), ion layer gas reaction (Muffler et al., 2000), atomic layer deposition (Zimmermann, Ruth, and Edoff 2006), sputtering (Klenk et al., 2014), evaporation (Romeo et al., 2004) and pulse laser deposition (PLD) (Deulkar, Huang, and Neumann-Spallart 2010). 50-100 nm thickness is coated for all technics.

4.4.2. Cadmium Sulphide (CdS) as a Buffer Layer

Cadmium sulphide (CdS) is an n-type semiconductor and it has direct bandgap value 2.42 eV (Lisco, Kaminski, Abbas, Bass, et al., 2015). Besides, CdS has high absorption coefficient. It is an ohmic contact to different material and a good transparent. Since it has good absorption features, CdS is used as a buffer layer in many solar cells devices such as Cu_2ZnSnS_4 (CZTS) (Tajima et al., 2017), $Cu(In,Ga)Se_2$ (CIGS) (Salomé et al., 2017).

CdS can be deposited using various technics such as chemical bath deposition (CBD) (Cantas 2017), deep coating (Oladeji et al., 2000), sputtering (Lisco, Kaminski, Abbas, Bowers, et al., 2015), spray pyrolysis (Ashour 2003) and thermal evaporation (Iacomi et al., 2007).

CdS can be formed from vapour phase of from liquid phase at high pressure because of its sublimation and melting point which are about 700^{o}C and 1750^{o}C, respectively. About electrical, structural and optical features of CdS films are considered, substrate (Ma, Ai, and Wu 2017), temperature (Liu et al., 2010), deposition time (Krishnakumar et al., 2011) and pH value (Zhang, Zhang, and Zhuang 2009) play an significant role. Generally, chemical bath deposition (CBD) technic is used for CdS thin film deposition because of low temperature process which is 27-80^{o}C and cheap (H. Chen et al., 2010). Deposition rate, thickness, pH, concentration and temperature can be controlled using chemical bath deposition technique.

There are also some necessities for buffer layer. Buffer layer should have high band gap in order to allow absorption to absorber layer. Moreover, thickness of the CdS

thin film should be lower than 100 nm to augment the transmission and performance. In the literature, efficiency for CZTS with CdS buffer layer still the highest (Tajima et al., 2017).

4.5. ZnO and Al:ZnO : Window Layer

ZnO and aluminium doped ZnO (AZO) films are used for window layer in CZTS solar cells. ZnO layer thickness is about 50 nm. AZO layer is used as a front contact and its thickness is about 300-500 nm. Beside this, AZO layer is used as a transparent conductive oxide (TCO) layer.

ZnO is getting attention for a long time because of its applications in many scientific areas. Especially, it is an important candidate for solar applications due to the its optoelectronic features in the UV range. ZnO which is from II-VI group is an n type semiconductor. It has 3.4 eV direct band gap (Srikant and Clarke 1998). This causes in high transparency in the visible spectrum. Lattice constants are a=0.325 nm and c=0.521 nm (Klingshirn 2007). In order to form ZnO layer, many deposition technics can be used for instance chemical vapour deposition, RF magnetron sputtering or spray pyrolysis. Generally, RF magnetron sputtering is preferred since this technic diminishes losses and gives good adhesion ability to material. Altering RF power or working pressure, we can control features of ZnO thin film. Moreover, ZnO layer hinders shunting because generated resistance by ZnO layer diminishes effect of recombination current (Rau and Schmidt 2001). It also restricts buffer layer interface from damage of ions during deposition.

As a transparent conductive oxide (TCO) layer allows all wavelength that under cut-off wavelength until absorber layer. In_2O_3:Sn (ITO) (Koseoglu et al., 2015), doped ZnO with gallium (GZO) (Lee et al., 2008) or aluminium (AZO) (Turkoglu et al., 2018) are the most used transparent conductive oxide concepts in solar cell applications (Gordon 2000). Since ITO is expensive and toxic, it is not preferred. Since AZO have better electrical and optical performance, it is preferred commonly. AZO is an n-type semiconductor and its band gap is 3.6 eV. Because of the carrier concentration, AZO has high electrical conductivity and high optical transparency. Besides, thickness of AZO layer is important for determining transmission and conductivity. When thickness of layer is thicker, it has better conductivity but it has worse transmission because thicker layers

provide enhancement in the surface morphology. Therefore, recombination of charge carriers cannot be formed, so we can say that there are more atoms in order to absorb radiation. Pulsed laser deposition (PLD) (Agura et al., 2003), sputtering (Jeong and Boo 2004) or chemical vapour deposition (Terasako et al., 2007) can be used to deposit AZO layer. To obtain high quality AZO layer, temperature must be higher than 300ºC. High temperatures supply enhancement of crystallinity of the films. But, these temperatures create many defects because of improved interfacial diffusion and occur high charge carrier recombination rate. Therefore, room temperature is necessary for deposition process in order to avoid inter-diffusion between layers of the device (Ferekides et al., 2000). But room temperature process for low resistivity and high transmittance is still under research.

4.6. SiN : Anti-reflective Coating

In order to improve solar cell performance, antireflection coating (ARC) is used. It is used to diminish loss mechanism for light. There are many antireflection coating (AR) materials such as TiO_2, ZnS and ZnO (C.-C. Lee and Tang 2006). Generally, silicon nitride (Si_3N_4) films are used for this purpose for solar cell devices due to its suitable optical features. Also, it has annealing induced capability for hydrogen passivation of grain boundaries and defects for silicon solar cells (Sheoran et al., 2008). Besides, it is stable for high temperature contact firing. Although, plasma enhanced chemical vapour deposition (PECVD) technic is popular for deposition this films (Kang et al., 2011), magnetron sputtering is also used (Barshilia, Deepthi, and Rajam 2007).

Table 4. 2. Optical properties of candidate materials
(Source: Sood et al., 2006)

Candidate Materials	**Transmission Range (μm)**	**Refractive Index**
CdTe	2-25	2.67
Si_3N_4	2.0-18	2.0
Diamond	0.4-300	2.37

Table 4.2 shows some materials properties for anti-reflective coating. Next chapter, we will explain experimental procedure that we used in this thesis. Systems that we used for deposition will be introduced. Each of system details will be described and picturized clearly. All parameters which will be used for formation of films will be tabled.

CHAPTER 5

EXPERIMENTAL PROCEDURES

In this thesis, study was divided two different parts. In the first part, we examined Mo and Ti foil substrate to investigate which substrate is more suitable for our work. In this part, any solar cell devices were not produced. In second part, we continued with Mo substrate. Two different effect was investigated on solar cell conversion efficiency including buffer layer thickness and sulfurization time.

5.1. Overview of Device Structure

Figure 5.1. shows fabricated CZTS solar cell device with (a) Zn(O,S) (b) CdS buffer layer. While magnetron sputtering technique was used for Zn(O,S) layer, chemical bath deposition (CBD) technique was utilized for CdS buffer layer.

Two stage process was performed to produce CZTS absorber layer. First, metallic precursor was deposited on Molybdenum (Mo) coated soda lime glass (SLG) using DC magnetron sputtering which provides advantages including easy adaptation to large scale and reproducible fabrication. (Tuna et al., 2010). Secondly, in order to complete CZTS structure, metallic precursors were sulfurized in sulphur atmosphere which is called sulfurization process.

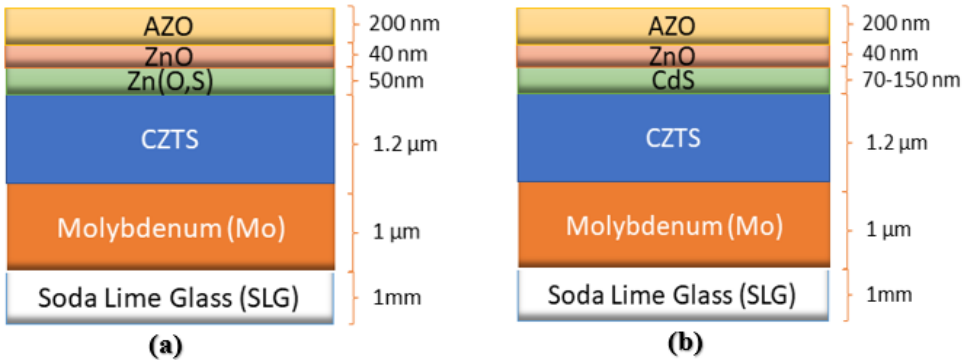

Figure 5. 1. Schematic illustration of CZTS solar cell device with (a) Zn(O,S) (b) CdS buffer layer.

5.1.1. Substrate Preparation

Mo coated SLG were used as substrate. Before deposition of Mo, SLGs were cleaned acetone, methanol and deionized water, subsequently. Then all samples exposed to Ar plasma for 15 minutes.

Ti substrates were used only for absorber layer characterization. Before the deposition of CZT layer, Ti foil substrates chemically etched in a mixed acid solution to remove oxide layer. Then, the HF acid solution in deionized water is performed to remove unwanted oxide layers. Ti foil substrates were etched for 1.5 minute in 90.0 ml deionized water. Then 10.0 ml diluted HF acid solution was utilized at room temperature. Obtained Ti foil thickness was about 150 μm after etching process.

5.1.2. Growth of Molybdenum Back Contact

As we mentioned in section 4.2., Mo deposited soda lime glass were obtained from TEKNOMA Technological Materials Industrial and Trading Inc. (www.teknoma.net). In order to coat Mo layer on SLG, DC magnetron sputtering was utilized. According to quality of Mo layer, parameters were optimized. The most important parameter is working pressure for determining adhesion of the films and resistivity. In order to achieve low resistivity, high density and smooth surface, low working pressure should be used. However, because of compressive stress, adhesion problems can occur. Besides, high deposition power and low deposition voltage diminish resistance. This causes better adhesion of the Mo film to SLG (Scofield et al., 1995). Bi-layer coating is used for good adhesion and electrical features. First, Mo is coated under high pressure (~12.5 mTorr) and after that second layer is deposited under low pressure (~2.5 mTorr).

To deposit Zn(O,S), ZnO and AZO layers, the magnetron sputtering system was used (Figure 5.2.). The magnetron sputtering system has 3 targets containing cooling system, gas and power access. In order to achieve high vacuum (~2.5×10^{-6} Torr), turbo molecular pump (TMP) and rough pump are used. While gate valve is used to control pressure, a cold cathode gauge shows the system pressure. After reaching a certain pressure value which is called base pressure, Ar gas (99.99%) is sent to form plasma using

mass flow controller. During the deposition process, system pressure is measured using baratron.

Figure 5. 2. Picture of magnetron sputtering system for deposition of Zn(O,S), ZnO and AZO layers.

Mo layer was deposited using DC sputtering. The measured total thickness of Mo films was about 1μm. Sample holder was rotated during deposition process in order to access uniform surface. Mo back contact layer is deposited on SLG substrates from 2-inch-targets with 99.95% purity. SLGs was located in chamber. System was evacuated to base pressure which is about 2.5×10^{-6} Torr. Ar gas flows (30 sccm) was introduced in the chamber. In order to remove contamination, pre-sputtering was started. After 10 minutes, shutter was opened. Mo coating was started under high pressure (~12.5 mTorr). To form bi-layer structure, rest of the deposition was done under low pressure (~2.5 mTorr). Valve position was altered to change the pressure. Target and substrate distance was 9 cm. Table 5.1 shows growth parameters for Mo coating.

As mentioned before, to deposit Zn(O,S), ZnO and AZO layers, the magnetron sputtering system was used (Figure 5.2.).

Table 5. 1. Growth Parameters for Mo layers.

	1st Layer of Mo	2nd Layer of Mo
DC Power	75 W	75 W
Gas Flow	30 sccm Ar	30 sccm Ar
Working Pressure	12.5 mTorr	2.5 mTorr
Valve Position	35 % Open	100 % Open
Deposition Time	140 min	70 min

5.1.3. Growth of CZTS Absorber Layer

Two step process was used to fabricate CZTS absorber layer. Firstly; Cu, Zn and Sn which are called CZT are coated using magnetron sputtering technique. Second step is sulfurization process. Metallic precursors are converted to CZTS absorber film form under sulphur atmosphere. Deposition of CZT metallic precursor and sulfurization process will be given in next section.

5.1.3.1. Metallic Precursor Growth

First step of the fabrication is growth of metallic precursor which consist of Cu-Sn-Zn using magnetron sputtering system. Mo coated SLG and Ti foil of Sigma-Aldrich were used as a substrate. To clean Mo coated SLG, acetone, ethanol and distilled water was used, respectively. Argon plasma was utilized to avoid contamination of surface. The metallic layers were growth using DC magnetron sputtering from 2-inch target of Cu (99.999%), Sn (99.999%) and Zn (99.999%) at room temperature (Figure 5.3). Target and substrate distance was fixed at 8 cm. According to target, holder could be rotated. Before the deposition, chamber was evacuated at 10^{-6} Torr using TMP. There was no heating for substrates. When we reached desired pressure, Ar gas (30 sccm) was sent

during the deposition. Our working pressure was $1.5x10^{-2}$ Torr. This pressure must be constant during the deposition.

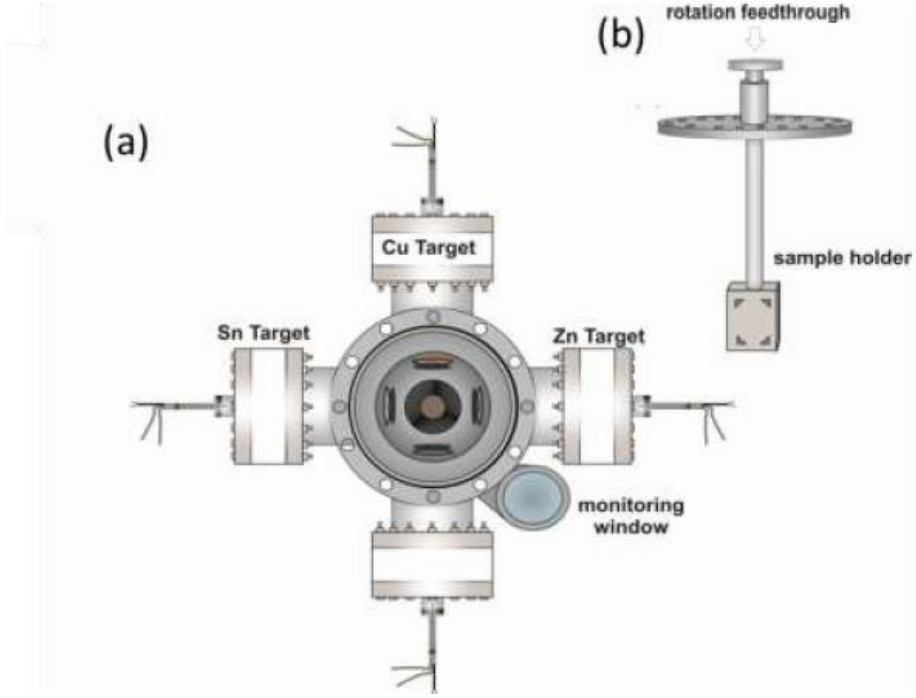

Figure 5. 3. (a) Schematic top view of multi target DC magnetron sputtering (b)Schematic view of rotating sample holder (Source: Yazici et al., 2015).

In this thesis, CZT thickness was about 575 nm. Thickness calibration of each layer was calculated before the growth. This thickness based on Cu-poor, Zn-rich situation. Each metallic layer was growth at various power. For Cu target, 41 W was used. For Sn target, 40 W was used. Finally, 20 W was used for Zn target. Deposition times were fixed as 4 min for Cu at the bottom layer, 6 min 9 s for Sn layer, 3 min 55 s for Zn layer and 1 min 50 s for Cu at the top layer. As seen Figure 5.4, Cu/Sn/Zn/Cu order was used. This stacking order supply many advantages. For instance; Cu can diffuse from bottom to top layer easily or Zn layer prevent the vacancies which causes from Cu diffusion. Besides, Sn evaporate easily because of low melting point (231.93^{o}C), this stacking order block the ZnS phase at surface.

SEM images and EDX results of CZT metallic precursor on Mo substrate was shown in Figure 5.5. Although there are little differences on surface, samples show uniform surface coverage. Particle size almost the same. Cu, Sn, Zn elements has 39.97%,

27.38% and 32.65% atomic ratios, respectively. These ratios indicate Cu-poor, Zn-rich composition.

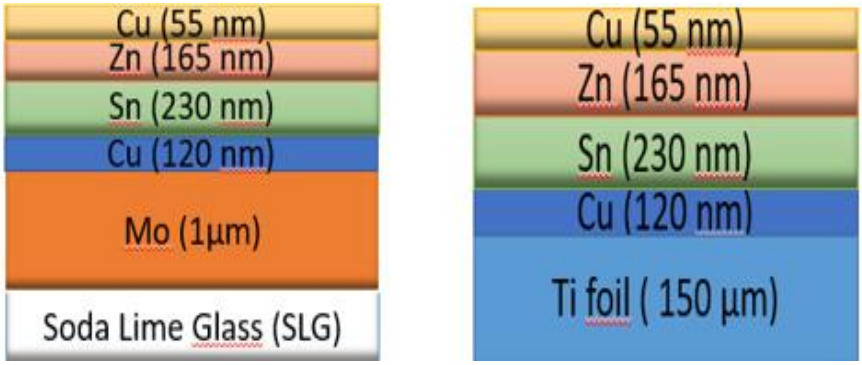

Figure 5. 4. Illustration of metallic precursors on Mo coated SLG and Ti foil.

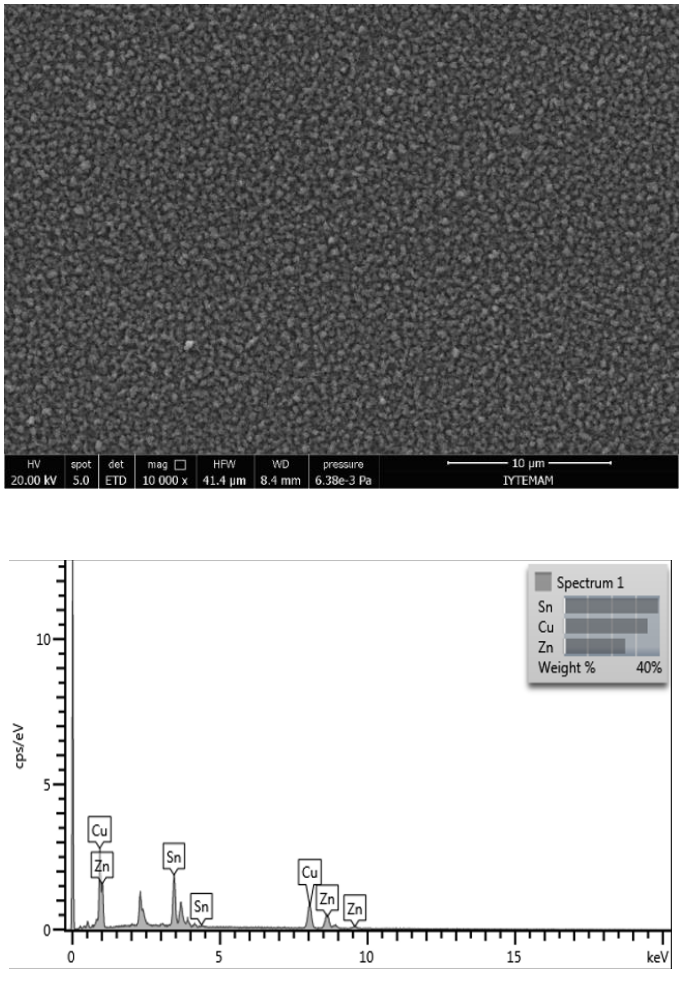

Figure 5. 5. SEM and EDS result of CZT metallic precursor on Mo coated SLG.

5.1.3.2. Sulfurization Process

Second step is sulfurization process. Metallic precursors on Mo and Ti substrates were annealed at 550^{o}C which is optimized temperature in sulphur (S) and Argon (Ar) atmosphere. For CZT films with Mo back contact, 600 mg S powder was utilized for solar devices. However, in order to compare Ti and Mo back contact effect, we used 50 mg S powder each of them. In this section, firstly we will give comparison parameters for Ti and Mo substrates. Then we will give our fundamental sulfurization parameters for solar cell devices.

Lindberg/Blue M tube furnace and a quartz glass tube was used for this procedure. It has 2.6 cm in diameter and its length is 60 cm (Figure 5.6). In addition, MKS 647C was used for flow of gas. First part of this section, the substrate with metallic precursors was placed in the middle of the graphite box. 50 mg S powder was equally added to each side of the graphite box, and then it was closed using a wire. The quartz tube was cleaned with 100 sccm argon gas flow for 10 min as preparation to sulfurization. At the beginning of the sulfurization process, graphite box was placed out of the furnace in quartz tube. When the furnace reached to 550°C which was kept for 15 min, the box pushed into the entrance of the furnace (point 1 of Figure 5.7.). All samples were pre-annealed at 150°C during 10 min at that point. After this part, the box was pushed into the middle of the furnace (point 2 of Figure 5.7.) where sulfurization process was kept for 15 min under 10 sccm Ar gas ambient. All sulfurization process was realized under atmospheric pressure in a quartz tube. Finally, furnace was turned off and was cooled down naturally accompanied with Ar gas flow.

Figure 5. 6. The sulfurization system and graphite box
(Source: Buldu 2017).

Second part of this section, CZT metallic precursor with Mo back contact annealed at 550ºC in S and Ar atmosphere. 600 mg S powder was used. Two-stage temperature range was applied. First, furnace reached to 270ºC within 5 minutes and during 3 minutes remain constant this temperature. Then, within the 5 minutes, furnace reached up to 550ºC. During 45 minutes and 30 minutes, CZT metallic precursors was sulfurized.

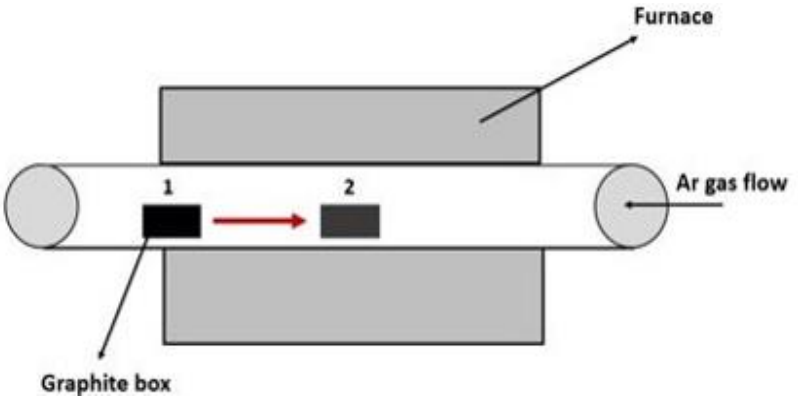

Figure 5. 7. Schematic illustration of sulfurization system.

Table 5. 2. Sulfurization Parameters of fabricated films.

	Ar (sccm)	**S (mg)**	**Pre-anneal (@150ºC)**	**Sulfurization(@550ºC) (minute)**
Ti-CZTS	30	50	✓	20
Mo-CZTS	30	50	✓	20
Mo-CZTS-A	30	600	X	30
Mo-CZTS-B	30	600	X	30
Mo-CZTS-C	30	600	X	30
Mo-CZTS-D	30	600	X	30
Mo-CZTS-E	30	600	X	45

5.1.4. Deposition of Zn(O,S) Buffer Layer

Zn(O,S) buffer layer was used for Mo-CZTS-D and Mo-CZTS-E. Zn(O,S) ($ZnO_{1-x}S_x$) buffer layers were deposited on CZTS layers using RF magnetron sputtering (Figure 5.2.) with ZnS target which has 2-inch diameter. First, Zn(O,S) films were growth on SLG to optimize thickness. After determining the deposition time for desired thickness, Zn(O,S) deposition can be started. Before the deposition, 10 minutes pre-sputtering process was applied to avoid contamination at the surface. Chamber was evacuated $2.5x10^{-6}$ Torr. Target and substrate distance was 8 cm. RF power which was 40 W was applied. In order to improve crystalline quality and adhesion, substrate was heated up to 200^{o}C. 50 sccm Ar and 0.5 sccm O_2 gas were used. Valve position was arranged 40% for pre-sputtering while 50% was arranged for sputtering.

Table 5. 3. Zn(O,S) Growth Parameters.

	RF Power (W)	**Substrate Temperature (^{o}C)**	**Valve Position (%)**	**Working Pressure (mTorr)**	**Ar (sccm)**	**O_2 (sccm)**	**Thickness (nm)**
Zn(O,S)	40	200	50	~ 5.75	50	0.5	50

5.1.5. Growth of CdS Buffer Layer

CdS buffer layer was used for Mo-CZTS-A, Mo-CZTS-B and Mo-CZTS-C. Chemical bath deposition technique was utilized for these CZTS films. Solution consist of 1.2 ml of 0.5 M cadmium acetate ($Cd(CH_3CO_2)_2$), 6 ml of 2 M ammonium acetate ($NH_4CH_3CO_2$), 7 ml of 0.5 M thiourea $SC(NH_2)_2$, 12 ml of 14.4 M (25 % of NH_3 solution) ammonium hydroxide (NH_4OH) and 270 ml de-ionized water, respectively. Chemical bath deposition system was show in Figure 5.8. When big glass temperature reached to 85^{o}C, 270 ml de-ionized water was added and waited for thermal balance. Then, substrates were placed into the water. After second equilibrium for temperature which is 85^{o}C again, cadmium acetate, ammonium acetate and ammonium hydroxide were put in glass, subsequently. CdS buffer layer was deposited on CZTS absorber layer using CBD

method at 85^{o}C with variety of times (90, 75 and 60 minutes for Mo-CZTS-A, Mo-CZTS-B, Mo-CZTS-C, respectively) in order to form p-n junction.

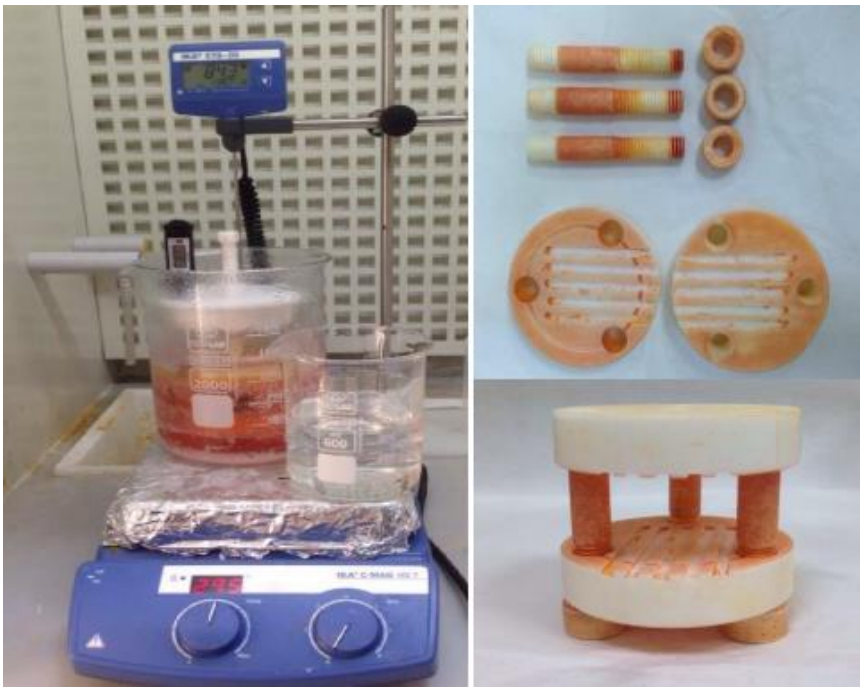

Figure 5. 8. Chemical Bath Deposition System
(Source: Cantas 2017).

5.1.6. Deposition of ZnO Window Layer

As mentioned before, ZnO is getting attention for a long time because of its applications in many scientific areas. Especially, it is an important candidate for solar applications due to the its optoelectronic features in the UV range. ZnO layer was deposited on CdS coated Mo-CZTS-A, Mo-CZTS-B, Mo-CZTS-C and Zn(O,S) coated Mo-CZTS-D and Mo-CZTS-E with 40 nm thickness using RF magnetron sputtering as seen Figure 5.2. ZnO (99.99%) target which has 2-inch diameter was used to fabricate ZnO layer. Chamber was evacuated $2.5x10^{-6}$ Torr. 80 sccm Ar was sent. Before the deposition, to avoid contamination of target surface, pre-sputtering was applied for 10 minutes. Then shutter was opened. Valve position was arranged to 50% and working pressure was 8.54 mTorr. RF power which was set 50 W was applied and target and substrate distance was 9 cm.

Table 5. 4. Growth Parameter of ZnO Layer.

	Substrate Temperature (ºC)	RF Power (W)	Valve Position (%)	Pressure (mTorr)	Ar (sccm)	Thickness (nm)
ZnO	25ºC (Room)	50	50	~8.54	80	40

5.1.7. Deposition of ZnO:Al Layer

AZO was deposited on CdS coated Mo-CZTS-A, Mo-CZTS-B, Mo-CZTS-C and Zn(O,S) coated Mo-CZTS-D and Mo-CZTS-E with a thickness of 250-300 nm using DC magnetron sputtering (Figure 5.2.). ZnO:Al_2O_3 (98 wt.% ZnO , 2 wt.% Al_2O_3) target which has 2-inch diameter was used. Chamber was evacuated $2.5x10^{-6}$ Torr. 50 sccm Ar gas flow was sent. Before the deposition, to avoid contamination of target surface, pre-sputtering was applied for 10 minutes. Valve position was arranged to 100% and working pressure was around 3.85 mTorr. Besides; in order to achieve improved crystallinity and low resistivity, sample holder was rotated using fixed speed during the growth (Figure 5.9.). This improves uniform coverage of the films. Target and substrate holder distance was fixed at 9.0 cm.

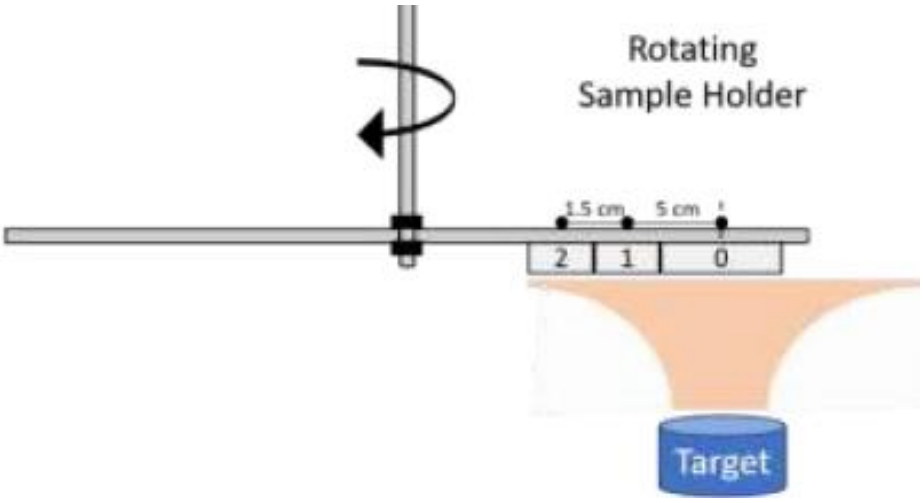

Figure 5. 9. Rotating Sample Holder of System.
(Source: Turkoglu et al., 2018)

Table 5. 5. Growth Parameters of AZO Layer.

	Substrate Temperature (ºC)	DC Power (W)	Valve Position (%)	Pressure (mTorr)	Ar (sccm)	Thickness (nm)
AZO	25ºC (Room)	50	100	~3.85	50	~250

5.1.8. Defining Area to Measure Solar Cell Performance

In order to measure solar cell performance; after the growth of AZO layer, removing the layers on top of the Mo outside the cell area, active area was defined. Area of 0.005-0.5 cm^2 were etched using help of a razor blade. Using silver epoxy, the cells were contacted via the window layer. To deliver photo-generated electrons to external load, these contacts extract these electrons. No anti-reflection coatings which improve cell performance were deposited to cells in this study. Figure 5.10 show the schematic of device structure and CZTS solar cell after defining the area. I-V measurement is important to define a cell characteristic.

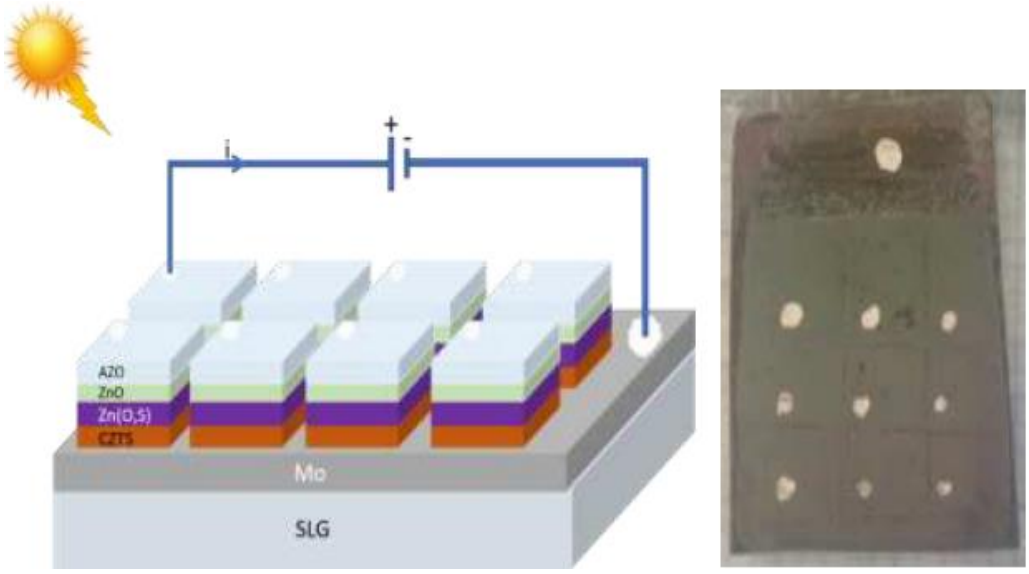

Figure 5. 10. Schematic Illustration of device structure and solar cell device and CZTS solar cell (Source: Turkoglu 2017).

5.2. Characterization Techniques

In the following sections, characterization techniques that we used for devices and materials summarized.

5.2.1. Profilometry

Profilometer uses a stylus in order to investigate surface. Stylus measures small surface variations in vertical line. All thin films CZTS solar cell thicknesses that we used in this thesis were determined using a Veeco DEKTAK 150 profilometer.

5.2.2. X-Ray Diffraction (XRD)

Crystal structure gives important information about material. To understand crystal structure, X-ray diffraction is utilized. The working principle based on the diffraction of an incident X-ray waves by a crystal lattice. Average space between layers or atoms, location of a single crystal or grain, crystal structure of a material, size, shape and internal stress of small crystalline regions can be investigated using X-ray diffraction technique. Angles and intensities are used for determining information about a structure.

For all samples used in cell fabrication, XRD was used to determine crystal structure of the films. XRD was performed in the Bragg-Brentano focusing geometry on a Phillips X'Pert Pro X-Ray diffractometry with Cu Kα radiation (λ=1.5406 Å). Data from XRD were collected from 2θ=20-80°. Step size is 0.016° and time step of 31 second for all films.

5.2.3. Scanning Electron Microscopy (SEM)

The scanning electron microscopy is a powerful technique for investigate surface morphology of the films. Electrons which are interact with films to image. The secondary electrons, back scattered electrons and X-Rays are occurred because of this interaction as seen Figure 5.11. All signals are detected using detectors and converted them as image

on screen. Depends on voltage and the density of the sample, depth of electron beam can be arranged. Besides, Energy Dispersive Spectroscopy (EDS) is used to reach chemical composition for a selected area.

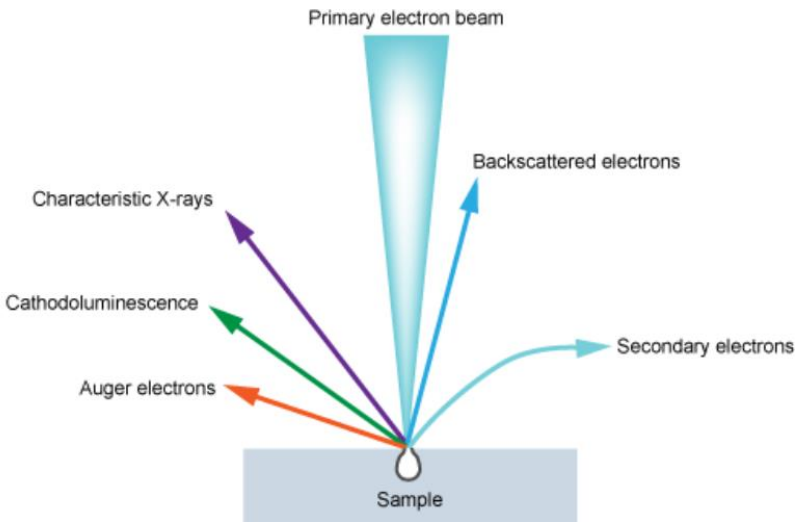

Figure 5. 11. Illustration of SEM working principle.

In this thesis, CZTS absorber layer surfaces were researched using scanning electron microscope (SEM; FEI-QuantaFEG 250). In addition this, Energy Dispersive Spectroscopy (EDS; Oxford X-act) was used. Under high vacuum, 15 kV acceleration voltage at different magnifications was used with ETD detector and 3 spot size.

5.2.4. Raman Spectroscopy

Raman spectroscopy is an important technic in order to investigate vibrational modes of materials. The working principle of this technique is about inelastic scattering (Raman scattering) of monochromatic light. Laser source is used in the visible region (390-700 nm), near infrared (700nm-1400nm) and near ultraviolet (300-400 nm). After light and sample interaction, frequency of absorbed light changes. Because of interactions between monochromatic light and vibrational energy level of sample's molecules, the shift in energy of the scattered light is detected by this technique. The intensity of shifted light versus frequency plot is obtained.

In this thesis, Micro Raman-spectroscopy (S&I Mono Vista Raman System, 0.750 mm Imaging Triple Grating Monochrometer) was used with the excitation wavelength of 514.5 nm Ion-Ar^{+} and 633 nm HeNe laser with 25mW power for CZTS samples. All measurements were taken with 600 grating and 100x objective. Using Si main mode at 521 cm^{-1}, calibration was done.

5.2.5. Spectrophotometric Analysis (Transmission and Reflection)

Reflection and transmission analysis of a material is evaluated using spectrophotometry. In this work, optical properties of fabricated solar cell devices were obtained thanks to a PerkinElmer Lambda 950 UV/VIS/NIR spectrophotometer the wavelength range between 200 and 2600 nm.

5.2.6. Light Beam Induced Current (LBIC) Measurement (2-D and 3-D Mapping)

The light beam induced current (LBIC) measurement technic is used for characterization of a solar cell using a light beam. This measurement allows characterization of spatial distribution of electrical parameters and defects. Beam probe scans the solar cell by obtaining current-voltage characteristics. A map of many solar cell parameters can be observed using this technic. Photo-generated current is occurred and we can achieve current as a function of its position. Changes in photo-generated current gives us defects. Figure 5.12. shows a simple LBIC system.

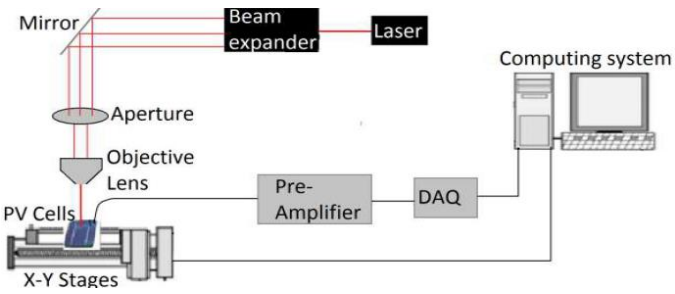

Figure 5. 12. Illustration of LBIC system
(Source: Bezuidenhout et al., 2012).

In this work, 50 μm step size and 80x80 matrice scanning was used. All measurements were taken at room temperature.

5.2.7. Electrical Characterization (Device Characterization)

V_{OC}, I_{SC}, FF and cell efficiency are important parameters to determine cell's performance. Figure 5.13. shows I-V measurement setup. A function generator was used for sweeping the voltage. Wave amplitude and frequency was fixed at 2Vp-p and 0.005 Hz, respectively. Function generator has two probes. One of them was located on a resistor with resistance of 10 Ω. Other one was located on CZTS cell. Two Keithley were used with a computer. Labview program was used for data analysis. To obtain voltage, probes of nanovoltmeter were put front and back contact of CZTS cells. To obtain current, the other probe was put on the ends of resistor. Halogen lamp was used to generate light with an intensity of $1kW/m^2$. Intensity of light was $1kW/m^2$. All measurements were taken at room temperature.

Thanks to I-V measurements under light illumination, we can obtain the values of I_{SC}, V_{OC}, I_M, V_M, FF and cell conversion efficiency. Also, loss parameters of solar cell, R_S and R_{SH}, are determined from and I-V measurement under dark. Figure 5.14. shows dark and light I-V curve on a measurement.

Figure 5. 13. I-V Measurement Setup.

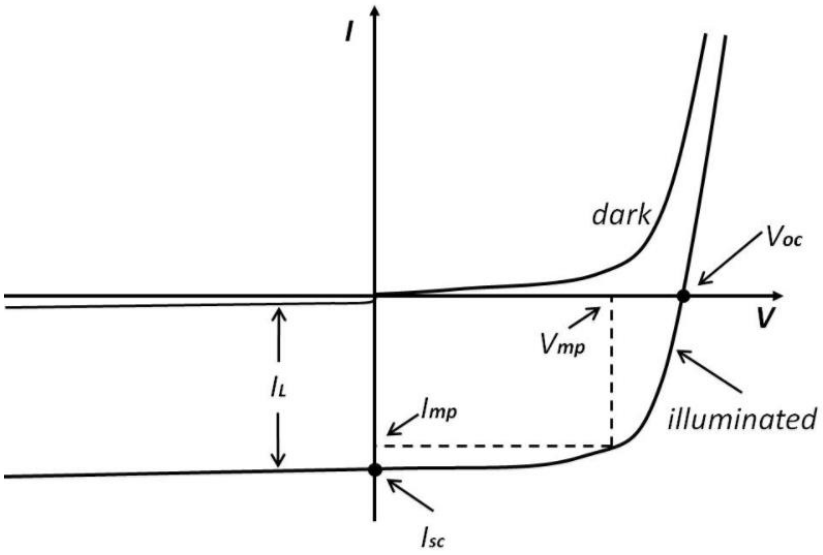

Figure 5. 14. Dark I-V and light I-V curve.

Next chapter, we will present our results. The solar cell device fabrication data will be discussed as well.

CHAPTER 6

RESULTS AND DISCUSSION

In this section CZTS absorber layer was characterized using many techniques such as SEM, EDS, Raman and XRD analysis. Firstly, different substrates for solar cell devices were discussed. Secondly, CZTS absorber layers on Mo coated SLG were characterized and devices which are fabricated from this samples were investigated.

6.1. Absorber Layer Characterization

6.1.1. Morphological Analysis (SEM Analysis)

6.1.1.1. SEM Analysis of CZTS Films on Different Substrates

Morphological analysis of an absorber layer is important. Grain boundaries on the absorber layer act as a recombination center and it causes a decrease device performance (Hegedus and Shafarman 2004). It is known from the literature that the uniform and compact morphology is beneficial for solar cell efficiency (Pawar et al., 2014). As a result, scanning electron microscopy (SEM) was used to determine the surface morphology. Figure 6.1. shows the SEM images of Mo-CZTS and Ti-CZTS. According to the SEM images of the films deposited on Mo substrate which was seen in Figure 6.1. (a) and (b), dense and more uniform structure was observed. As seen the films deposited on Ti foil substrate which was seen Figure 6.1. (c) and (d)., it was observed different shapes because of different formations in all probability. Therefore; it can be said that Mo substrate is more applicable to fabricate a CZTS absorber layer. In addition, taking into account of the most dominant peaks which were 28.44° and 28.49° in XRD analysis and the crystalline size of samples was obtained using Scherrer Formula. 63 nm for Mo-CZTS and 31,6 nm for Ti-CZTS was calculated. As the crystalline size decreases, grain boundaries increase causing resistivity boost which is detrimental for solar cell efficiency(Khalkar et al., 2014).

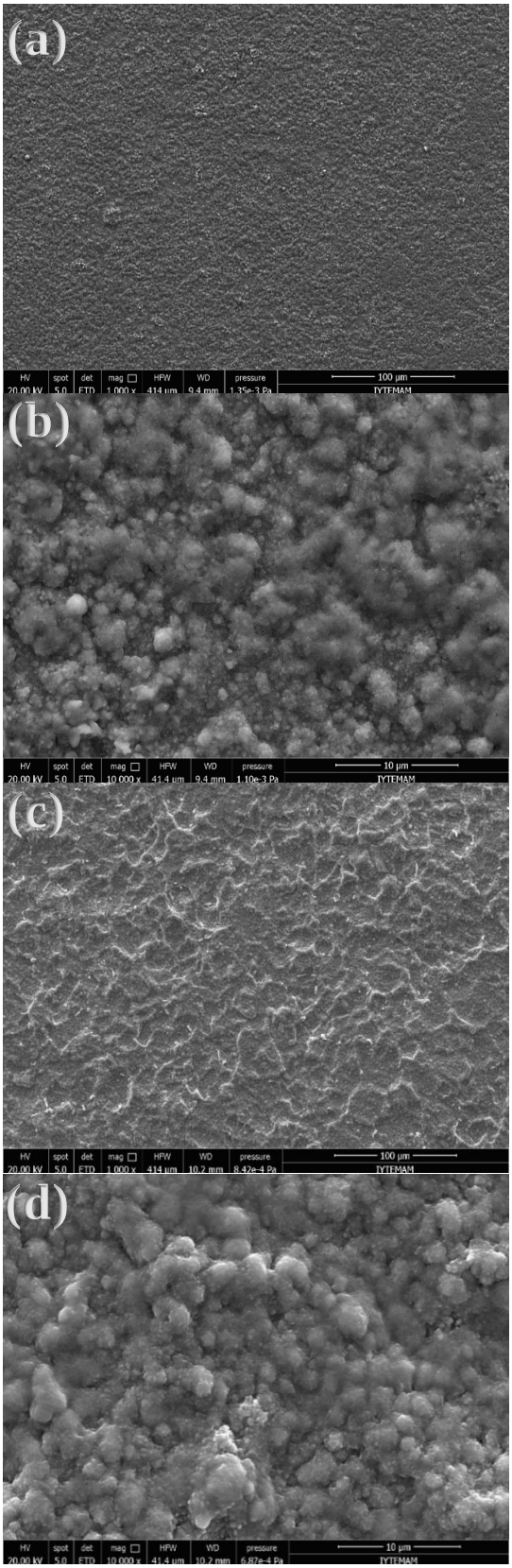

Figure 6. 1. SEM images of (a) and (b) for Mo-CZTS and (c) and (d) for Ti-CZTS.

In our CZTS laboratory group, the temperature dependent measurement has been studied along with the substrate effect, and it will be further expanded in the future (Buldu 2018).

6.1.1.2. SEM Analysis of CZTS Films on Mo Coated SLG

As mentioned before, scanning electron microscopy (SEM) was used to investigate the surface morphology of the grown films. This technique uses electrons which interact with the sample' atoms to form an image. Besides, it is also possible to determine the chemical composition of selected area on the sample surface by using Energy Dispersive Spectroscopy (EDS). Elemental compositional CZTS films were determined using EDS technique which has 1 μ penetration depth and 10% accuracy.

Figure 6.2. shows SEM measurements of (a)Mo-CZTS-A, (b) Mo-CZTS-B and (c) Mo-CZTS-C. As mentioned before, these three samples were sulfurized with the same parameters. Besides, we used these samples for device fabrication in order to understand dependence of CdS buffer layer thickness on solar cell conversion efficiency. In addition; Figure 6.3. shows SEM measurements of (a) Mo-CZTS-D and (b) Mo-CZTS-E. These samples were fabricated to determine sulfurization time effect on solar cell conversion efficiency. For two samples, Zn(O,S) buffer layer was used as an n-type layer.

Mo-CZTS-A, B and C were produced with the same growth and sulfurization parameters in order to understand CdS buffer layer thickness effect on solar cell performance. Because of same parameters have been applied, there is no huge differences between them. Grain boundaries are important for CZTS absorber layer as mentioned before (Khalkar et al., 2014). In literature, large grain size is observed for Cu-rich composition (Scragg 2010). According to XRD analysis, we detected small grain size because of Cu-poor composition. Cu-rich composition causes Cu_2S secondary phases. Control of this phase is important as well as large grains of films. EDS analysis were used to determine chemical compositions.

Mo-CZTS-D and Mo-CZTS-E were fabricated with the same growth process but different sulfurization time. SEM images of these samples were shown in Figure 6.3. It is clearly seen that there were different formations which has different colors. They can be undesirable secondary phases. In addition, they can be detected using EDS technique. Using some etchant, it is possible to avoid these secondary phases.

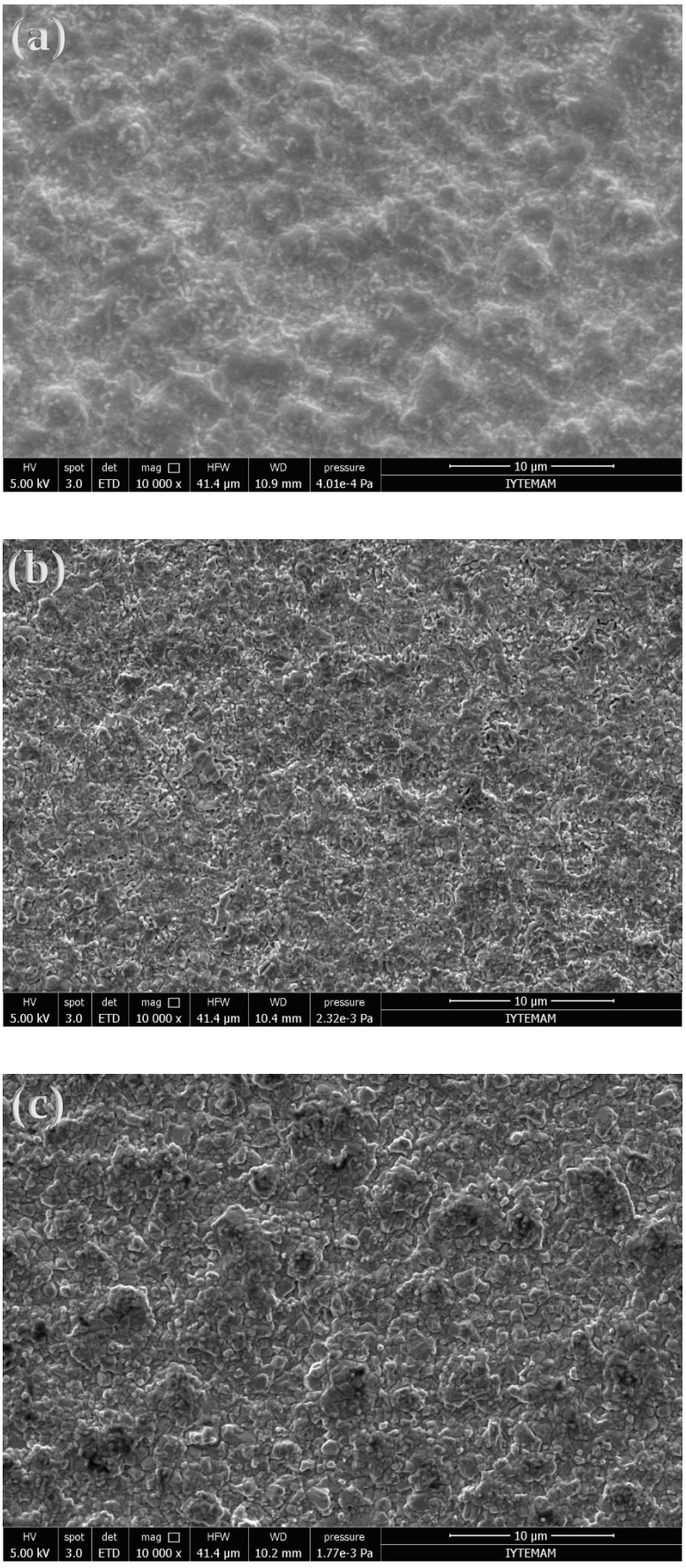

Figure 6. 2. SEM images of (a) Mo-CZTS-A (b) Mo-CZTS-B and (c) Mo-CZTS-C.

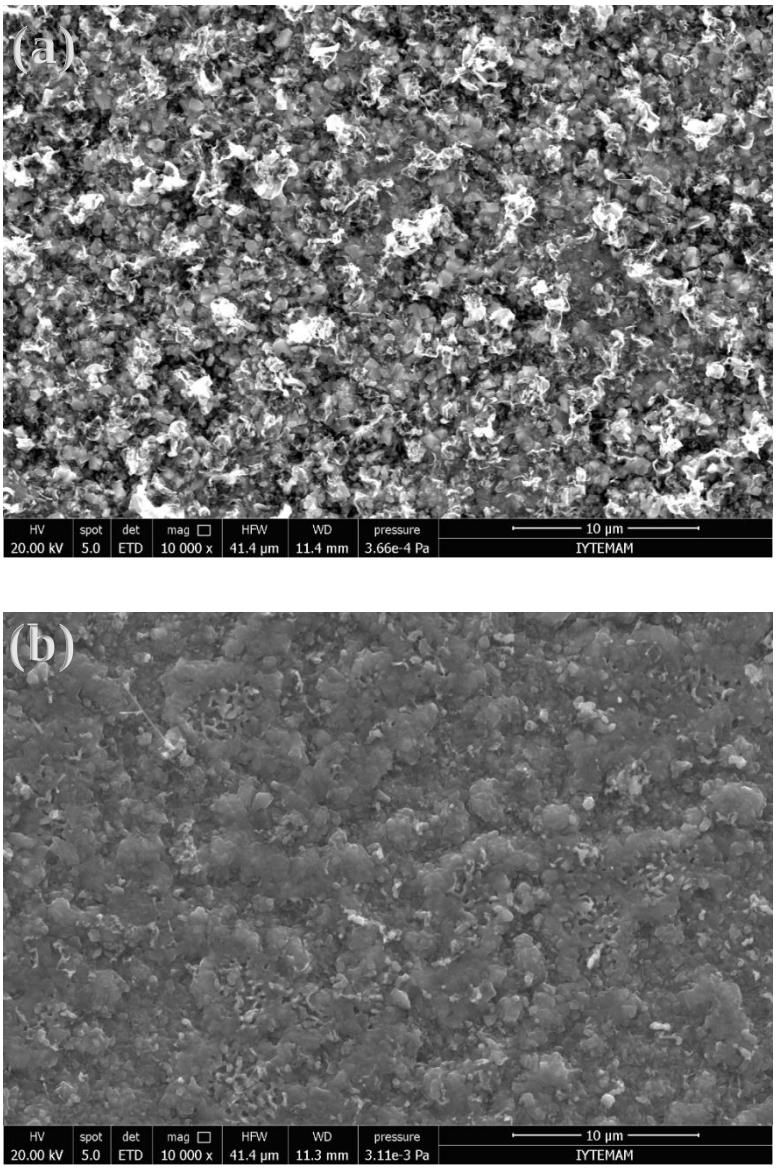

Figure 6. 3. SEM images of (a) Mo-CZTS-D and (b) Mo-CZTS-E.

Mentioned before, there are some parameters to determine solar cell such as open circuit voltage or short circuit voltage. Causes that affect these parameters are very important. Especially secondary phases cause some changes in the solar cell surface. For instance, during sulfurization process, MoS_2 phase can occur (Barkhouse, Haight, et al., 2012).. Because of it has low band gap (1.29 eV) this phase diminishes the V_{OC} of the cells (Byungha Shin, Oki Gunawan, Yu Zhu, Nestor A. Bojarczuk 2013). This type of decompositions at CZTS/Mo interfaces improve the recombination. Besides, it causes low V_{OC}, J_{SC} and FF of device. As seen in Figure 6.4., it was obtained; long sulfurization

time cause thicker MoS_2 secondary phase. According to MoS_2 occurrence, performance of the cell prone to change. This performance of the cells will be mentioned in next section

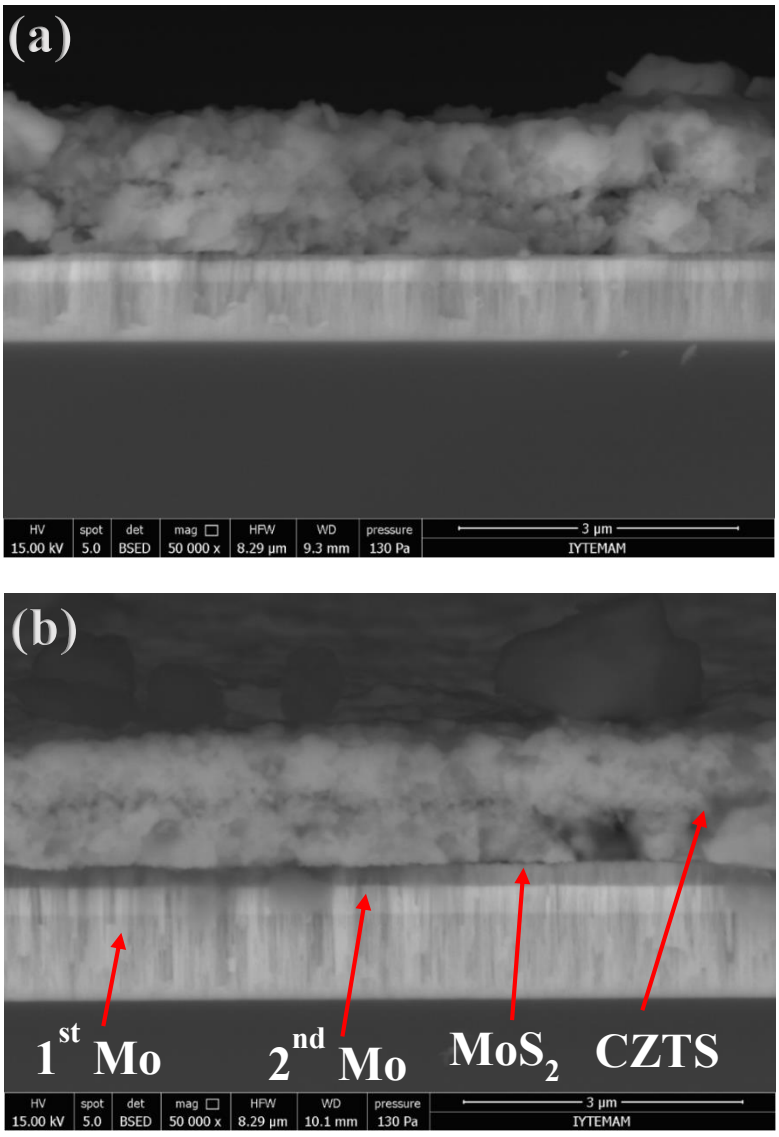

Figure 6. 4. Cross section SEM images of (a) Mo-CZTS-D and (b) Mo-CZTS-E.

6.1.2. Chemical Composition (EDS Analysis)

To form Cu-poor Zn-rich composition, each layer was calibrated with a specific thickness. According to literature; Cu-poor Zn-rich composition increase the solar cell performance. Cu vacancies improve p-type conductivity of CZTS film (S. Chen et al., 2010). On the other hand; Zn-rich compositions which means increase the Zn_{Sn} formation

acceptors and reduce the Sn_{Zn} donor enhance the conductivity also (Yeh et al., 2016). However, Zn amount is important because high Zn amount is detrimental for solar cell performance while Cu/Zn ratio will be low. Chemical composition plays a huge role for CZTS structure. EDS analysis was used to obtain elemental ratios.

6.1.2.1. EDS Analysis of CZTS Films on Different Substrates

The atomic composition of CZTS thin film was investigated by using EDS analysis (Table 6.1.). Sulfurized films were fabricated as Cu-poor and Zn-rich compositions that is important to obtain high efficient CZTS solar cells (Katagiri et al., 2001). In literature, the most suitable ratios for Cu/(Zn+Sn) and Zn/Sn are given as 0.8 and 1.2, respectively. (Barkhouse, Gunawan, et al., 2012). Furthermore, non-uniformity occurs because of Cu/Sn fluctuations. Cu movement from bottom to upper surface during sulphurization process, as well as inhibition of Cu-Sn reaction, are needed for presence of Cu_2SnS_3 (Pawar et al., 2010). As seen in Table 6.1., Cu, Sn and Zn compositions were nearly similar, while sulphur content was seen dissimilar. It is given in the literature that as sulfur content increase in the alloy, kesterite CZTS formation is improved and secondary phases are started to disappear (Sripan et al., 2016). As seen Table 1, amount of sulphur for Mo-CZTS is greater than Ti-CZTS. Therefore, it can be observed that molybdenum substrate seems more suitable for solar cell applications.

Table 6. 1. EDS results of CZTS films on Mo coated SLG and Ti foil.

	Cu (atomic%)	**Sn (atomic%)**	**Zn (atomic%)**	**S (atomic%)**	**Cu / (Zn+Sn)**	**Zn/Sn**	**Cu/Sn**
Mo-CZTS	21.09	12.04	12.43	54.44	0.86	1.03	1.75
Ti-CZTS	22.94	12.46	13.06	51.54	0.89	1.04	1.84

6.1.2.2. EDS Analysis of CZTS Films on Mo Coated SLG

Table 6.2. shows chemical composition of CZTS films on Mo coated SLG substrate. The elemental ratios for Cu/(Zn+Sn), Zn/Sn and Cu/Sn should be 0.8, 1.2 and 1.8, respectively (Katagiri et al., 2009). The stoichiometry is important for performance of the cell. Cu-poor, Zn-rich composition was obtained for Mo-CZTS-A, B and C. Mo-CZTS-D and E show Cu-poor, Zn-poor and Sn-rich composition. As sulfurization time increase, Sn concentration diminishes. In the literature, Sn loss is the biggest problem for films.

Table 6. 2. Atomic compositions and ratios of CZTS films.

	Cu (atomic%)	**Sn (atomic%)**	**Zn (atomic%)**	**S (atomic%)**	**Cu / (Zn+Sn)**	**Zn/Sn**	**Cu/Sn**
Mo-CZTS-A	20.96	11.09	13.48	54.47	0.85	1.22	1.88
Mo-CZTS-B	20.33	11.36	13.41	54.90	0.82	1.18	1.78
Mo-CZTS-C	20.72	11.33	13.57	54.37	0.83	1.20	1.82
Mo-CZTS-D	20.16	12.28	11.79	55.77	0.83	0.96	1.64
Mo-CZTS-E	20.30	11.67	12.39	55.63	0.84	1.06	1.73

6.1.3. X-Ray Diffraction (XRD) Analysis

As we mentioned before, XRD analysis give information about crystal structure of material. CZTS data base (JCPDS-26-0575) was used in XRD analysis. However, XRD analysis is not sufficient for determining the CZTS structure due to overlap of secondary phases such as Cu_2SnS_3 (CTS) and ZnS peaks with CZTS peaks. To overcome this problem, Raman analysis were performed. Raman results which belongs to samples

will be given in next topic. Thanks to these analysis, separated peaks will be obtained belongs to CZTS.

6.1.3.1. XRD Analysis of CZTS Films on Different Substrates

Figure 6.5. shows the XRD spectrum of sulfurized CZTS films on Mo coated SLG substrates. This analysis was performed in order to detect the formation of secondary phases and investigate the quality of crystalline structure. The peaks were obtained at 2Θ = 23.09, 28.44, 29.68, 32.96, 37.91, 44.94, 47.30, 56.12, 58.92, 69.20 and 76.40 correspond to the (110), (112), (103), (200), (211), (105), (220), (312), (224), (008) and (332) planes respectively, for Mo-CZTS (JCPDS 00-026-0575). Peaks were obtained as a result of (112), (220) and (312) planes were the most dominant ones. They indicate the formation of CZTS kesterite structure (JCPDS 00-026-0575). The peaks were obtained at 40.41° and 73.56° were associated with Mo substrate (JCPDS 00-004-0809). Moreover, MoS_2 was detected at 78.94° (JCPDS 00-024-0515).

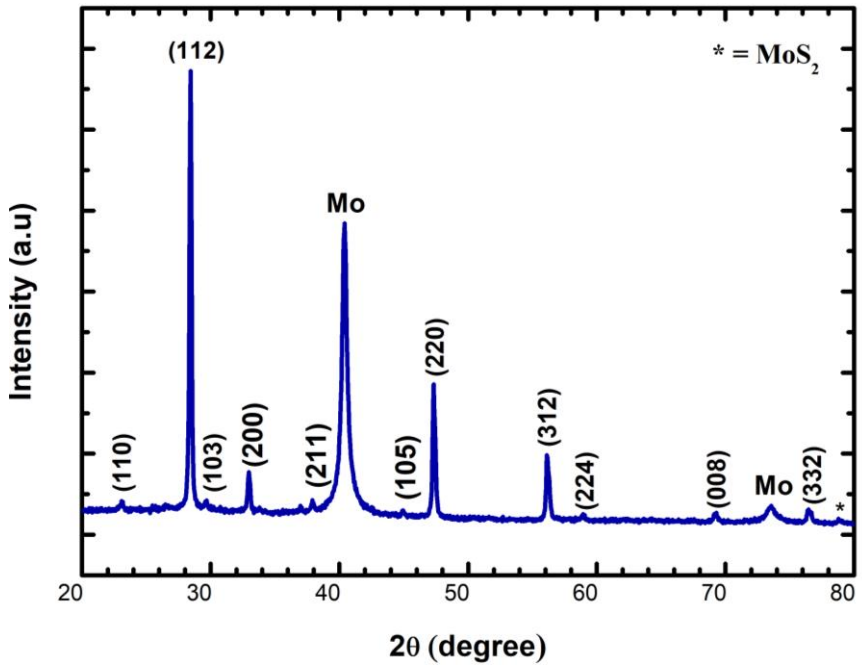

Figure 6. 5. XRD spectrum of sulfurized CZTS films on Mo coated SLG substrate.

Figure 6.6. shows the XRD spectrum of sulfurized CZTS films deposited on Ti foil. The peaks were obtained at 2Θ = 23.15, 28.49, 29.65, 33.01, 44.95, 47.32, 56.13, 58.85 and 76.42 correspond to the (110), (112), (103), (200), (105), (220), (312), (224) and (332) planes respectively for Ti-CZTS (JCPDS 00-026-0575). Also SnS_2 phase was detected at 69.27° (JCPDS 00-031-1399).

These peaks are fundamental ones for CZTS kesterite structure (JCPDS 00-026-0575). In addition, peaks which belong to Ti substrate at 38.36°, 40.19°, 53.14° and 70.60° were observed (JCPDS 00-044-1294).

When two different substrates were used for films, both of them exhibited the characteristic of CZTS peaks. (112) diffraction peak was intense and sharp which indicates good crystalline structure for each sample. Crystallinity is crucial for high quality absorber layer.

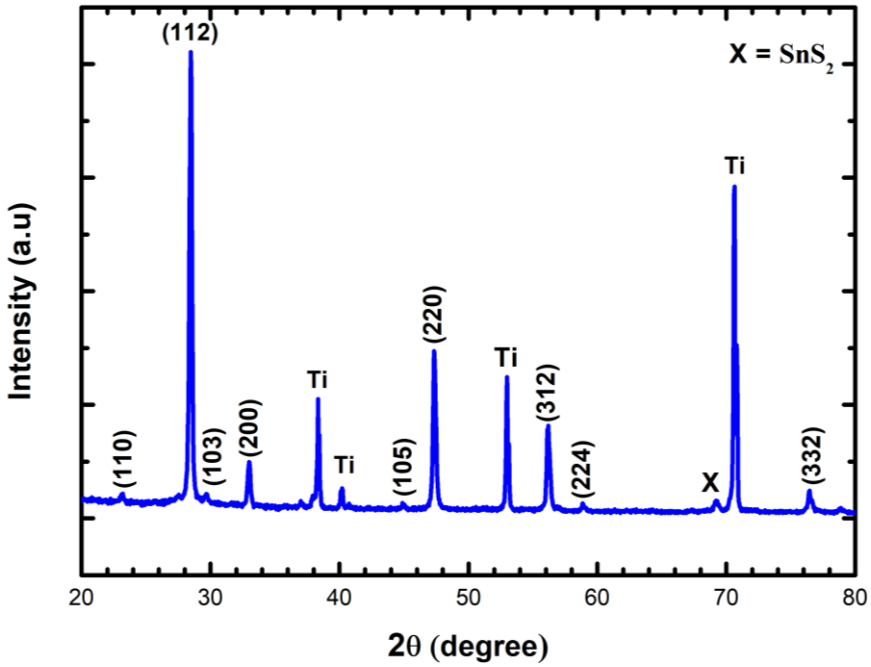

Figure 6. 6. XRD spectrum of sulfurized CZTS films on Ti foil.

In addition, taking into account of the most dominant peaks were 28.44° and 28.49°, the crystalline size of samples was obtained using Scherrer Formula. 63 nm for Mo-CZTS and 31,6 nm for Ti-CZTS were reached. As crystalline size decreases, grain boundaries increase causing resistivity boost which is detrimental for solar cell efficiency

(Khalkar et al., 2014). Bigger grain boundaries are beneficial for solar cell device performance

6.1.3.2. XRD Analysis of CZTS Films on Mo Coated SLG

Figure 6.7. shows XRD spectra of sulfurized CZTS films as called Mo-CZTS-A, Mo-CZTS-B and Mo-CZTS-C. When three samples are considered, there is no difference between peaks locations. Thus, all data for three sample were plotted in the same spectra. The peaks were obtained at 2Θ = 23.15, 28.47, 29.72, 32.99, 37.94, 44.97, 47.38, 56.19, 58.93, 69.19 and 76.48 correspond to the (110), (112), (103), (200), (211), (105), (220), (312), (224), (008) and (332) planes respectively, for Mo-CZTS-A, Mo-CZTS-B and Mo-CZTS-C (JCPDS 00-026-0575). All XRD patterns of sulfurized films matched with CZTS fundamental peaks. In addition, (112) diffraction peak was intense and sharp which indicates good crystalline structure for each sample. Besides, the films showed secondary phases such as MoS_2, MoO_2 and ZnO. The peaks belong the Mo substrate were detected at 2Θ=40.38 (JCPDS 00-004-0809). Besides, crystallite size was calculated approximately 50 nm using Scherrer Calculation formula.

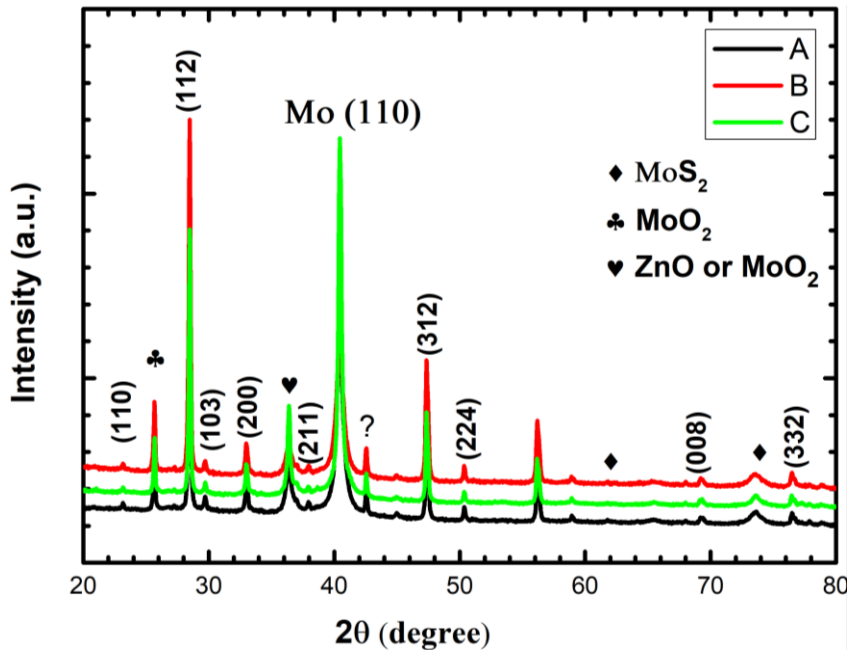

Figure 6. 7. XRD spectra of sulfurized films as called Mo-CZTS-A, Mo-CZTS-B and Mo-CZTS-C.

Figure 6.8. shows XRD spectra of CZTS films as called Mo-CZTS-D and Mo-CZTS-E. All data for two sample were plotted in the same graph. The peaks located at 2Θ = 28.33, 32.75, 36.26, 40.30, 47.20 and 56.05 correspond to the (112), (200), (202), (220) and (312) planes respectively, for Mo-CZTS-D, and E (JCPDS 00-026-0575). A peak from Mo substrate was seen at 40.30° (JCPDS 00-042-1120). To obtain crystallite size, Scherrer's formula was used;

$$D = \frac{0.9\lambda}{\beta cos\theta} \tag{6.1}$$

where D is average crystallite size (diameter), 0.9 is called the particle shape factor, λ is wavelength of Cu-K α which is 0.15406 nm and β is full width at half-maximum (FWHM) in radians, Θ is the Bragg angle in degrees. Obtained crystallite sizes were approximately 63 nm for Mo-CZTS-D and 81.9 nm for Mo-CZTS-E. It can be seen that large grain size effects solar cell performance (Mkawi et al., 2014). To do this long sulfurization process should be applied. Besides; no peak from secondary phases was obtained.

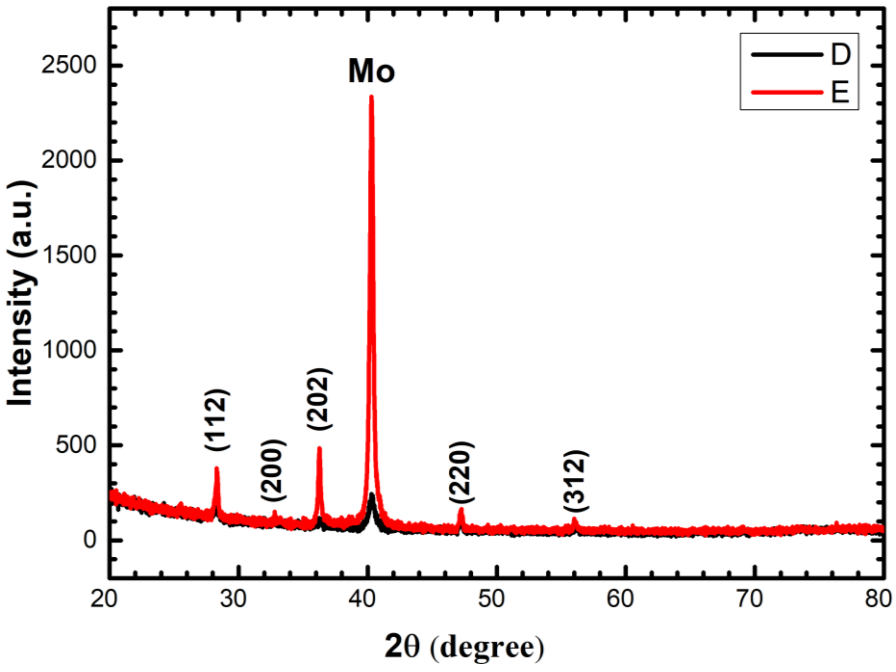

Figure 6. 8. XRD spectra of CZTS films as called Mo-CZTS-D and Mo-CZTS-E.

6.1.4. Raman Analysis

Since XRD peaks from the secondary phases of ZnS (JCPDS: 00-05-0566) and Cu_2SnS_3 (JCPDS: 00-027-0198) are close to CZTS peak, they are not sufficient to distinguish the formation of CZTS. Therefore, Raman spectroscopy measurements will be used to confirm CZTS kesterite structure (Jiang and Yan 2013).

6.1.4.1. Raman Analysis of CZTS Films on Different Substrates

Figure 6.9. shows the Raman spectrum of CZTS films on Mo substrate. Peaks at 256 cm^{-1} and 337 cm^{-1} are the characteristic peaks of CZTS (Cormier and Snyders 2015). Besides, MoS_2 is observed at 410 cm^{-1} in Raman spectra which was seen XRD spectra.

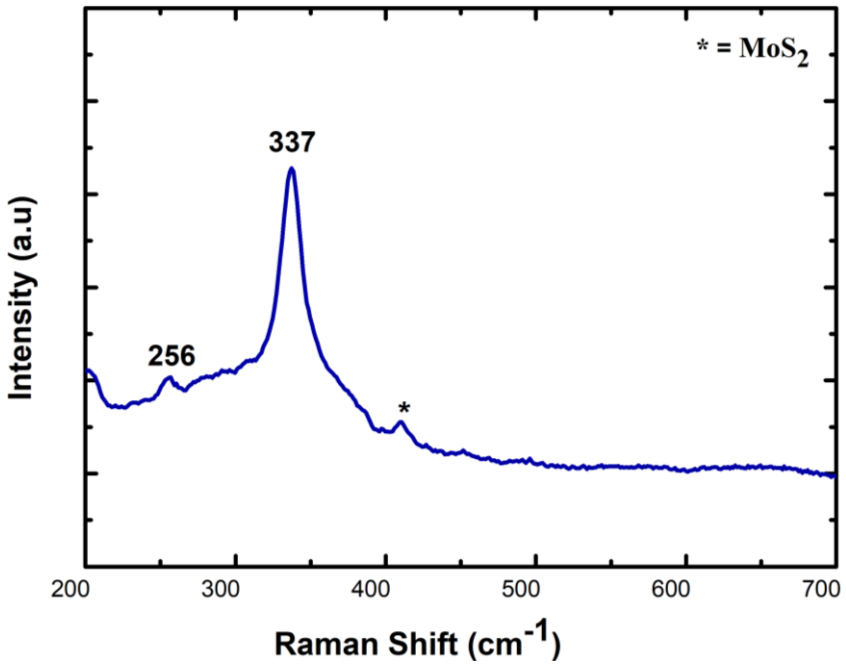

Figure 6. 9. Raman spectrum of CZTS films on Mo coated SLG substrate.

Although Raman penetration is 150 nm, MoS_2 phase was detected because CZTS formation was not continuous. This was an evidence for presence of vacancy. Secondary phases are harmful for solar cell devices. Since MoS_2 restrict the hole transportation from

CZTS to Mo layer (Yang et al., 2015), it leads to disintegration of the CZTS absorber layer as a result of high temperature sulfurization (Scragg et al., 2012). Moreover, there is no remarkable observation of phase separation between Cu_2SnS_3 phase peaks at 336 and 351 cm^{-1} and ZnS at 355 cm^{-1} (K. Wang et al., 2011).

Figure 6.10. shows Raman spectrum for Ti-CZTS. The main peaks for CZTS kesterite structure were detected at 255 cm^{-1}, 338 cm^{-1} and 670 cm^{-1} (Cormier and Snyders 2015). In addition, SnS_2 phase was detected at 310 cm^{-1} which was observed XRD analysis.

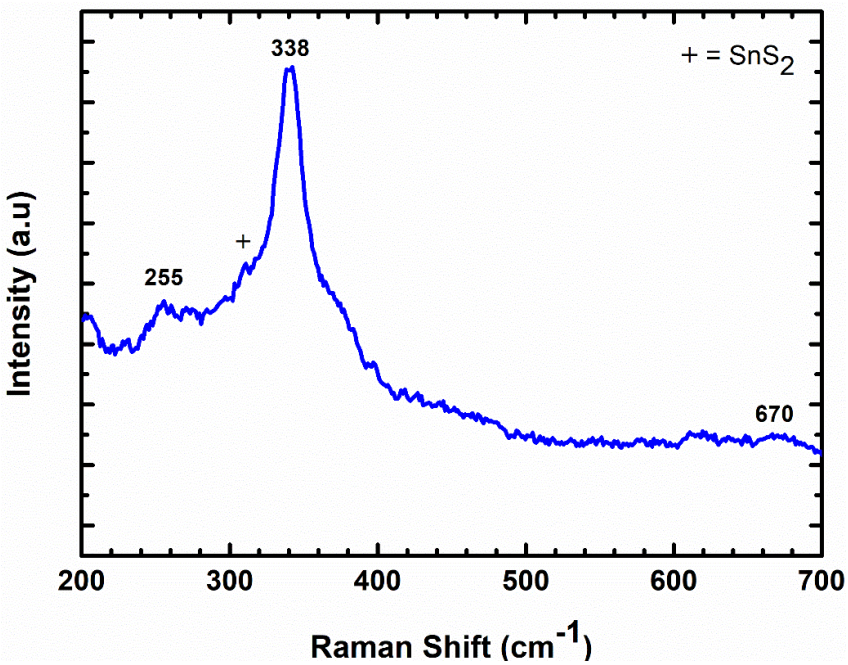

Figure 6. 10. Raman spectrum of CZTS films on Ti foil.

6.1.4.2. Raman Analysis of CZTS Films on Mo Coated SLG

As we mentioned before; CZTS absorption coefficient is higher than 10^4 cm^{-1}. Therefore, penetration depth of Raman laser for 514 and 632 nm wavelength are 150 and 170 nm, respectively (Fernandes, Salomé, and Da Cunha 2011). Anions and cations vibration is detected in definite frequency range. Zn cations, S anions and Cu cations vibrations have states between 250 and 300 cm^{-1}. Between 310 to 340 cm^{-1}, phonon states occurred by S anions. States from 340 to 370 consist Sn cations and S anions vibrations

(Khare et al., 2012). 633 nm wavelength laser was used for Raman analysis of Mo-CZTS-A, B, C, D and E. Below 200 cm^{-1} modes were not studied.

Figure 6.11. shows Raman spectra of sulfurized CZTS films as called Mo-CZTS-A, Mo-CZTS-B and Mo-CZTS-C. When three samples are considered, there was no difference between peaks locations. Thus, all data for three sample were plotted in the same graph. The shift to lower frequency was observed for Mo-CZTS-A, Mo-CZTS-B and Mo-CZTS-C. Generally, this situation is seen for low crystallite size which must be lower than 50 nm (Guc et al., 2016).

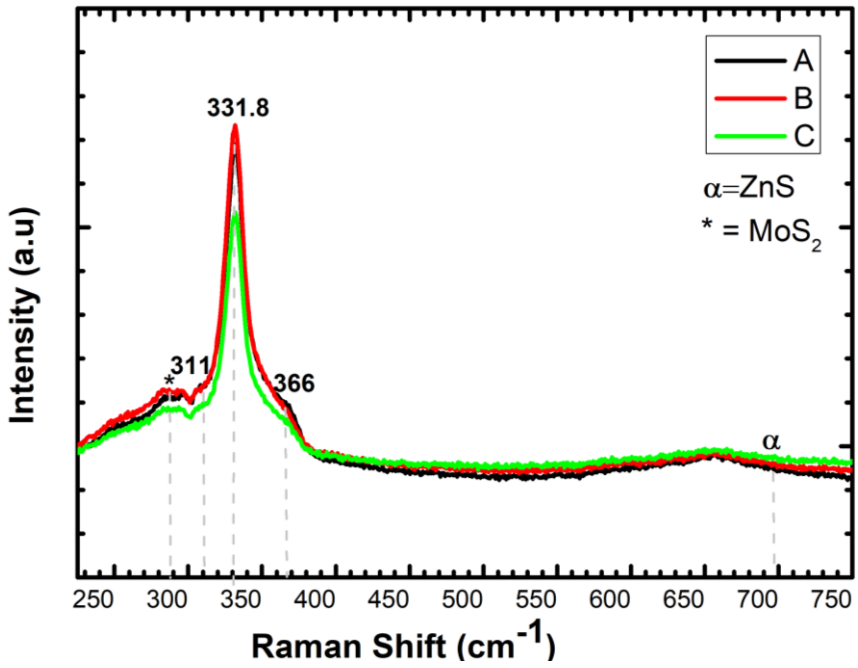

Figure 6. 11. Raman spectra of CZTS films as called Mo-CZTS-A, Mo-CZTS-B and Mo-CZTS-C.

The CZTS Raman peaks were detected nearly at 311, 331 and 366 cm^{-1} wavelengths. The weak peak observed at 697 cm^{-1} wavelength belongs to ZnS phase (Fernandes, Salomé, and Cunha 2011). In addition, when we looked at XRD results of these samples, we observed that MoS_2 occurrence. In Raman analysis, 288 cm^{-1} peak can be attributed to MoS_2 or CZTS phase. XRD and Raman analysis is related to each other. Therefore, it can said that this peak refers to MoS_2 phase (Fernandes, Salomé, and Cunha 2011).

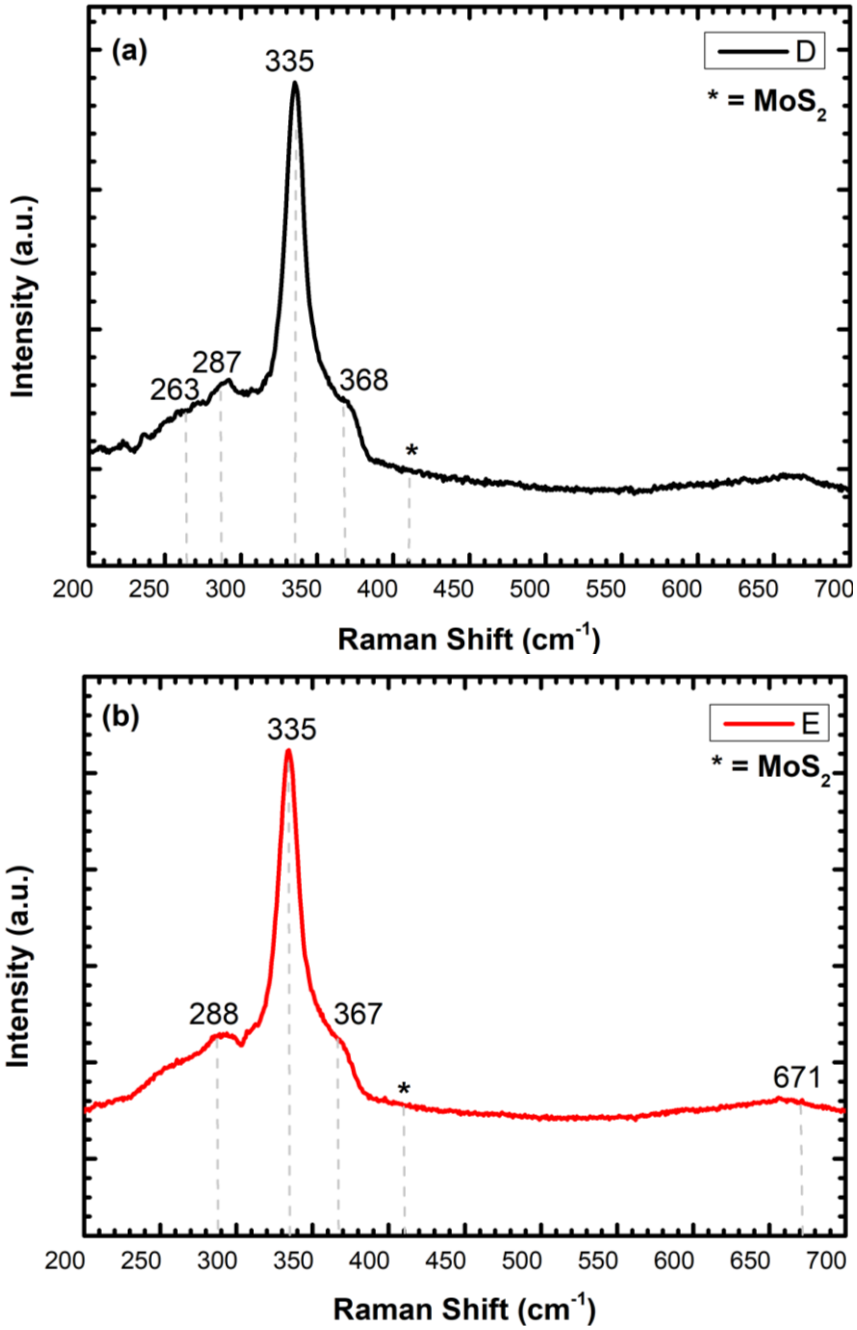

Figure 6. 12. Raman spectra of (a) Mo-CZTS-D and (b) Mo-CZTS-E.

In general, main CZTS Raman peaks were detected at 337-338 cm^{-1}. This attributes vibration of S anions in kesterite CZTS. Because of deconvolution, main peaks were observed at 331.4 cm^{-1} for these samples. According to literature, the peak detected at 330 or 331 cm^{-1} is called partial disorder kesterite phase. Generally, this phase was seen in non-stoichiometric films (Kaushik, Rao, and Subrahmanyam 2017). Change in crystal symmetry of CZTS films causes to change from kesterite structure to disorder kesterite.

Peak position at 668 cm^{-1} shows as a broad band. It can be attributes second order of the main Raman band of CZTS. This peak refers to enhanced crystalline quality of the material (Pal et al., 2013).

Figure 6.12. shows Raman spectra of sulfurized CZTS films which labelled are (a)Mo-CZTS-D and (b)Mo-CZTS-E. While peaks at 263, 287, 335 and 368 cm^{-1} were observed for Mo-CZTS-D, peaks at 288, 335, 367 and 671 was detected for Mo-CZTS-E. These peaks are main peaks for CZTS structure (Cormier and Snyders 2015). MoS_2 phase was observed at 410 cm^{-1} for two samples.

According our Raman analysis, we can say that CZTS structure was formed and hence, these samples ready for device fabrication.

6.1.5. Optical Characterization

The optical properties of absorber layer play a huge role in solar cell performance. Samples were prepared without Mo back contact. Our stacking order was growth on SLG. Then sulfurization process was applied with the same condition. Using transmittance and reflectance measurements, the optical band gap was predicted at room temperature. Using Equation 6.2. absorption coefficient α of CZTS sample can be calculated;

$$\alpha = \frac{1}{t} ln \left[\frac{(1-R)^2}{T}\right] \tag{6.2.}$$

where R is reflection, T is transmission and t is thickness of the sample. If we want to obtain band gap energy, we should use the equation;

$$(\alpha hv) = A[hv - E_g]^n \tag{6.3.}$$

where α is absorption coefficient, E_g is band gap energy, A is constant and n=1/2 for direct transition. Graph of $(\alpha hv)^2$ versus photon energy gives us the optical band gap of CZTS samples. Figure 6.13. shows $(\alpha hv)^2$ vs. hv plot of CZTS sample which is band gap 1.59 eV. Besides, transmittance graph was also shown in this graph. In the visible region, transmission of sample has 0.01-1.10% values. In near infrared region, it is about 0.10-45.24%.

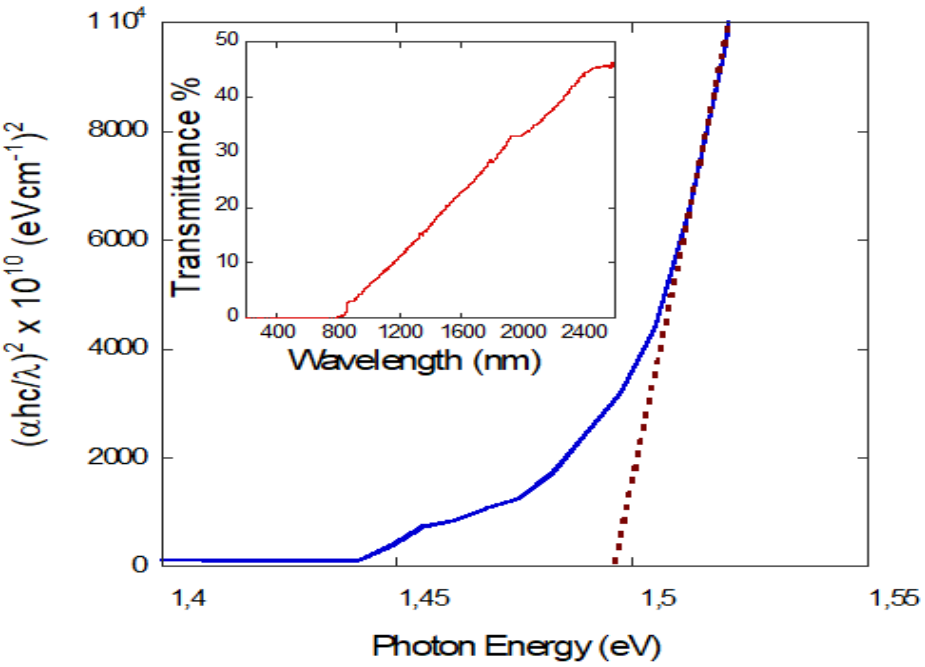

Figure 6. 13. Graph of $(\alpha hv)^2$ versus photon energy and transmittance spectrum.

Optical properties were obtained and band gap was calculated to be 1.5 eV which is acceptable according to literature (Malerba et al., 2014). Secondary phases cause high band gap energy. Therefore, CZTS structure fabrication is important thinking band gap energy. Since secondary phases that have low band gap energy presence is more acceptable.

6.1.6. Electrical Characterization

In this part, temperature dependence of the resistivity measurements were investigated in the range of 80 – 300 K. To investigate; Van der Pauw method was used. To apply a magnetic field, a conductor which is perpendicular to the current flow direction produces an electric field perpendicular to the current and the magnetic field. In the p-type semiconductor sample, the current and holes flow in y-direction, the magnetic field is in the z-direction. The current is performed and then the voltage is measured across the diagonal of the sample. Hall measurement is an effective technic to investigate electrical properties of a solar cell. If electrical properties understand clearly, steps to be taken can be specific. In the literature, CZTS characterization supports with electrical charaacterization.

The same stacking order which is Cu/Sn/Zn/Cu was growth on SLG without Mo back contact. Sulfurization process was applied with the same conditions. Figure 6.14. shows the resistivity versus temperature graph. The lowest resistivity value that we found as 187 Ω.cm at room temperature for this sample. The highest resistivity value was found 5009 Ω.cm at 80 K. It can see clearly that the resistivity gradually increases with the decrease in temperature due to a semiconductor behaviour. In this work; hole mobility of CZTS absorber layer was obtained lower than 1 as 0.01 $cm^2/V.s$ at room temperature. Generally; in the range of 1-10 $cm^2/V.s$ is reported in the literature (Ito and Nakazawa 1988). Some reports obtained this value as 0.1-60 $cm^2/V.s$ (Zhao et al., 2017). Lower mobility gives information about optimized thickness of absorber layer. Carrier concentration and hall mobility was calculated for 1500 nm thick sample. $R_H = 1/(n * e)$ gives us hall coefficient. e is electron charge and its value is $1.602x10^{19}$ Coulombs.

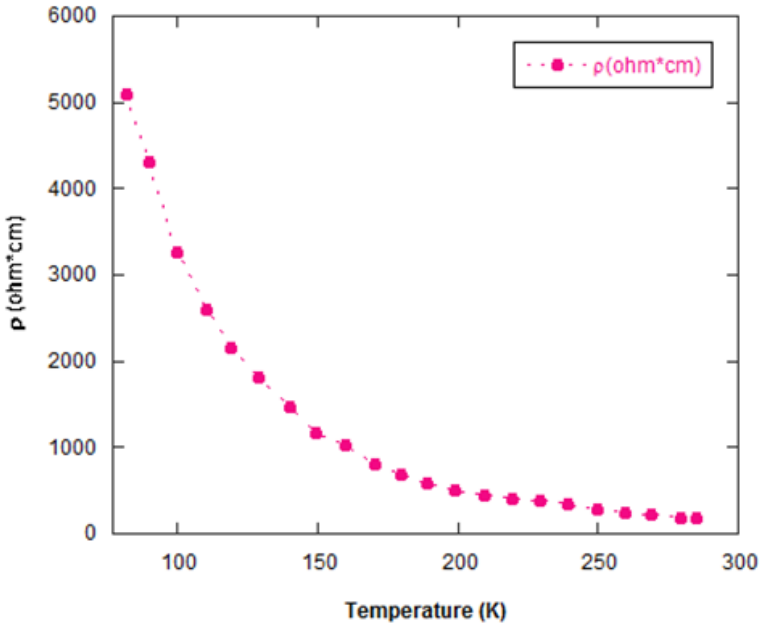

Figure 6. 14. The resistivity vs temperature curve of CZTS sample.

The hole mobility value was measured as 0.77 $cm^2/V.s$ and the hole carrier concentration value was found 4.29×10^{16} cm^{-3} at room temperature by van der pauw method. As a result, the electrical properties of the sample are showed p-type semiconductor behaviour.

6.2. Light Beam Induced Current (LBIC) Measurements

There are many parameters that affect the solar cell performance such as V_{OC}, I_{SC}, homogeneity. Determined parameter allows high performance solar cell fabrication. Light beam induced current (LBIC) measurement is one of the analysis that examine these parameters using 2D-3D mapping. As mentioned before, point by point scanning of the selected region by focused light beam allows to create distribution. Beam probe scans the solar cell by obtaining current-voltage characteristics. A map of many solar cell parameters can be observed using this technic. Photo-generated current is occurred and we can achieve current as a function of its position. Thanks to this measurement, it is possible to detect electrically active defects existing inside semiconductor structure. Figure 5.2. shows illustration of light beam induced current system.

For instance; V_{OC} homogeneity can be observed. On the other hand, in a solar cell, performance should be measure from the weakest point. Therefore, this point can be obtained using this technique. Besides, V_{OC} depending on the temperature gives us visually the presence and distribution of the center that affect the performance of the solar cell. This method is used to characterize the existing local inhomogeneities that will ultimately affect the performance.

Especially; it is used for detection homogeneities depend on deposition technique in solar cell that formed by binary, ternary and quaternary compound.

Finally; if distribution occur depending on the compositional difference that can occur is supported with EDX mapping or Raman, this technique gives the identity of the composition which will be the highest efficiency throughput directly over the whole. Figure 6.15. shows 2D mapping of V_{OC} and I_{SC} distribution for Mo-CZTS-D and Figure 6.16. shows 2D mapping of V_{OC} and I_{SC} distribution for Mo-CZTS-E. It is obviously seen that maps have different colours distribution. This colours can be considered as mapping of crucial parameters. Uniform colour distribution should be reached. It is important to find out which colour is suitable.

It is concluded that Voc and Isc were not uniform in solar cell surface. Areas indicated that there are defects with in the cell. Because of impurities that form the fabrication process diminishes the performance of the solar cell. It can be clearly seen that there was a huge inhomogeneity.

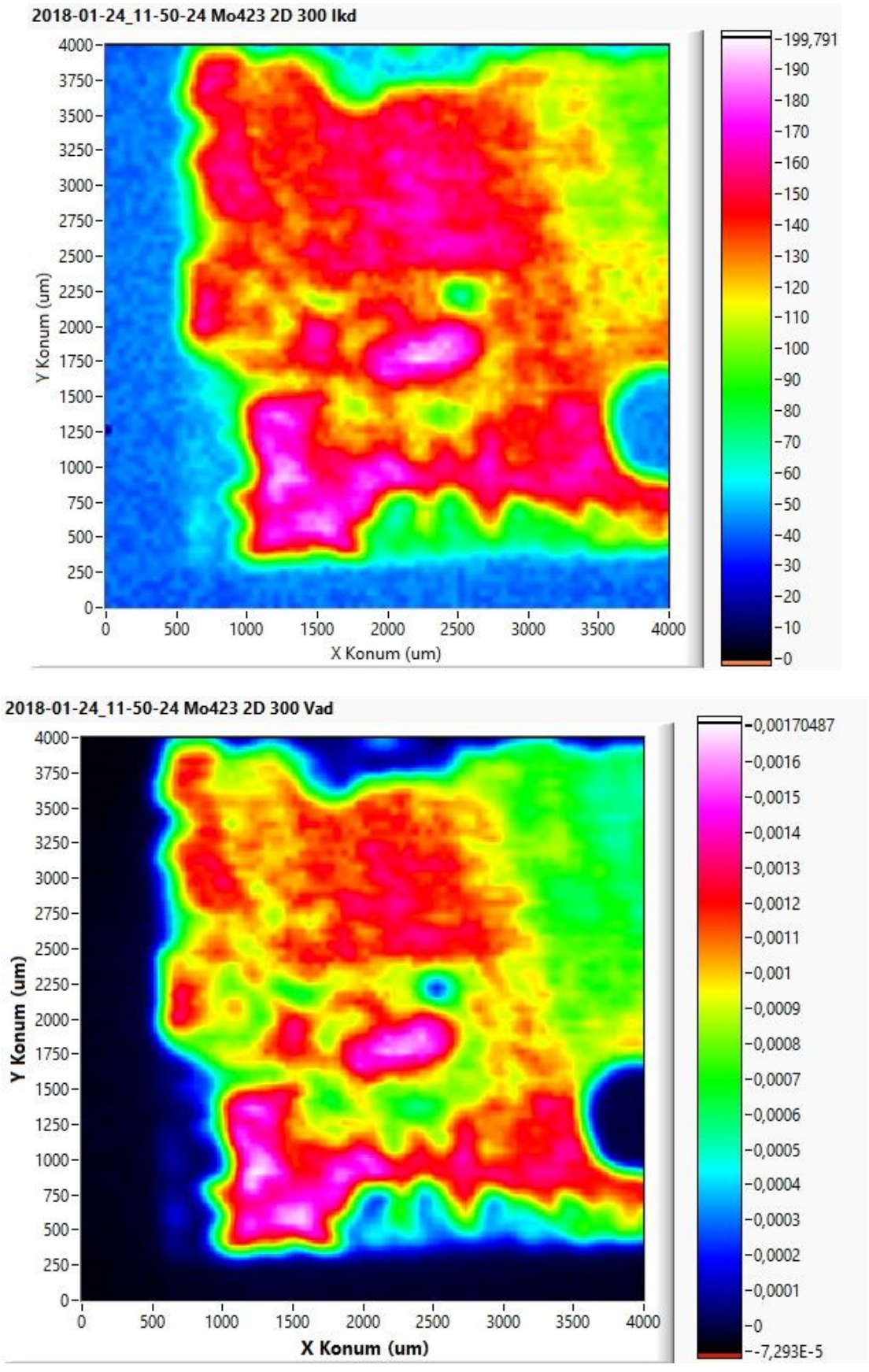

Figure 6. 15. 2D distribution of (a)I_{SC} (b)V_{OC} for Mo-CZTS-D.

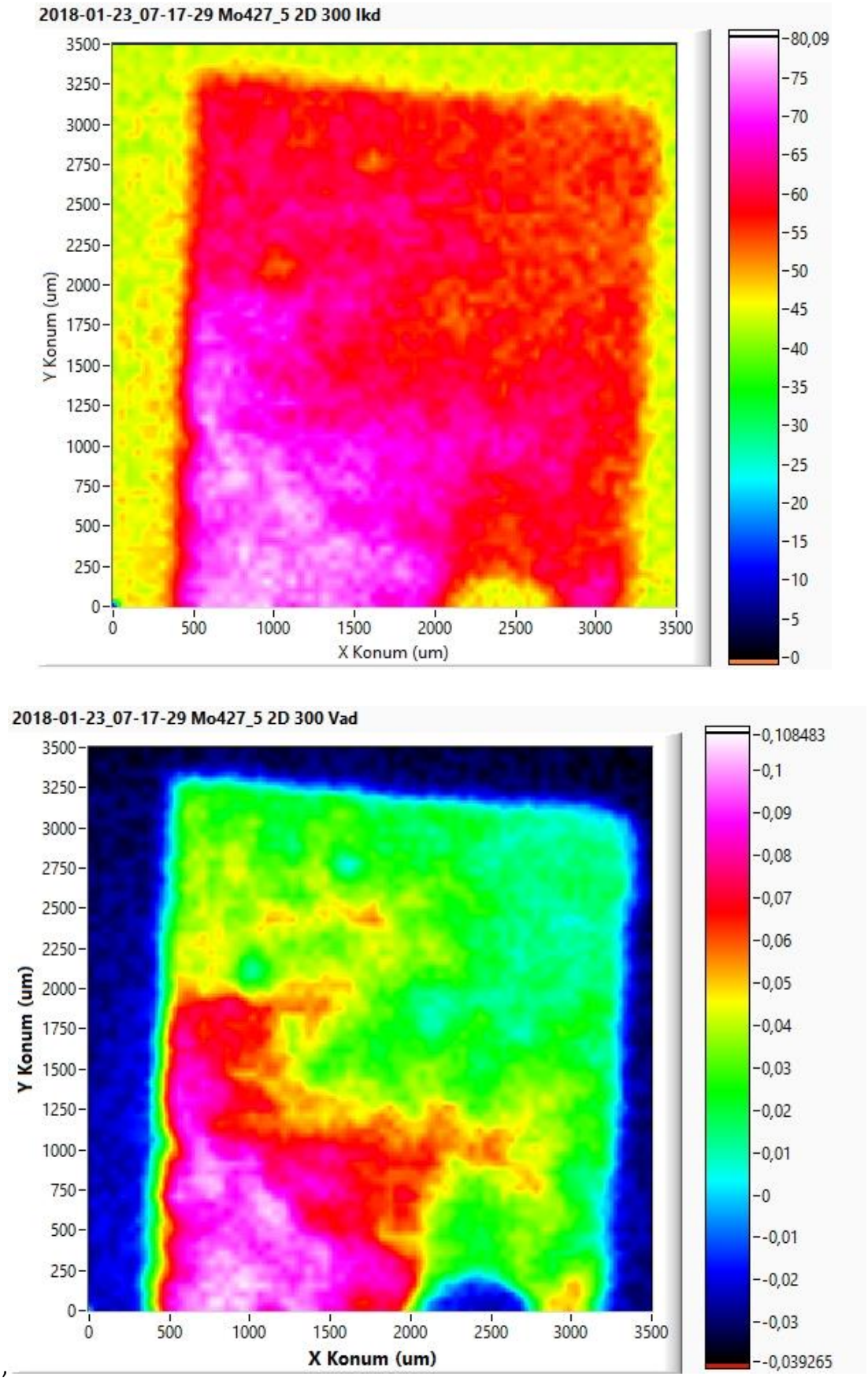

Figure 6. 16. 2D distribution of (a) I_{SC} (b)V_{OC} for Mo-CZTS-E.

In Figure 6.15. and 6.16., it is seen that V_{OC} and I_{SC} were not uniform in solar cell surface. Current can be obtained as a function of a position on the cell thanks to this maps. It is clear that each point adds different contribution to the current (Todorov et al., 2013). Especially, there was a huge inhomogeneity for Mo-CZTS-E. When the other analysis was considered for Mo-CZTS-D and E, short sulfurization time which is 45 minutes is still the better.

6.3. Device Characterization

In this thesis, only Mo coated SLG was used as the back contact material for a solar cell device. Firstly, we examined SLG/Mo/CZTS/CdS/ZnO/AZO structure. There different thicknesses were used for buffer layer. Deposition time effect on solar cell conversion efficiency was investigated. Therefore, previously we will look at J-V measurement for Mo-CZTS-A, B and C. Figure 6.17. shows the J-V measurement results for these samples. As we mentioned before, CdS calibration was done before. It can be some changes in calibration because of roughness of SLG or CZTS films. Experimental conditions can be change during the depositions. Also, our highest efficiency was very low when we compared to the literature. We will discuss all thing that affect the performance of solar cell.

Figure 6.17. (a) shows Mo-CZTS-A. For this formation, 140 nm CdS buffer layer was growth. V_{OC}, J_{SC}, I_{SC}, FF and η was determined from the J-V curve 277.5 mV, 0.79 mA/cm^2, 0.112 mA, 42.8 % and 0.093 %, respectively. The cell area was 0.142 cm^2. Figure 6.17. (b) shows Mo-CZTS-B. For this structure, 134 nm CdS buffer layer was formed. V_{OC}, J_{SC}, I_{SC}, FF and η was determined from the J-V curve 298 mV, 2.80 mA/cm^2, 0.58 mA, 34 % and 0.291 %, respectively. The cell area was 0.207cm^2. Figure 6.17. (c) shows Mo-CZTS-C. For this sample, 102.5 nm CdS buffer layer was deposited. V_{OC}, J_{SC}, I_{SC}, FF and η was determined from the J-V curve 415 mV, 2.59 mA/cm^2, 0.34 mA, 52 % and 0.562 %, respectively. The cell area was 0.131 cm^2. Table 6.3. shows all photovoltaic device properties for three sample.

It can be clearly understood that deposition time effects the conversion efficiency of solar cell. The thinnest CdS coated solar cell device showed the highest photovoltaic characteristic but this thickness is not the optimum thickness for CdS layer. When the thickness of CdS buffer layer is high, the generated electron-hole pairs do not contribute

to the photocurrent and causes the optical losses. The enhancement in photovoltaics properties was observed when thicknesses of CdS was reduced (Cantas et al., 2018). It might be the consequences of thinnest MoS_2 layer for Mo-CZTS-C which has the highest efficiency. When CdS thickness was reduced, V_{oc} improves. Although development of J_{sc} with diminishing CdS layer, because of reduction of absorption loss in the wavelength between 492 and 455 which is called blue region, it was a tiny reduction for the sample Mo-CZTS-C. It might causes diminish in interface recombination. For very thin buffer layer, space charge region width diminishes and photo-generated carriers reduce. Therefore; buffer layer thickness optimization is very important. More photons are absorbed from the thick buffer layer, so light cannot achieve to CZTS absorber layer. Carrier collection is hard for thick CdS layer because of path of light is long also. Therefore, it causes optical loss.

As mentioned before, when our efficiencies compared to the literature, it was very low. XRD analysis showed that there were some secondary phases such as MoS_2, MoO_2, ZnO. Besides, we detected MoS_2 phase in Raman analysis for three sample. Generally, MoS_2 forms during the sulfurization process. In the literature, MoS_2 reported n-type or p-type (Dolui, Rungger, and Sanvito 2013). Nearly 300 nm thick MoS_2 layer forms Schottky-type barrier with back contact, it improves the series resistance and diminish the open circuit voltage (K. Wang et al., 2010). Because n-type MoS_2 layer forms barrier and hinders the charge carriers, generally p-type MoS_2 layers is preferred. We haven't any cross section images to see MoS_2 layer between absorber layer and back contact. According to XRD and Raman analysis, there is a MoS_2 formation for three sample. It must be thick MoS_2 layer which is n-type because of low efficiency. Besides, MoO_2 phase was detected. Reports claim that it is beneficial for certain amount since it reduces the MoS_2 formation. (Lopez-Marino et al., 2016).

Table 6. 3. Summarize of device properties of SLG/Mo/CZTS/CdS/ZnO/AZO solar devices for different CdS buffer layer thickness.

	CdS Thickness (nm)	**V_{OC} (mV)**	**J_{SC} (mA/cm^2)**	**FF (%)**	**Ƞ (%)**
Mo-CZTS-A	140	277.5	0.79	42.8	0.093
Mo-CZTS-B	134	298	2.80	34	0.291
Mo-CZTS-C	102.5	415	2.59	52	0.562

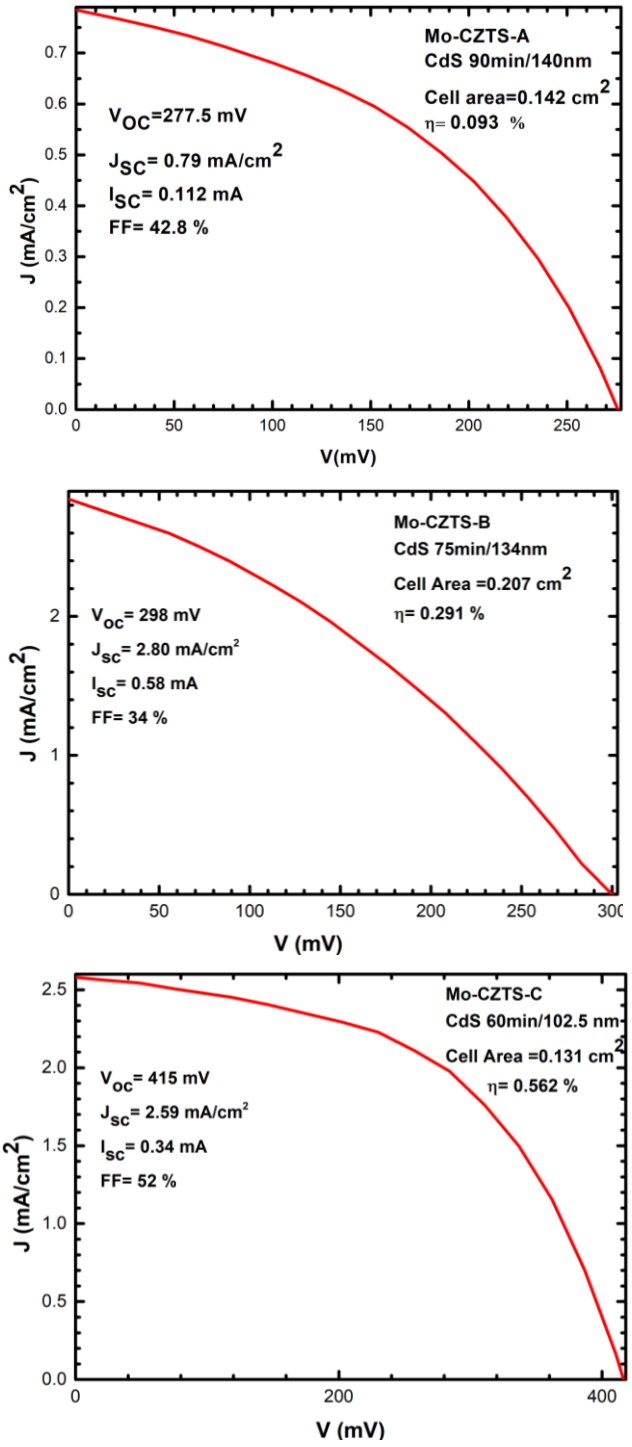

Figure 6. 17. J-V curve of (a) Mo-CZTS-A (b) Mo-CZTS-B and (c) Mo-CZTS-C.

For Mo-CZTS-B, it can be seen that FF decreasing. XRD and Raman analysis said that ZnO or ZnS secondary phases were formed. Their band gaps are 3.3 and 3.7 eV, respectively. Occurred secondary phase's band gap higher than band gap of CZTS, the positive conduction band offset (CBO) where it occurs buffer layer's conduction band

minimum lower than the absorber layer relating to conduction band minimum (CBM) of CZTS occurs and this offset blocks majority and minority carriers. Conductivity decreases but recombination of charge carriers does not rise since secondary phase acts as a sink for one type carrier and it decreases the current density (Wujisiguleng 2014). If secondary phase's band gap lower than the band gap of CZTS, negative CBO occurs relating to conduction band minimum of CZTS. These phases act as a recombination center for minority and majority carriers. V_{OC} limits. Separation is blocked and carrier collection reduces the solar cell efficiency. We showed that V_{OC} didn't decrease but FF decreased when we looked at all table. We can attribute alteration of FF for Mo-CZTS-B because secondary phase which has higher band gap than absorber layer was occurred much higher than other two sample.

Secondly, we examined SLG/Mo/CZTS/Zn(O,S)/ZnO/AZO structure. We investigated sulfurization time effect on solar cell conversion efficiency. Table 6.4. shows all parameters of cell and Figure 6.18. shows the J-V measurement for Mo-CZTS-D and Mo-CTZS-E. As we seen, efficiency of CZTS samples were very low. J-V curves were not like standard shape. When Raman and SEM analysis considered, it was detected MoS_2 phase. This phase indicate that CZTS absorber layer is not continuous. This situation causes serious shunting. Actually, this shunting explains low efficiencies. However, when we compared sulfurization time effect on solar cell efficiency, it can be say that 45 minutes is better for CZTS solar cell fabrications.

Table 6. 4. Summarize of device properties of SLG/Mo/CZTS/Zn(O,S)/ZnO/AZO solar devices for different sulfurization time.

	Sulfurization Time (min)	**V_{OC} (mV)**	**J_{SC} (mA/cm^2)**	**FF (%)**	**η (%)**
Mo-CZTS-D	30	499	1.48	23	0.17638
Mo-CZTS-E	45	568	1.73	17	0.17676

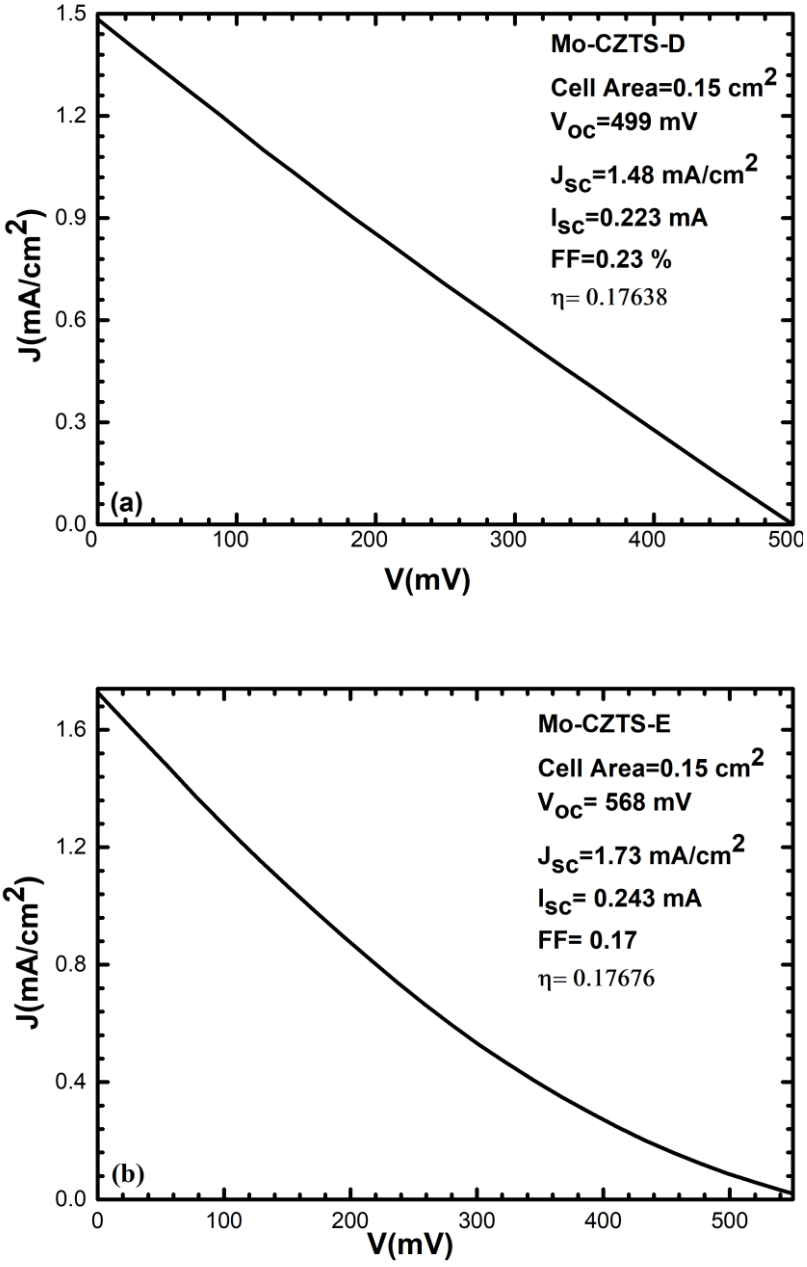

Figure 6. 18. J-V curve of (a) Mo-CZTS-D and (b) Mo-CZTS-E.

CHAPTER 7

CONCLUSION

Cu_2ZnSnS_4 (CZTS) is a promising candidate as an absorber layer for thin film solar cells due to not only its low cost but also nontoxic properties contrary to CdTe and $Cu(In,Ge)Se_2$ (CIGS). Besides, components of CZTS are earth abundant when compared to the CIGS. Recently, Cu_2ZnSnS_4 (CZTS) and similar chalcogenides have taken remarkable attention because of their low cost and being environmentally friendly. Even though the highest efficiency for thin film solar cells have reached over 20% for CIGS ($Cu(In,Ga)Se_2$), compounds of this chalcopyrite absorber layer contains rare elements of indium (In) and gallium (Ga) as well as toxic element of selenium (Se). Due to these drawbacks, the long term production is restricted. In order to avoid these kind of problems, researchers have focused on less toxic, more abundant and cheaper elements for thin film solar cells. Among them, Cu_2ZnSnS_4 (CZTS) is a good candidate for absorber layer, since it has 1.4–1.6 eV bandgap energy and it has high absorption coefficient which is higher than 10^4 cm^{-1}.

In this thesis, we investigated characterization of CZTS thin films as an absorber layer for solar cell devices using DC magnetron sputtering. Three different effects were studied. Substrate selection, buffer layer thickness and sulfurization time effect on solar cell conversion efficiency were studied. Growth process was done under vacuum condition. Pressure was about 10^{-6} Torr. First part of this study Mo coated SLG and Ti foil was used as a back contact. Mo coated SLG was used for second and third part of study as a back contact. All thin film samples were sulfurized to complete CZTS structure. Secondly, CdS buffer layer was growth on CZTS structure with varying thicknesses. Its effects on conversion efficiency was investigated. Third part of this study was about sulfurization time effect on solar cell efficiency. For this part, Zn(O,S) buffer layer was used alternatively. Variety of characterization techniques was used such as Scanning Electron Microscopy (SEM), X-Ray Diffraction (XRD), Raman Spectroscopy, Energy Dispersive Spectroscopy (EDS), Spectrophotometric Analysis (Transmission-Reflection), Hall Effect measurements and Light Beam Induced Current (LBIC) Measurement.

According to the analysis, Cu-poor and Zn-rich compositions was achieved. The compositions were uniform for precursors. CZTS structure was formed. Large grain size is beneficial for solar cell performance. Also, secondary phases are non-desirable situation. Thus, Mo coated SLG was more suitable for device fabrication. In order to investigate CdS buffer layer thickness effect on solar cell conversion efficiency, all layers were growth on Mo coated SLG substrate. Mo-CZTS-C showed better performance when we compared with Mo-CZTS-A and Mo-CZTS-B. Simply, light must achieve CZTS absorber layer with generated electron-hole pairs. Thus, thickness optimization was very important for solar performance. Because, buffer layer thickness was high, generated electron- hole pairs didn't contribute photo-current. This situation caused optical losses. In addition, we detected that when CdS buffer layer thickness reduced, V_{OC} improved. Also we can say that thinner layer might be diminish interface recombination. Our efficiencies were low when we compared to literature. It can attribute to detected MoS2 secondary phases. Because, this phase caused resistance between back contact and CZTS absorber layer.

Last part of this study, we examined sulfurization time effect on conversion solar cell efficiency. Again, all layers were growth on Mo coated SLG substrate. The only difference for structure was buffer layer type from second part of this study. Zn(O,S) was used as a buffer layer. 30 min and 45 min was tried for sulfurization process. Quite low efficiencies were achieved. Cross section images showed that MoS_2 phase was formed. This situation caused shunting in the cell. However, CZTS absorber layer characterization of these samples indicated good crystallite CZTS structure and large grains. When we compared sulfurization time, Mo-CZTS-D which was sulfurized 45 min at Ar atmosphere showed better performance.

REFERENCES

Agura, H., Suzuki A., Matsushita, T., Aoki, T., & Okuda, M. (2003). Low Resistivity Transparent Conducting Al-Doped ZnO Films Prepared by Pulsed Laser Deposition. Thin Solid Films, 445,263–67.

Araki, H., Mikaduki, A., Kubo, Y., Sato, T., Jimbo,K., Maw, W., Katagiri, H., Yamazaki, M., Oishi, K., & Takeuchi. A. (2008). Preparation of Cu_2ZnSnS_4 Thin Films by Sulfurization of Stacked Metallic Layers. Thin Solid Films, 517(4),1457–1460.

Ashour, A. (2003). Physical Properties of Spray Pyrolysed CdS Thin Films. Turkish Journal of Physics, 27(6), 551–558.

Barkhouse, D., Haight, R., Sakai, N., Hiroi, H., Sugimoto, H., & Mitzi, D. (2012). Cd-Free Buffer Layer Materials on $Cu_2ZnSn(S_xSe_{1-x})_4$: Band Alignments with ZnO, ZnS, and In_2S_3. Applied Physics Letters, 100(19).

Barkhouse, D. A., R, Gunawan, O., Gokmen, T., Todorov, T., & Mitzi., D. (2012). Device Characteristics of a 10.1% Hydrazine-Processed Cu_2 $ZnSn(Se,S)_4$ Solar Cell. Progress in Photovoltaics: Research and Applications, 20(1), 6–11.

Barshilia, C., Deepthi, B., & Rajam K. (2007). Deposition and Characterization of CrN/Si_3N_4 and $CrAlN/Si_3N_4$ Nanocomposite Coatings Prepared Using Reactive DC Unbalanced Magnetron Sputtering. Surface and Coatings Technology, 201(24), 9468–9475.

Bharam, V., (2012). *Advantages and Challenges of Silicon in the Photovoltaic Cells*, Final Term Paper.

Birkmire, R. W., & McCandless, B. E. (2010). CdTe Thin Film Technology: Leading Thin Film PV into the Future. Current Opinion in Solid State and Materials Science, 14(6), 139–42.

BP. (2017). BP Statistical Review of World Energy 2017'. British Petroleum, no. 66: 1–52.

Buffière, M., Brammertz, G., Oueslati, S., Anzeery, H. El., Bekaert, J., Messaoud, K. Ben, Köble, C., Khelifi, S., Meuris, M., & Poortmans, J. (2014). Spectral Current-Voltage Analysis of Kesterite Solar Cells. Journal of Physics D: Applied Physics, 47(17).

Buldu, D. G. (2017). I*nvestigation of Sulfurization Temperature Effects On Cu_2ZnSnS_4 Thin Films Prepared by Magnetron Sputtering Method on Flexible Titanium Foil Substrates for Thin Film Solar Cells* (Master's Thesis), Izmir Institute of Technology.

Buldu, D.G., Cantas, A., Turkoglu, F., Akca, F. G., Meric, E., Ozdemir, M., Tarhan, E., Ozyuzer, L., Aygun, G. (2018). Influence of Sulfurization Temperature On Cu_2ZnSnS_4 Absorber Layer on Flexible Titanium Substrates for Thin Film Solar Cells. Physica Scripta, 93 024002.

Cantas, A., Turkoglu, F., Meric, E.,. Akca, F. G., Ozdemir, M., Tarhan, E., Ozyuzer, L., Aygun, G. (2018) 'Importance of CdS Buffer Layer Thickness on Cu_2ZnSnS_4 Based Solar Cell Efficiency. Journal of Physics D: Applied Physics 51 275501.

Cantas, A. (2017). X-*Ray Photoelectron Spectroscopy Analysis of Magnetron Sputtered Cu_2ZnSnS_4 Based Thin Film Solar Cells With CdS Buffer Layer* (PhD Thesis), Izmir Institute of Technology.

Carlson, D. E., & Wronski, C. R. (1976). Amorphous Silicon Solar Cell'. Applied Physics Letters, 28(11), 671–73.

Chen, H., Li, W., Liu, H., & Zhu, L. (2010). A Suitable Deposition Method of CdS for High Performance CdS-Sensitized ZnO Electrodes: Sequential Chemical Bath Deposition. Solar Energy, 84(7), 1201–1207.

Chen, S., Gong, X. G., Walsh, A., Wei, S., S. (2010). Defect Physics of the Kesterite Thin-Film Solar Cell Absorber Defect Physics of the Kesterite Thin-Film Solar Cell Absorber Cu_2ZnSnS_4. Applied Physics Letters, 96(2), 021902.

Chittick, R.C., Alexander, J. H., & Sterling, H. F. (1969). The Preparation and Properties of Amorphous Silicon. Journal of the Electrochemical Society, 116(1), 77-81.

Cormier, P, Snyders, R. (2015). One-Step Synthesis of Cu_2ZnSnS_4 Thin Films by Reactive Magnetron. Acta Materialia, 96, 80–88.

Deulkar, S H, Huang, J. L., & Spallart, M. N. (2010). Zinc Oxysulfide Thin Films Grown by Pulsed Laser Deposition. Journal of Electronic Materials, 39(5),589–594.

Dolui, K., Rungger, I., & Sanvito, S. (2013). Origin of the N-Type and p-Type Conductivity of MoS_2 Monolayers on a SiO_2 Substrate. Physical Review B - Condensed Matter and Materials Physics, 87,165402.

Ennaoui, A., Steiner, L. M., Weber, A., Ras, D. A., Kötschau, I., Schock, H. W., Schurr, R., Hölzing, A., Jost, Z., Hock, R., Voβ, T., Schulze J., & Kirbs, A. (2009). Cu_2ZnSnS_4 Thin Film Solar Cells from Electroplated Precursors: Novel Low-Cost Perspective. Thin Solid Films, 517(7), 2511–2514.

Ferekides, C. S., Marinskiy, D., Viswanathan, V., Tetali, B., Palekis, V., Selvaraj, P., Morel, D. L. (2000). High Efficiency CSS CdTe Solar Cells. Thin Solid Films, 361–362, 520–26.

Fernandes, P. A., Salomé, P. M P., & Cunha. A. F. (2011). Study of Polycrystalline Cu_2ZnSnS_4 Films by Raman Scattering. Journal of Alloys and Compounds 509(28), 7600–7606.

Gordon, R. G. (2000). Criteria for Choosing Transparent Conductors. MRS Bulletin, 25(8), 52–57.

Green, M. A., Hishikawa, Y., Dunlop, E. D., Levi, D. H., Ebinger, J., H., & Ho-Baillie , A. W. Y. (2018). Solar Cell Efficiency Tables (Version 51). Progress in Photovoltaic Research and Applications, 26(1), 3-12.

Green, M. A., Hishikawa, Y., Wilhelm, W., Dunlop, E. D., Levi, D. H., Ebinger, J., H., & Ho-Baillie , A. W. Y. (2017). Solar Cell Efficiency Tables (Version 50). Progress in Photovoltaics: Research and Applications, 25(7), 668–676.

Guc, M., Levcenko, S., Bodnar, I. V., Roca, V. I., Fontane, X., Volkova, L. V., Arushanov, E., & Rodríguez, A. P. (2016). Polarized Raman Scattering Study of Kesterite Type Cu_2ZnSnS_4 Single Crystals. Scientific Reports, 6, 19414.

Hall, S.R., Szymanski, J.T., & Stewart. J.M. (1978). Kesterite, $Cu_2(Zn,Fe)SnS_4$ and Stannite $Cu_2(Fe,Zn)SnS_4$, Structurally Similar but Distinct Minerals. Canadian Mineralogist, 16, 131–37.

Hegedus, S. S., & Shafarman, W. N. (2004). Thin-Film Solar Cells: Device Measurements and Analysis. Progress in Photovoltaics: Research and Applications, 12(2-3), 155–76.

Hergert, F., & Hock, F. (2007). Predicted Formation Reactions for the Solid-State Syntheses of the Semiconductor Materials Cu_2SnX_3 and Cu_2ZnSnX_4 (X = S, Se) Starting from Binary Chalcogenides. Thin Solid Films, 515(15), 5953–5956.

Iacomi, F., Purica, M., Budianu, E., Prepelita, P., & Macovei D. (2007). Structural Studies on Some Doped CdS Thin Films Deposited by Thermal Evaporation. Thin Solid Films, 515 (15): 6080–6084.

Ito, K., & Nakazawa T. (1988). Electrical and Optical Properties of Stannite-Type Quarternary Semiconductor Thin Films. Japanese Journal of Applied Physics, 27, Part 1, 11.

Jackson, P., Hariskos, D., Wuerz, R., Kiowski, O., Bauer, A., Friedlmeier, T. M., & Powalla, M. (2014). Properties of $Cu(In,Ga)Se_2$ Solar Cells with New Record Efficiencies up to 21.7%. Physica Status Solidi RRL, 1-4

Jeong, S. H., & Boo, J. H. (2004). Influence of Target-to-Substrate Distance on the Properties of AZO Films Grown by RF Magnetron Sputtering. Thin Solid Films, 447–448, 105–110.

Jha, S. K., Bilalovic, J., Jha, A., Patel, N., & Zhang, H. (2017). Renewable Energy: Present Research and Future Scope of Artificial Intelligence. Renewable and Sustainable Energy Reviews, 77, 297–317.

Jiang, M., Yan, X. (2013). Cu2ZnSnS4 Thin Film Solar Cells: Present Status and Future Prospects. Intech.

Jimbo, K., Kimura, R., Kamimura, T., Yamada, S., Maw, W. S., Araki, H., Oishi, K., & Katagiri, H. (2007). Cu_2ZnSnS_4-Type Thin Film Solar Cells Using Abundant Materials. Thin Solid Films, 515 (15): 5997–5999.

Kang, M. H., Ryu, K., Upadhyaya, A., & Rohatgi, A. (2011). Optimization of SiN AR Coating for Si Solar Cells and Modules through Quantitative Assessment of Optical and Efficiency Loss Mechanism. Progress in Photovoltaics: Research and Applications, 19(8), 983–990.

Katagiri, H., Ishigaki, N., Ishida, T., & Saito. K. (2001). Characterization of Cu_2ZnSnS_4 Thin Films Prepared by Vapor Phase Sulfurization. Japanese Journal of Applied Physics, Part 1: Regular Papers and Short Notes and Review Papers, 40(2A), 500–504.

Katagiri, H., Jimbo, K., Maw, W. S., Oishi, K., Yamazaki, M., Araki, H., & Takeuchi A. (2009). Development of CZTS-Based Thin Film Solar Cells. Thin Solid Films, 517(7), 2455–2460.

Katagiri, H., Jimbo, K., Yamada, S., Kamimura, T., Maw, W. S., Fukano, T., Ito, T.,& Motohiro, T. (2008). Enhanced Conversion Efficiencies of Cu_2ZnSnS_4-Based Thin Film Solar Cells by Using Preferential Etching Technique. Applied Physics Express, 1(4), 0412011–12.

Katagiri, H., Saitoh, K., Washio, T., Shinohara, H., Kurumadani, T., & Miyajima. S. (2001). Development of Thin Film Solar Cell Based on Cu_2ZnSnS_4 Thin Films. Solar Energy Materials and Solar Cells, 65(1-4), 141–148.

Katagiri, H., Sasaguchi, N., Hando, S., Hoshino, S., Ohashi, J., & Yokota, T., (1997). Preparation and Evaluation of Cu_2ZnSnS_4 Thin Films by Sulfurization of E-B Evaporated Precursors. Solar Energy Materials and Solar Cells, 49(1–4),407–414.

Kaushik, D. K., Rao, T. N., & Subrahmanyam, A. (2017). Studies on the Disorder in DC Magnetron Sputtered Cu_2ZnSnS_4 (CZTS) Thin Films Grown in Sulfide Plasma. Surface and Coatings Technology, 314, 85–91.

Kavitha, N., Chandramohan, R., Valanarasu, S., Vijayan, T. A., Rosario, S. R. & Kathalingam A. (2016). Effect of Film Thickness on the Solar Cell Performance of CBD Grown CdS/PbS Heterostructure. Journal of Materials Science: Materials in Electronics, 27(3),2574–2580.

Kazmerski, L L, White, F R., Morgan, G K., (1976). Thin-Film $CuInSe_2$/CdS Heterojunction Solar Cells. Applied Physics Letters, 29(268).

Khalkar, A., ,Lim, K. S., Yu, S. M., Kim, J. H., & Yoo, J. B. (2014). Sulfurization Approach Using Sulfur Vapor, Graphite Box and H_2S Gas Atmospheres for Co-Sputtered Cu_2ZnSnS_4 Thin Film. 2014 IEEE 40th Photovoltaic Specialist Conference PVSC 2014, 390–394.

Khare, A., Himmetoglu, B., Johnson, M., Norris, D. J., Cococcioni, M., & Aydil, E. S. (2012). Calculation of the Lattice Dynamics and Raman Spectra of Copper Zinc Tin Chalcogenides and Comparison to Experiments. Journal of Applied Physics, 111(8) 083707

Klenk, R. (2001). Characterisation and Modelling of Chalcopyrite Solar Cells. Thin Solid Films, 387(1–2), 135–140.

Klenk, R., Steigert, A., Rissom, T., Greiner, D., , Kaufmann, C. A. Unold, T., & Steiner, M. C. L. (2014). Junction Formation by Zn(O,S) Sputtering Yields CIGSe-Based Cells with Efficiencies Exceeding 18%. Progress in Photovoltaics: Research and Applications, 22(2), 161–165.

Klingshirn, C. (2007). ZnO: Material, Physics and Applications. Chemical Physisc and Phsical Chemistry, 8(6), 782-803.

Koseoglu, H., Turkoglu, F., Kurt, M., Yaman, M. D., Akca, F. G., Aygun, G., & Ozyuzer L. (2015). Improvement of Optical and Electrical Properties of ITO Thin Films by Electro-Annealing. Vacuum, 120(Part B), 8–13.

Krishnakumar, V., Han, J., Klein, A., & Jaegermann. W. (2011). CdTe Thin Film Solar Cells with Reduced CdS Film Thickness. Thin Solid Films, 519(21), 7138–7141.

Kumar, M., & Kumar, A. (2017). Performance Assessment and Degradation Analysis of Solar Photovoltaic Technologies: A Review. Renewable and Sustainable Energy,Reviews 78, 554–587.

Kumar, M., Dubey, A., Adhikari, N., Venkatesan, S., & Qiao. Q., (2015). Strategic Review of Secondary Phases, Defects and Defect-Complexes in Kesterite CZTS–Se Solar Cells. Energy & Environmental Science, 8 (11), 3134–3159.

Kushiya, K. (2004). Development of Cu(InGa)Se_2-Based Thin-Film PV Modules with a Zn(O,S,OH)X buffer Layer. Solar Energy 77(6), 717–724.

Bezuidenhout, L. J., Dyk E. E, Vorster, F. J., & Plessis Mc. (2012). On the Characterisation of Solar Cells Using Light Beam Induced Current Measurements. 1-9.

Lee, C. C., & Tang., C. J. (2006). TiO_2--Ta_2O_5 Composite Thin Films Deposited by Radio Frequency Ion-Beam Sputtering. Applied Optics, 45(36), 9125–9131.

Lee, C., Dwivedi, R. P., Lee, W., Hong, C., Lee, W. I., & Kim, H. W. (2008). IZO/Al/GZO Multilayer Films to Replace ITO Films. Journal of Materials Science: Materials in Electronics, 19(10), 981–985.

Li, J. V., Kuciauskas, D., Young, M. R., & Repins, I. L. (2013). Effects of Sodium Incorporation in Co-Evaporated $Cu_2ZnSnSe_4$ Thin-Film Solar Cells. Applied Physics Letters, 102(16), 163905.

Lisco, F., Kaminski, P. M., Abbas, A., Bass, K., Bowers, J. W., Claudio, G., Losurdo, M., & Walls J. M. (2015). The Structural Properties of CdS Deposited by Chemical Bath Deposition and Pulsed Direct Current Magnetron Sputtering. Thin Solid Films, 582:323–327.

Lisco, F., Kaminski, P. M., Abbas, A., Bowers, J. W., Claudio, G., Losurdo, M., & Walls, J. M. (2015). High Rate Deposition of Thin Film Cadmium Sulphide by Pulsed Direct Current Magnetron Sputtering. Thin Solid Films, 574, 43–51.

Liu, F., Lai, Y., Liu, J., Wang, B., Kuang, S., Zhang, Z., Li, J., & Liu, Y. (2010). Characterization of Chemical Bath Deposited CdS Thin Films at Different Deposition Temperature. Journal of Alloys and Compounds, 493(1–2), 305–308.

Loferski, J. J. (1956). Theoretical Considerations Governing the Choice of the Optimum Semiconductor for Photovoltaic Solar Energy Conversion. Journal of Applied Physics, 27(7), 777–784.

Lopez, M. S., Rodriguez, M. E., Sanchez, Y., Alcobe, X., Oliva, F., Xie, H., Neuschitzer, M., Giraldo, S., Placidi, M., Caballero, R., Roca, V. I., Rodriguez, A. P., Saucedo, E. (2016). The Importance of Back Contact Modification in $Cu_2ZnSnSe_4$ Solar Cells: The Role of a Thin MoO_2 Layer. Nano Energy, 26, 708–721.

Ma, L., Ai, X., & Wu, X. (2017). Effect of Substrate and Zn Doping on the Structural, Optical and Electrical Properties of CdS Thin Films Prepared by CBD Method. Journal of Alloys and Compounds, 691, 399–406.

Maeda, T., Nakamura, S., & Wada T. (2011). First-Principles Calculations of Vacancy Formation in In-Free Photovoltaic Semiconductor $Cu_2ZnSnSe_4$. Thin Solid Films, 519(21), 7513–7516.

Malerba, C., Biccari, F., Leonor, C., Ricardo, A., Valentini, M., Chierchia, R., Müller, M., Santoni, A., Esposito, E., Mangiapane, P., Scardi, P., Mittiga, A. (2014). CZTS Stoichiometry Effects on the Band Gap Energy. Journal of Alloys and Compounds, 582, 528–534.

Marchionna, S., Garattini, P., Donne, A. L., Acciarri, M., Tombolato, S., & Binetti, S. (2013). Cu_2ZnSnS_4 Solar Cells Grown by Sulphurisation of Sputtered Metal Precursors. Thin Solid Films, 542, 114–118.

Markvart, T. (2013). Solar Cells - Materials, Manufacture and Operation. Journal of Chemical Information and Modeling, 53.

McCrone, A., Moslener, U., D'Estais, F., & Grünig. C. (2017). Global Trends in Renewable Energy Investment 2017. Frankfurt School UNEP Collaborating Centre for Climate and Sustainable Energy Finance.

Mkawi, E. M., Ibrahim, K., Ali, M. K. M., Saron, K. M. A., Farrukh M. A., & Allam. N. K. (2014). Influence of Substrate Temperature on the Properties of Electrodeposited Kesterite Cu_2ZnSnS_4 (CZTS) Thin Films for Photovoltaic Applications. Journal of Materials Science: Materials in Electronics, 26(1), 222–228.

Moholkar, A. V., Shinde, S. S., Babar, A. R., Sim, K. U., Kwon, Y. B., Rajpure, K. Y., Patil, P. S., Bhosale, C. H., & Kim, J. H. (2011). Development of CZTS Thin Films Solar Cells by Pulsed Laser Deposition: Influence of Pulse Repetition Rate. Solar Energy, 85(7), 1354–1363.

Moll, J. L. (1958). The Evolution of the Theory for the Voltage-Current Characteristic of P-N Junctions. Proceedings of the IRE, 46(6).

Muffler, H. J., Bär, M., Fischer, C. H., Gay, R., Karg, F., &,Steiner, M. C. L. (2000). Ilgar Technology. VIII. Sulfidic Buffer Layers for $Cu(InGa)(S,Se)_2$solar Cells Prepared by Ion Layer Gas Reaction (ILGAR). In Conference Record of the IEEE Photovoltaic Specialists Conference, 2000 610–613.

Nelson, J. (2003). The Physics of Solar Cells. Properties of Semiconductor Materials.

Oladeji, I. O., Chow, L., Liu, J. R., Chu, W. K., Bustamante, A. N. P., Fredricksen, C., & Schulte, A. F. (2000). Comparative Study of CdS Thin Films Deposited by Single, Continuous, and Multiple Dip Chemical Processes. Thin Solid Films, 359(2),154–159.

Paier, J., Asahi, R., Nagoya, A., & Kresse G. (2009). Cu_2ZnSnS_4 as a Potential Photovoltaic Material: A Hybrid Hartree-Fock Density Functional Theory Study. Physical Review B - Condensed Matter and Materials Physics, 79(11),115126.

Pal, M., Mathews, N. R., Gonzalez, R. S., & Mathew, X. (2013). Synthesis of Cu_2ZnSnS_4 Nanocrystals by Solvothermal Method. Thin Solid Films, 535(1),78–82.

Pawar, S. M., Inamdar, A. I., Pawar, B. S., Gurav, K. V., Shin, S. W., Yanjun, X., Kolekar, S. S., Lee, J. H., Kim, J. H., & Im, H. (2014). Synthesis of Cu_2ZnSnS_4 (CZTS) Absorber by Rapid Thermal Processing (RTP) Sulfurization of Stacked Metallic Precursor Films for Solar Cell Applications Materials Letters, 118, 76–79.

Pawar, S M, Pawar, B S., Moholkar, A V., Choi, D S., Yun, J H., Moon, J H., Kolekar, S. S., & Kim, J. H. (2010). Single Step Electrosynthesis of Cu_2ZnSnS_4 (CZTS) Thin Films for Solar Cell Application. Electrochimica Acta, 55(12), 4057–4061.

Persson, C. (2010). Electronic and Optical Properties of Cu_2ZnSnS_4 and $Cu_2ZnSnSe_4$. Journal of Applied Physics, 107(5), 053710.

Petrich, M. (2007). Amorphous Silicon Alloys 7, 220.

Platzer-Björkman, C., Törndahl, T., Abou-Ras, D., Malmström, J., Kessler, J., & Stolt, L. (2006). Zn(O,S) Buffer Layers by Atomic Layer Deposition in Cu(In,Ga)Se_2 Based Thin Film Solar Cells: Band Alignment and Sulfur Gradient. Journal of Applied Physics, 100(4), 044506.

Rau, U., & Schmidt, M. (2001). Electronic Properties of ZnO/CdS/Cu(In,Ga)Se_2 Solar Cells - Aspects of Heterojunction Formation. Thin Solid Films 387(1–2),141–146.

Romeo, A., Gysel, R., Buzzi, S., Abou-Ras, D., Bätzner, D. L., Rudmann, D., Zogg, H., & Tiwari, A. N. (2004). Properties of CIGS Solar Cells Developed with Evaporated II-VI Buffer Layers. Technical Digest of the International PVSEC-14, 10–12.

Sah, C. T., Noyce, & Shockley. W. (1957). Carrier Generation and Recombination in P-N Junctions and P-N Junction Characteristics. Proceedings of the IRE 45(9), 1228–1243.

Salomé, P. M. P., Keller, J., Törndahl, T., Teixeira, J. P., Nicoara, N., Andrade, R. R., Stroppa, D. G., Gonzalez, J. C., Edoff, B., Leitao, J. P., Sadewasser, S. (2017). CdS and $Zn_{1-x}Sn_xO_y$ Buffer Layers for CIGS Solar Cells. Solar Energy Materials and Solar Cells, 159, 272–281.

Schorr, S. (2011). The Crystal Structure of Kesterite Type Compounds: A Neutron and X-Ray Diffraction Study. Solar Energy Materials and Solar Cells, 95(6),1482–1488.

Schorr, S., Weber, A., Honkimäki, V., & Schock. H. W. (2009). In-Situ Investigation of the Kesterite Formation from Binary and Ternary Sulphides. Thin Solid Films, 517(7),2461–2464.

Scofield, J. H., Duda, A., Albin, D., Ballard, B. L., & Predecki, P. K. (1995). Sputtered Molybdenum Bilayer Back Contact for Copper Indium Diselenide-Based Polycrystalline Thin-Film Solar Cells. Thin Solid Films, 260(1),26–31.

Scragg, J. J., Wätjen, J. T., Edoff, M., Ericson, T., Kubart, T., & Björkman, C. P. (2012). A Detrimental Reaction at the Molybdenum Back Contact in $Cu_2ZnSn(S,Se)_4$ Thin-Film Solar Cells. Journal of the American Chemical Society, 134(47), 19330–19333.

Scragg, J. J., (2010). *Studies of Cu_2ZnSnS_4 Films Prepared by Sulfurisation of Electrodeposited Precursors.* (Ph.D Thesis) 262.

Sekular, R., & Blake, R. (1985). Perception. New York: Alfred A. Knopf Inc.

Seyboth, K., Sverrisson, F., Appavou, F., Brown, A., Epp, B., Leidreiter, A., Lins, C., et al. (2016). Renewables 2016 Global Status Report. Global Status Report.

Shah, A. V., Schade, H., Vanecek, M., Meier, J., Vallat-Sauvain, E., Wyrsch, N., Kroll, U., Droz, C., & Bailat, J. (2004). Thin-Film Silicon Solar Cell Technology. Progress in Photovoltaics: Research and Applications, 12(23), 113–142.

Sheoran, M., Kim, D. S., Rohatgi, A., Dekkers, H. F. W., Beaucarne, G., Young, M., & Asher. S. (2008). Hydrogen Diffusion in Silicon from Plasma-Enhanced Chemical Vapor Deposited Silicon Nitride Film at High Temperature. Applied Physics Letters, 92(17),172107.

Shi, C., Shi, G., Chen, Z., Yang, P., & Yao, M. (2012). Deposition of Cu_2ZnSnS_4 Thin Films by Vacuum Thermal Evaporation from Single Quaternary Compound Source. Materials Letters, 73, 89–91.

Shin, B., Gunawan, O., Zhu, Y., Bojarczuk, N. A., Chey, S. J., & Guha, S., (2013). Thin Film Solar Cell with 8.4% Power Conversion Efficiency Using an Earth-Abundant Cu_2ZnSnS_4 Absorber. Progress in Photovoltaics: Research and Applications, 21(1) 72–76.

Shockley, W. (1949). The Theory of P-n Junctions in Semiconductors and p-n Junction Transistors. Bell System Technical Journal, 28(3), 435–489.

Shockley, W., & Queisser, H. J. (1961). Detailed Balance Limit of Efficiency of p-n Junction Solar Cells. Journal of Applied Physics, 32(3), 510–519.

Singh, D. J. (2016). Optical and Electronic Properties of Semiconducting Sn_2S_3. Applied Physics Letters, 109(3), 032102.

Sinsermsuksakul, P., Hartman, K., Kim, S. B., Heo, J., Sun, L., Park, H. H., Chakraborty, R., Buonassisi, T., & Gordon, R. G. (2013). Enhancing the Efficiency of SnS Solar Cells via Band-Offset Engineering with a Zinc Oxysulfide Buffer Layer. Applied Physics Letters, 102(5), 053901

Sood, A. K, Puri, Y. R., Becker, L., Tidrow, M. Z., Balcerak, R. S., Brill, G., Wijewarnasuriya, P., Dhar, N., Boieriu, P., Fulk, C., Sivananthan, S., Yehoda, J. (2006). Development of High-Performance Radiation-Hardened Antireflection Coatings for LWIR and Multicolor IR Focal Plane Arrays. Proceedings of the SPIE - The International Society for Optical Engineering, 620613–15.

Srikant, V., & Clarke, D. R. (1998). On the Optical Band Gap of Zinc Oxide. Journal of Applied Physics, 83(10),5447–5451.

Sripan, C., Ganesan, R., Vinod, E. M., & Viswanath, A. K. (2016). The Effect of Sulfur on the Phase Formation of Cu_2ZnSnS_4 Solar Cell Material. Materials Letters, 180, 295–297.

Sze, S. M., & Ng., K. K. (2006). Physics of Semiconductor Devices. Physics of Semiconductor Device.

Tajima, S., Umehara, M., Hasegawa, M., Mise, T., & Itoh, T. (2017). Cu_2ZnSnS_4 Photovoltaic Cell with Improved Efficiency Fabricated by High-Temperature Annealing after CdS Buffer-Layer Deposition. Progress in Photovoltaics: Research and Applications, 25(1), 14–22.

Terasako, T., Yagi, M., Ishizaki, M,. Senda, Y., Matsuura, H., & Shirakata, S. (2007). Growth of Zinc Oxide Films and Nanowires by Atmospheric-Pressure Chemical Vapor Deposition Using Zinc Powder and Water as Source Materials. Surface and Coatings Technology, 201(22–23), 8924–8930.

Todorov, T. K., Tang, J., Bag, S., Gunawan, O., Gokmen, T., Zhu, Y., & Mitzi, D. B. (2013). Beyond 11% Efficiency: Characteristics of State-of-the-Art $Cu_2ZnSn(S,Se)_4$ Solar Cells. Advanced Energy Materials, 3(1), 34–38.

Tuna, O., Selamet, Y., Aygun, G., & Ozyuzer, L. (2010). High Quality ITO Thin Films Grown by DC and RF Sputtering without Oxygen. Journal of Physics D: Applied Physics, 43(5).

Turkoglu, F., Koseoglu, H., Zeybek, S., Ozdemir, M., Aygun, G., Ozyuzer, L. (2018) Effect of Substrate Rotation Speed and Off-Center Deposition on the Structural , Optical , and Electrical Properties of AZO Thin Films Fabricated by DC Magnetron Sputtering' Journal of Applied Physics, 123(16), 165104.

Turkoglu, F. (2017). Magnetron Sputtering Growth Of AZO / ZnO / Zn(O,S) Multilayers For Cu_2ZnSnS_4 Thin Film Solar Cells: Material And Device Characterization (Ph.D Thesis), Izmir Institute of Technology.

Wang, K., Gunawan, O., Todorov, T., Shin, B., Chey, S. J., Bojarczuk, N. A., Mitzi, D., & Guha, S. (2010). Thermally Evaporated Cu_2ZnSnS_4 Solar Cells. Applied Physics Letters, 97(14), 143508.

Wang, K., Shin, B., Reuter, K. B., Todorov, T., Mitzi, D. B., & Guha, S. (2011). Structural and Elemental Characterization of High Efficiency Cu_2ZnSnS_4 Solar Cells. Applied Physics Letters, 98(5), 98–101.

Wang, W., Winkler, M. T., Gunawan, O., Gokmen, T., Todorov, T. K., Zhu, Y., & Mitzi, D. B. (2014). Device Characteristics of CZTSSe Thin-Film Solar Cells with 12.6% Efficiency. Advanced Energy Materials, 4(7), 1–5.

Washio, T., Shinji, T., Tajima, S., Fukano, T., Motohiro, T., Jimbo, K.,b& Katagiri. H. (2012). 6% Efficiency Cu_2ZnSnS_4-Based Thin Film Solar Cells Using Oxide Precursors by Open Atmosphere Type CVD. Journal of Materials Chemistry, 22(9), 4021-4024.

Wu, C., Hu, Z., Wang, C., Sheng, H., Yang, J., & Xie, Y. (2007). Hexagonal Cu_2SnS_3 with Metallic Character: Another Category of Conducting Sulfides. Applied Physics Letters, 91(14), 143404.

Wujisiguleng, B. (2014). *First Principles Study on Band Offsets at the Cu_2ZnSnS_4-Based Heterointerfaces. Journal of Chemical Information and Modeling.* (Ph.D Thesis), Nagoya Institute of Technology.

Yang, K-J., Sim, J-H., Son, D. H., Kim, D-H., Kim, G. Y., Jo, W., Song, S., Kim, J., Nam, D., Cheong, H., Kang, J-K. (2015). Effects of the Compositional Ratio Distribution with Sulfurization Temperatures in the Absorber Layer on the Defect and Surface Electrical Characteristics of Cu_2ZnSnS_4 Solar Cells. Progress in Photovoltaics: Research and Applications, 23, 1771–1784.

Yazici, S., Olgar, M. A., Akca, F. G., Cantas, A., Kurt, M., Aygun, G., Tarhan, E., Yanmaz, E., & Ozyuzer, L. (2015). Growth of Cu_2ZnSnS_4 Absorber Layer on Flexible Metallic Substrates for Thin Film Solar Cell Applications. Thin Solid Films, 589, 563–573.

Yeh, M. Y., Lei, P. H., Lin, S. H., & Yang, C. (2016). Copper-Zinc-Tin-Sulfur Thin Film Using Spin-Coating Technology. Materials, 9(7).

Yoo, H., & Kim, J. (2011). Comparative Study of Cu_2ZnSnS_4 Film Growth. Solar Energy Materials and Solar Cells, 95(1),239–244.

Zhang, X., Zhang, G., & Zhuang, D. (2009). The Influence of Ph Value to the Properities of Cds Thin Film. Taiyangneng Xuebao/Acta Energiae Solaris Sinica 30(7).

Zhao, J., Jeon, I., Yi, Q., Jain, M., Rummeli, M. H., Song, P., Matsuo, Y., & Zou, G. (2017). An Efficient Organic Solvent-Free Solution-Processing Strategy for High-Mobility Metal Chalcogenide Film Growth. Green Chemistry, 19(4), 946–591.

Zhu, H., Wei, J., Wang, K., Wu D., Al-Hasan, A. Y., Altermatt, P. P., Kiesewetter, T. (2011). The History of Solar. Solar Energy Materials and Solar Cells, 93,1461–1470.

Zhu, X. G., Long, S. P., & Ort, D. R. (2008). What Is the Maximum Efficiency with Which Photosynthesis Can Convert Solar Energy into Biomass? Current Opinion in Biotechnology, 19(2), 153–159.

Zimmermann, U., Ruth, M., & Edoff, M. (2006). Cadmium-Free CIGS Mini-Modules with Zn(O,S)-Based Buffer Layers. 21st European Photovoltaic Solar Energy Conference, 1831–1834.